VIRUS REMOVAL AND INACTIVATION IN A PHOTOCATALYTIC MEMBRANE REACTOR: DISINFECTION MECHANISMS AND EFFECT OF WATER QUALITY

By

Bin Guo

A DISSERTATION

Submitted to
Michigan State University
in partial fulfillment of the requirements
for the degree of

Environmental Engineering – Doctor of Philosophy

2016

ABSTRACT

VIRUS REMOVAL AND INACTIVATION IN A PHOTOCATALYTIC MEMBRANE REACTOR: DISINFECTION MECHANISMS AND EFFECT OF WATER QUALITY

By

Bin Guo

Waterborne diseases pose great health threat to humans and result in huge economic losses. One of the effective way to avoid the infections by waterborne microorganisms is water disinfection. Conventional disinfection methods include chlorination, chloramination and ozonation. However, the inevitable production of disinfection by-products (DBPs) and the inability to inactivate certain resistant microbial species are drawbacks of the conventional disinfection methods. In addition, with the transition to lower quality water sources and an increasing role of water reuse, conventional disinfection methods may no longer be sufficient. Alternative treatment methods with higher efficiency and smaller energy demand are urgently required.

Numerous studies have been conducted to explore the application of photocatalytic membrane reactors (PMRs) in water treatment. Most of these studies have focused on the removal of chemicals, often employing dyes as model pollutants. PMRs applications to water disinfection, however, are very limited. Only five studies employed concurrent filtration and photocatalytic disinfection. In four of the five publications, the same type of bacterium was used as the bacterial model. In the present work, a novel hybrid photocatalytic UV-membrane filtration system was designed and applied for water disinfection. To the best of our knowledge, this is the first application of a PMR for virus removal and inactivation in water. Two types of viruses and two types of waters were used to test the performance of the hybrid system. The hybrid system is shown to retain the advantages of photocatalytic UV disinfection and membrane filtration and to

synergistically mitigate drawbacks of each of these two processes. In addition, batch experiments were also conducted to understand the mechanism of photocatalytic inactivation of viruses in water and to examine the effect of water quality on the photocatalytic inactivation of viruses. Water quality affects the kinetics of photocatalytic inactivation, which fits Collins-Selleck model in DI water and a first-order reaction in pre-filtered surface water.

This thesis is dedicated to my family.
Thank you for always loving and supporting me.

ACKNOWLEDGEMENTS

First of all, I would like to express my sincere thanks to my advisor, Dr. Volodymyr Tarabara, for his patience and guidance throughout my graduate study.

I am also grateful to my dissertation committee members: Dr. Irene Xagoraraki, Dr. Thomas W. Hamann and Dr. Kristin N. Parent, for their time and valuable input throughout the entire project.

In addition, I would also like to thank Lori Larner, Margaret Conner, Laura Taylor, Mary Mroz, Laura Post, Joseph Nguyen, Craig Burck and Yanlyang Pan, for their administrative and technical support during my graduate study.

Furthermore, my appreciation also extended to my former and current group members for the inspiring discussions and their positive attitudes in and outside the lab, which bring me a very pleasant time at Michigan State University. The collaboration with many of them is really an enjoyable experience for me, and all their great contribution and generous sharing of experiences are highly appreciated.

Finally, I would like to express my gratitude to my beloved family members, especially my mother, my aunts and my husband, Dr. Yunyi Jia. Without their continuous support and encouragement I would not be where I am. And all your love and understanding will always be my strongest backing.

TABLE OF CONTENTS

LIST OF TABLES

LIST OF FIGURES

KEY TO ABBREVIATIONS

AOP	Advanced oxidation process
BDF	Buffered demand-free
CPE	Cytopathic effects
DBPs	Disinfection by-products
DDI	distilled deionized water
DNA	Deoxyribonucleic acid
DOC	Dissolved organic carbon
DOM	Dissolved organic matter
DI	Deionized water
EDTA	Ethylenediaminetetraacetic acid
FBS	Fetal bovine serum
HAdV	Adenoviruses
HAdV40	Human adenovirus serotype 40
H_2O_2	Hydrogen peroxide
H_3PO_4	Phosphoric acid
KI	Potassium iodide
KIO_3	Potassium iodate
LBL	Layer-by-layer
LRV	The log removal
MB	Methylene blue
MEM	Minimum essential medium

MF	Microfiltration
MPN	Most probable number
NaOH	Sodium hydroxide
NEAA	Non-essential amino acid
NF	Nanofiltration
NOM	Natural organic matter
O_3	Ozone
OH·	Hydroxyl radicals
P22	Enterobacteria phage P22
PBS	Phosphate buffered saline
PBW	Phosphate buffered water
pCBA	para-Chlorobenzoic Acid
PDADMAC	Polydiallyldimethylammonium chloride
PFU	Plaque forming unit
qPCR	Real-time polymerase chain reaction
RNA	Ribonucleic acid
RO	reverse osmosis
ROS	Reactive oxygen species
SDW	Sterile distilled water
SEM	Scanning electron microscopy
SEW	Steriie estuarine water
SUVA	Specific UV absorbance
TiO_2	Titanium dioxide

TOC	Total organic carbon
TSA	Trypticase soy agar
TSB	Trypticase soy broth
UF	Ultrafiltration

CHAPTER 1. INTRODUCTION

1.1 Importance and challenges of current water disinfection technologies

Waterborne diseases, which are caused by pathogenic microorganisms and/or chemicals transmitted in the contaminated water, pose a major threat to human health world-wide. According to the report by World Health Organization (WHO) [1, 2], as of 2013, 700 million people still lack access to an improved drinking water sources and ~ 1.5 million people die from waterborne disease (e.g. diarrhea) annually, mostly children in developing countries. Every year huge amounts of financial and human resources are spent to prevent and reduce the risk of waterborne infectious.

Water disinfection has been considered as a promising technology to prevent or decrease the deaths from waterborne diseases caused by pathogens. Conventional disinfection methods include chlorination, chloramination and ozonation. By adding strong oxidants, harmful pathogens (e.g. viruses, bacteria and protozoa) are inactivated in the treatment, storage and distribution systems. However, the traditional technologies have their drawbacks. These include: 1) formation of disinfection by-products (DBPs) that are carcinogenic [3, 4]; 2) some pathogens, such as *Legionella*, *Cryptosporidium*, *Giardia lamblia* cysts, have been proved to be resistant to disinfection by chlorine [5, 6]. A suite of alternative treatment processes — advanced oxidation process (AOP) – that utilize the strong oxidizing property of hydroxyl radicals (·OH) has been developed. Although proven to be a powerful treatment alternative, AOPs is not free of its own drawbacks (Table 1.1) [7-9]. With the increasing awareness of persistent microbial pathogens detected in treated wastewater and drinking water sources worldwide, a sufficient, economical and environment-friendly treatment technology is necessary and urgent.

Table 1.1 Disadvantages of selected advanced oxidation processes

AOPs	Disadvantages
UV/H_2O_2	• Treatment effectiveness is greatly affected by the water quality (e.g. alkalinity, turbidity) • Excess peroxide can limit the effectiveness • The production of ·OH is limited by the small molar extinction coefficient of H_2O_2
O_3/H_2O_2	• Treatment performance depends on pH and water quality • O_3 production is expensive • Control of O_3/H_2O_2 dosage ratio is difficult • Additional treatment of excess H_2O_2 and O_3
O_3/UV	• Treatment effectiveness is dependent on pH • High amount of O_3 and energy consumption • The presence of UV absorbing compounds is problematic • May require O_3 off-gas treatment
UV/H_2O_2	• Treatment effectiveness is dependent on pH • Turbidity and UV absorbing compounds is problematic • Less stoichiometrically efficient at generating ·OH
$O_3/H_2O_2/UV$	• Turbidity and UV absorbing compounds is problematic • May require O_3 off-gas treatment • Control of O_3/H_2O_2 dosage • High energy and cost consumption

1.2 Implication of photocatalysis in disinfection: mechanisms and applications

Photocatalysis is classified as an AOP because the oxidation in this process occurs primarily though reactions with hydroxyl radicals (·OH) which are non-selective and potent oxidizers for organic matter in water [10, 11]. The term photocatalyst refers to a semiconductor that is able to convert light energy to the chemical energy of electron-hole pairs. Although many semiconductor materials such as TiO_2, ZnO, Fe_2O_3, WO_3, BiOBr, Bi_3O_4Br and CuS have been investigated as photocatalysts [12-18], titanium dioxide (TiO_2) is still the most popular catalyst because of its high photoactivity, chemical stability, commercial availability, no demonstrable toxicity and low cost [19, 20].

1.2.1 Mechanisms

There are three polymorphs of TiO_2: anatase (tetragonal minerals), rutile and brookite (a rare orthorhombic mineral). With the different crystalline structures, these three types of TiO_2 exhibit different properties. Many studies show that the rutile is the most stable form but less active, whereas anatase is metastable but the most effective photocatalyst [21-23]. It was believed that the photoactivity is associated with the energy structure, recombination rate of electron-hole pairs [24, 25] as well as the surface physical/chemical properties [26]. Moreover, nanosized TiO_2 usually show higher photoactivity due to the quantum size effect and the larger surface area. Miyagi et al. [25] also pointed out that the mixture of anatase and rutile was more effective in photocatalytic process than the pure anatase form of TiO_2 . Thus, the commercial available Degussa P25 TiO_2, which contains ~ 80% anatase and 20% rutile, is the catalyst most frequently used in the fundamental studies of microbial disinfection.

Because of the relatively wide band gap (3.2 eV for anatase), non-modified TiO_2 can be excited only under UV irradiation with a wavelength less than 400 nm [19, 27]. When a photon with energy that is equal to or greater than the band gap energy is absorbed by TiO_2, an electron in the valence band may be excited to the conduction band, resulting in the formation of electron-hole pairs in femtoseconds [7, 28]:

$$TiO_2 \xrightarrow{h\nu} e^- + h^+ \quad (1)$$

With the formed hole h^+ and the presence of appropriate scavengers (e.g. H_2O and/or OH^-), ·OH can be produced [29]:

$$H_2O + h^+ \rightarrow H^+ + \cdot OH \quad (2)$$

$$OH^- + h^+ \rightarrow \cdot OH \quad (3)$$

Meanwhile, the electron e^- may react with dissolved oxygen to produce other reactive oxygen species (ROS) like superoxide radical ion ($O_2^{\cdot -}$) and hydrogen peroxide (H_2O_2), which ultimately lead to the production of ·OH [30]:

$$O_2 + e^- \rightarrow O_2^{\cdot -} \quad (4)$$

$$O_2^{\cdot -} + h^+ \rightarrow HO_2^{\cdot} \quad (5)$$

$$HO_2^{\cdot} + h^+ + e^- \rightarrow H_2O_2 \quad (6)$$

$$H_2O_2 + e^- \rightarrow \cdot OH + OH^- \quad (7)$$

$$H_2O_2 + O_2^{\cdot -} \rightarrow \cdot OH + OH^- + O_2 \quad (8)$$

1.2.2 Factors influencing photocatalytic activity

The efficiency of photocatalytic activity depends upon many factors, including loading of the photocatalyst, initial concentration of the substrate, characteristics of UV lamp and the components of the solution.

1.2.2.1 Loading of photocatalysts

Generally, the reaction rate is proportional to the mass of catalysts in the initial step due to the higher number of available sites on the catalyst [31]. However, when the mass of catalysts is above the optimized amount, the reaction rate is independent of catalysts. The rate may remain constant or even decrease because of the increased solution opacity and agglomeration of catalyst particles [32-35].

1.2.2.2 Initial concentration of the substance

The degradation rate increases with an increase in the initial concentration of the substrate till a certain level. A further increase in the concentration leads to the decreased degradation rate [35]. It has been reported by Molinari et al. [26] that the increased substrate concentration may cause light scattering, thus reducing the generation of ·OH.

1.2.2.3 Characteristics of UV lamp

Several studies have reported that the wavelength and the intensity of the light source affect the photocatalytic activity [36-38]. However, the influence decreases with an increase in light intensity: the dependence changes from a linear relationship at low light intensity (<20 mW/cm^2) to saturation at high light intensity (>25 mW/cm^2) [35, 39].

1.2.2.4 The components of the solution

The photocatalytic activity is strongly affected by the pH of the solution. The agglomeration of TiO_2 particles was reported under acidic condition [40], thus alkaline solution is preferred for photocatalytic activity. In addition, it is commonly considered that ·OH is easier to be produced in

alkaline solution due to the presence of sufficient hydroxide ions (eq. (3)). However, decreased photocatalytic activity was observed by Molinari et.al. [26], and the possible reason may be the repulsion force between the negatively charged TiO_2 surface and the hydroxide ions. Besides, the photocatalytic activity is also related to the presence of oxygen and inorganic ions (e.g. Cl^-, NO_3^-, CO_3^-, etc.). As an electron scavenger (eq. (4)) and a strong oxidant, oxygen is known to promote photocatalytic reactions [26]. The presence of inorganic species may have positive or negative effects depending on the reaction mechanism [34, 35, 41].

1.2.3 Applications: photocatalytic antimicrobial activity

The use of TiO_2 for the photoinactivation of *Lactobacillus acidophilus*, *Saccharomyces cerevisiae*, and *Escherichia coli* was first reported by Matsunaga et al. in 1985 [42]. Later on many studies showed TiO_2 was an effective catalyst for the inactivation of a great range of microorganisms especially bacteria [43-46] and viruses [43, 47-50] (Table 1.2).

The mechanism of bacterial inactivation by photocatalysis was initially proposed as depleting coenzyme A by dimerization and therefore inhibiting respiration [43, 51]. However, with the development of analysis technology, more evidences show that the lethal action is due to the damage to the membrane of bacterial cells. For example, a rapid leakage of potassium ions (K^+) followed by a slow release of cellular components, such as RNA and protein, were observed from treated *Streptococcus sobrinus* AHT cell by Satio et al. [52]. Later, Sunada et al. [53] reported the destruction of endotoxin indicating that TiO_2 photocatalysts destroy the outer cell membrane of Gram-negative bacteria *E. coli*. It was suggested that the ROS generated on the TiO_2 surface may attack the polyunsaturated phospholipids in the bacterial cell membrane, resulting in breakdown

Table 1.2 Selected representative studies of microbial disinfection by UV/TiO_2

Immobilization	Quantity of catalysts	UV wavelength	Microorganism	Removal efficiency	References
TiO_2 layer	-	300-400 nm	Bacteriophage kNM1149	99.6% after 6h	Belhacova, L., et al. [54]
TiO_2 suspension	1.0 or 2.0 g/L, 50 mL	300-420 nm	*Escherichia coli*	99% after 2h	Cho, M., et al. [55]
TiO_2 suspension	1.0 g/L, 50 mL	<300 nm	*Escherichia coli,* Bacteriophage MS-2	~90% after 2h >99% after 2h	Cho, M., et al. [56]
TiO_2-coated glass	400nm thick	300-400 nm	Bacteriophage T4, *Escherichia coli*	100% after 3h	Ditta, I.B., et al. [57]
TiO_2 suspension	-	100-280 nm	*Escherichia coli* K12 PHL849, *Escherichia coli* K12 PHL1273	~100% after 5h	Guillard, C., et al. [58]
TiO_2 layer	-	254 nm	Coliphage	98~100% after 89-104s	Guimaraes, J.R., et al. [59]
TiO_2 film	100nm thick	300–400 nm	*Lactobacillus casei* phage PL-1	99.9% after 24h	Kashige, N., et al. [60]
TiO_2 layer	-	-	Bacteriophage Qβ	>99% after 1h	Lee, S., et al. [61]

of cell membrane and the further damage of the cytoplasmic membrane and intracellular components [53, 62]. The cytoplasmic membrane contains the necessary enzymes which are closely associated with the synthesis, assembly, and transport functions of viable cells. Therefore, any disruption to the cell membrane will threaten to cell survival [63]. In addition, DNA damage was reported in many studies when microorganisms are subjected to treatment by TiO_2 photocatalysis [64-69]. Although DNA damage was considered as an event that follows destruction of cell membrane, it is still responsible for the cell death. Moreover, following the cell death, complete mineralization of bacteria in water has also been reported [70-72].

It is well known that ROS generated on the TiO_2 surface is responsible for the microorganism inactivation [62]. Nevertheless, ·OH among all types of ROS is proposed as the most important component [55, 56, 73-76]. For example, Ogino et al. [77] and Takashima et al. [78] showed that the inactivation of bacteria *E. coli* in closely correlated with the concentration of ·OH. Another study by Cho et al. [76] also indicated that ·OH to be a major contributor to the inactivation of *Cryptosporidium parvum*. However, it is noteworthy that photocatalytic inactivation of microorganism is very complex and may vary from case to case. Thus the contribution of other ROS, such as H_2O_2 and $O_2^{\cdot-}$ to the overall performance should not be neglected.

1.3 Photocatalytic membrane reactors (PMRs): configurations and applications

Since its first industrial application in 1950s, membrane filtration has been considered as a highly automated, operationally simple and efficient technology [79]. With the increasing attention on microorganisms in water and the higher removal requirement from regulatory agencies, membrane filtration is widely applied in water industry. However, several challenges still limit its practical application: a) membrane fouling b) trade-off between the permeability and selectivity c) lack of

degradation capacity. Therefore, additional processes for membrane cleaning and concentrate treatment are required. Photocatalyzed oxidation, as an effective chemical process, was first used to degrade cyanide in water [80]; since then its application in water purification has been extensively studied [28, 81-85] and a number of studies have verified its applicability to water disinfection [47, 86-91].

Photocatalytic membranes combine photocatalysis with membrane separation. The hybrid technology is a potential alternative that may overcome the obstacles associated with conventional membrane filtration and photocatalytic oxidation. In addition to size exclusion, photocatalytic membranes reactively degrade organic pollutants [92-95], disinfect water [96-101], and may possess self-cleaning properties with respect to common membrane foulants [102-106].

Typically, “photocatalytic membrane reactors” (PMRs) refers to the hybridization of photocatalysis with membrane process. Compared to the conventional photoreactors, PMRs have many advantages: 1) membrane serves as a barrier to retain the catalysts; 2) PMR enables the control of the residence time of the pollutants in the reactor; 3) PMR enables simultaneous photocatalysis and product separation; 4) PMR avoids the additional treatment processes used for the separation of catalysts, lowering the consumption of energy.

1.3.1 PMRs configurations

According to the state of the catalysts, PMRs can be simply divided into two groups: 1) reactors with suspended catalysts 2) reactors with catalysts immobilized in/on the membrane. In the first case, the active surface is large and the system has been found to be more efficient [107-110].

However, the recovery of the catalysts and the membrane fouling may be the problems [111]. In contrast, the separation of catalysts is easier in the immobilized system, but the fixation of catalysts results in the limited mass transfer and a potential loss of available active surface [112].

1.3.1.1 PMRs with suspended catalysts

Most studies describe PMRs that utilize as the driving force for separation; the corresponding membrane processes include microfiltration (MF) [113-117], ultrafiltration (UF) [109, 118-121] and nanofiltration (NF) [122-125]. The use of reverse osmosis (RO) [126, 127] is rare, because usually RO is not applied for the feed water containing suspended solids. However, photocatalysis combined with RO for water treatment were still investigated in some studies. For example, Lehr et al. [126] observed less membrane fouling by applying RO with suspended catalysts. Additionally, Tay et al. [127] reported that no fouling occurred using photocatalytic RO membrane for the pretreatment of water containing humic acid.

Since the catalyst is suspended and not attached to the membrane, the location of the light source is more flexible than that in PMRs with immobilized catalyst. The most commonly used configurations are: 1) light irradiation above the feed tank 2) light irradiation above the membrane module 3) light irradiation above the additional reservoir located between feed tank and the membrane module. To choose the configuration in terms of the light source, many factors (e.g. properties of feed solution, treatment target, cost of installation, etc.) need to be considered. Besides the position of light source, other parameters that affect the performance of PMRs with suspended catalysts are: driving force, characteristics of the membrane module (e.g. type of membrane, hydraulic properties in the membrane module), operational mode (e.g. pressurized or

depressurized), composition of feed solution, efficacy of photocatalytic degradation (impact factors are discussed in section 1.2.1), etc. [109, 111, 113-119, 121-123, 128].

1.3.1.2 PMRs with immobilized catalysts

In the PMRs with immobilized catalysts, the membrane has a dual function: a support for the photocatalysts and a barrier for the target compounds. Depending on the different membrane structures, the photocatalytic activity may occur on the membrane surface or within the membrane pores. Therefore, in the PMRs with immobilized catalysts, membrane itself is the only component that needs to be irradiated.

There are various methods of fabricating photocatalytic membranes. Membranes may be coated with catalyst material or membrane material itself can be catalytic. A variety of materials, including inorganic, organic and metallic, have been investigated as the support where the catalysts can be deposited or imbedded. In particular, for TiO_2 catalysts, polymer and ceramic membranes are the most often used supports [99, 129-131]. Taking ceramic membranes as an example, two asymmetric configurations are widely used. In the first case (Fig. 1.1a), the photocatalytic layer is on the same side with the membrane separation layer. The major advantage of this configuration is that the organic contaminants can be decomposed, therefore, the membrane fouling can be relieved. However, since the light source is on the feed side, low turbidity of the feed solution is necessary to maintain the sufficient irradiation. In the second case (Fig. 1.1b), the photocatalytic layer is separate from the separation layer. Although membrane fouling and the production of concentrated stream are observed in this configuration, this configuration can be used for the turbid water treatment. Also, any organic contaminants transported through the membrane may be decomposed

by the ROS in the permeate; thus this type of photocatalytic membrane can be applied to purify turbid water.

Some photocatalytic membranes are made of the pure photocatalyst materials. One classical example is the development of TiO_2 nanofibers, nanowire or nanotubes [98, 100, 132, 133]. Zhang et al. [134] reported that photocatalytic TiO_2 nanowire is more effective in mitigating membrane fouling. Moreover, an increased permeate flux was observed with the UV irradiation enhanced by TiO_2 nanotubes [135].

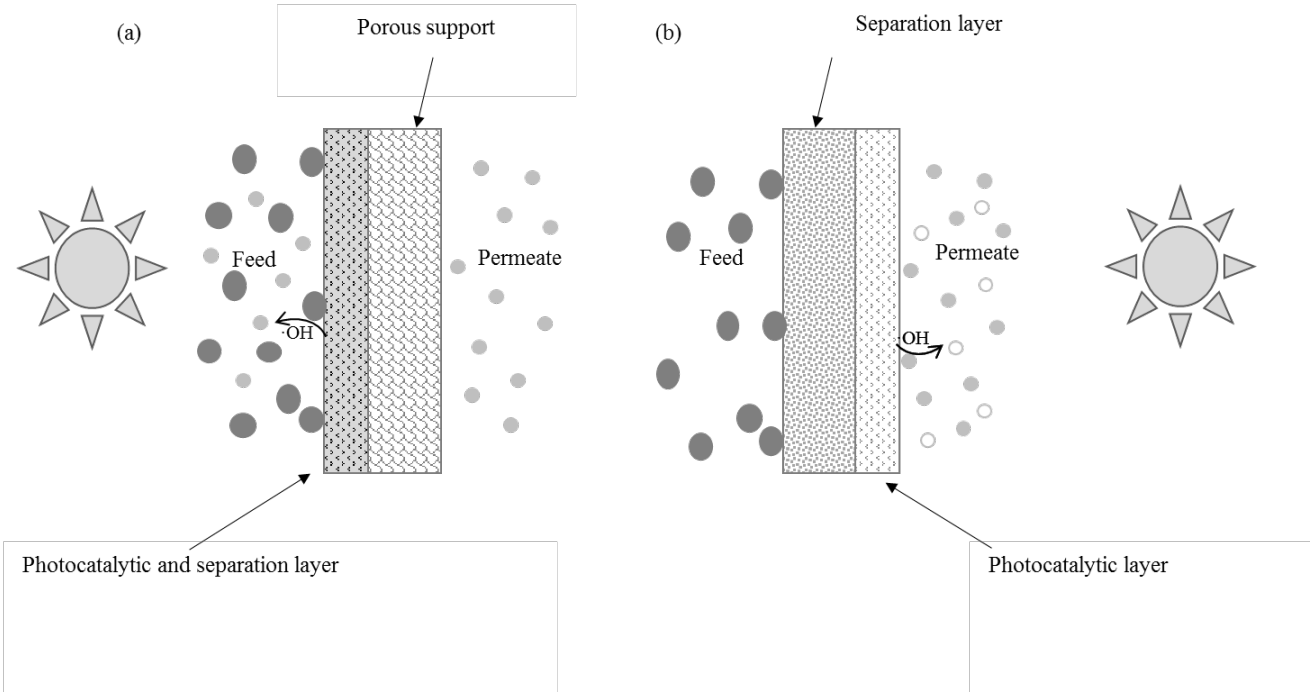

Figure 1.1 Two types of configurations of photocatalytic ceramic membranes

1.3.2 Applications of PMRs in water treatment

1.3.2.1 Application of PMRs for chemical removal

Numerous studies have shown that the PMR is a promising technology for water treatment and has been widely applied for removal of various chemical pollutants including pharmaceuticals [117, 123, 124, 136], humic acid [119, 128, 134, 135, 137], dyes [97, 100, 113, 118, 125, 129, 131, 138], bisphenol A [115, 116], 2,4-dichlorophenol [139], phenol [140], etc. Mutiple studies have shown that the removal efficiency of organic pollutants is higher than 90%. For example, Zhang et al. [134] found that the TiO_2 nanowires could remove 100% humic acid and 93.6% total organic carbon (TOC) in a continuous operation mode. The same in the continuous flow reactor, Romanos et al. [141] indicated that 90% methyl orange (MO) was removed by TiO_2/Al_2O_3 membrane in 10 hours. In another study, 95%-100% removal of MO was reported [142] by using TiO_2-Al_2O_3-ZrO_2 nanofiber membrane. More than 99% removal of Reactive Black 5 in 60 min was obtained by Damodar et al. [102].

1.3.2.2 Application of PMRs for water disinfection

The application of PMRs to water disinfection is very limited. Some studies showed that the photocatalytic membranes, such as TiO_2 film [97], TiO_2 deposited thin-film-composite [130], TiO_2 entrapped PVDF membrane [102], silver decorated carbon nanofibers [143], have antibacterial properties. In these studies the physical (e.g. permeability) and chemical (e.g. photocatalytic disinfection) properties were quantified in the separation tests. For example, Kim et al. [130] reported less flux decline and higher salt rejection with UV irradiated photocatalytic membrane using deionized water (DI) with the addition of sodium chloride, while a complete disinfection of

Escherichia coli (*E. coli*) was observed by pipetting *E. coli* cell dilution onto the membranes and illuminated by a UV lamp for up to 4 hours.

To the best of our knowledge, there have been only five reports on the concurrent filtration and photocatalytic disinfection of microorganism [98, 100, 144-146]. In four of these studies [98-100, 144], gram-negative bacterium *E. coli* was used as the model pathogen, and three of the four also used silver as a component of the photocatalytic membranes. Only one study of the five investigated the photocatalytic disinfection of viruses. Although bacteriophage f2, a single-stranded RNA virus, is used as a representative in this study, the system configuration in this case is a PMR with suspended catalysts which is quite different from the previous four studies which have immobilized catalysts. Therefore, the application of PMRs with immobilized catalysts for water disinfection needs to be explored.

1.4 Dissertation overview

The objective of this study is to develop an effective PMR for water disinfection and to understand the mechanisms and impacts of water quality on the photocatalytic inactivation of virus in the PMR. In chapter 2, we report on the design of a hybrid photocatalytic UV-membrane filtration system and its application to the treatment of DI water seeded with a bacteriophage. To our knowledge, this work is the first application of a PMR with immobilized catalysts to virus disinfection. The efficacy of the hybrid process is compared with other three processes: microfiltration only, UV disinfection only, and non-photocatalytic UV-membrane process. Batch disinfection tests are also conducted to understand the mechanisms of virus inactivation. In chapter 3, a UV-resistant human virus and several more complex water matrices are used to explore the

efficiency of the hybrid photocatalytic UV-membrane filtration system. Since the introduction of complex water matrix, not only the mechanism of virus inactivation but also the effect of water quality on virus inactivation is evaluated as well.

REFERENCES

REFERENCES

[1] WHO and UNICEF: Progress on drinking water and sanitation, Hydrologie Und Wasserbewirtschaftung, 58 (2014) 244-245.

[2] W.H. Organization, F. United Nations Children's, Global water supply and sanitation assessment 2000 report, Global water supply and sanitation assessment 2000 report, (2000) vii + 80 pp.-vii + 80 pp.

[3] S.D. Richardson, M.J. Plewa, E.D. Wagner, R. Schoeny, D.M. DeMarini, Occurrence, genotoxicity, and carcinogenicity of regulated and emerging disinfection by-products in drinking water: A review and roadmap for research, Mutation Research-Reviews in Mutation Research, 636 (2007) 178-242.

[4] H. Yang, H. Cheng, Controlling nitrite level in drinking water by chlorination and chloramination, Separation and Purification Technology, 56 (2007) 392-396.

[5] AWWA, J. Edzwald, Water Quality & Treatment: A Handbook on Drinking Water, 4th Edition ed., New York1990.

[6] S. Regli, Disinfection requirements to control for microbial contamination Regulating Drinking Water Quality Charles E. Gilbert and Edward J. Calabrese1992.

[7] R. Andreozzi, V. Caprio, A. Insola, R. Marotta, Advanced oxidation processes (AOP) for water purification and recovery, Catalysis Today, 53 (1999) 51-59.

[8] R. Munter, Advanced oxidation processes–current status and prospects, Proc. Estonian Acad. Sci. Chem, 50 (2001) 59-80.

[9] J. Prado, S. Esplugas, Comparison of different advanced oxidation processes involving ozone to eliminate atrazine, Ozone-Science & Engineering, 21 (1999) 39-52.

[10] W.H. Glaze, J.-W. Kang, D.H. Chapin, The Chemistry of Water Treatment Processes Involving Ozone, Hydrogen Peroxide and Ultraviolet Radiation, Ozone: Science & Engineering, 9 (1987) 335-352.

[11] D. Ljubas, Solar photocatalysis - a possible step in drinking water treatment, Energy, 30 (2005) 1699-1710.

[12] A. Markowska-Szczupak, K.L. Wang, P. Rokicka, M. Endo, Z.S. Wei, B. Ohtani, A.W. Morawski, E. Kowalska, The effect of anatase and rutile crystallites isolated from titania P25 photocatalyst on growth of selected mould fungi, Journal of Photochemistry and Photobiology B-Biology, 151 (2015) 54-62.

[13] V. Siyahi, A. Habibi-Yangjeh, S. Latifi-Navid, A. Asadi, Microwave-assisted one-pot preparation of AgBr/ZnO nanocomposites as highly efficient visible-light photocatalyst for inactivation of Escherichia coli, Materials Express, 5 (2015) 201-210.

[14] Z. Miao, S. Tao, Y. Wang, Y. Yu, C. Meng, Y. An, Hierarchically porous silica as an efficient catalyst carrier for high performance vis-light assisted Fenton degradation, Microporous and Mesoporous Materials, 176 (2013) 178-185.

[15] X. Gao, X. Su, C. Yang, F. Xiao, J. Wang, X. Cao, S. Wang, L. Zhang, Hydrothermal synthesis of WO_3 nanoplates as highly sensitive cyclohexene sensor and high-efficiency MB photocatalyst, Sensors and Actuators B-Chemical, 181 (2013) 537-543.

[16] Y. Huo, Z. Xie, X. Wang, H. Li, H. Manh, R.A. Caruso, Methyl orange removal by combined visible-light photocatalysis and membrane distillation, Dyes and Pigments, 98 (2013) 106-112.

[17] J. Wang, Y. Yu, L. Zhang, Highly efficient photocatalytic removal of sodium pentachlorophenate with Bi3O4Br under visible light, Applied Catalysis B-Environmental, 136 (2013) 112-121.

[18] V.K. Gupta, D. Pathaniac, S. Agarwal, P. Singh, Adsorptional photocatalytic degradation of methylene blue onto pectin-CuS nanocomposite under solar light, Journal of Hazardous Materials, 243 (2012) 179-186.

[19] R. Daghrir, P. Drogui, D. Robert, Modified TiO_2 for environmental photocatalytic applications: A review, Industrial and Engineering Chemistry Research, 52 (2013) 3581-3599.

[20] K. Rajeshwar, Photoelectrochemistry and the environment, Journal of Applied Electrochemistry, 25 (1995) 1067-1082.

[21] U. Diebold, Structure and properties of TiO2 surfaces: a brief review, Applied Physics a-Materials Science & Processing, 76 (2003) 681-687.

[22] X.S. Ye, J. Sha, Z.K. Jiao, Z.F. Peng, L.D. Zhang, Structural phase transition in nanostructured TiO2, Journal of Materials Science & Technology, 13 (1997) 359-360.

[23] B. Ohtani, Y. Ogawa, S. Nishimoto, Photocatalytic activity of amorphous-anatase mixture of titanium(IV) oxide particles suspended in aqueous solutions, Journal of Physical Chemistry B, 101 (1997) 3746-3752.

[24] W.Q. Fang, X.-Q. Gong, H.G. Yang, On the Unusual Properties of Anatase TiO2 Exposed by Highly Reactive Facets, Journal of Physical Chemistry Letters, 2 (2011) 725-734.

[25] T. Miyagi, M. Kamei, T. Mitsuhashi, T. Ishigaki, A. Yamazaki, Charge separation at the rutile/anatase interface: a dominant factor of photocatalytic activity, Chemical Physics Letters, 390 (2004) 399-402.

[26] R. Molinari, A. Caruso, L. Palmisano, 3.07 - Photocatalytic Processes in Membrane Reactors, in: L. Giorno (Ed.) Comprehensive Membrane Science and Engineering, Elsevier, Oxford, 2010, pp. 165-193.

[27] R. Leary, A. Westwood, Carbonaceous nanomaterials for the enhancement of TiO2 photocatalysis, Carbon, 49 (2011) 741-772.

[28] M.N. Chong, B. Jin, C.W.K. Chow, C. Saint, Recent developments in photocatalytic water treatment technology: A review, Water Research, 44 (2010) 2997-3027.

[29] M.R. Hoffmann, S.T. Martin, W.Y. Choi, D.W. Bahnemann, Environmental applications of semiconductor photocatalysis, Chemical Reviews, 95 (1995) 69-96.

[30] A.L. Linsebigler, G.Q. Lu, J.T. Yates, Photocatalysis on TiO_2 surfaces: principles, mechanisms, and selected results, Chemical Reviews, 95 (1995) 735-758.

[31] A. Fujishima, K. Honda, Electrochemical photolysis of water at a semiconductor electrode, Nature, 238 (1972) 37-+.

[32] S.P. Kamble, S.B. Sawant, V.G. Pangarkar, Batch and continuous photocatalytic degradation of benzenesulfonic acid using concentrated solar radiation, Industrial & Engineering Chemistry Research, 42 (2003) 6705-6713.

[33] S. Kaneco, M.A. Rahman, T. Suzuki, H. Katsumata, K. Ohta, Optimization of solar photocatalytic degradation conditions of bisphenol A in water using titanium dioxide, Journal of Photochemistry and Photobiology a-Chemistry, 163 (2004) 419-424.

[34] K. Kabra, R. Chaudhary, R.L. Sawhney, Treatment of hazardous organic and inorganic compounds through aqueous-phase photocatalysis: A review, Industrial & Engineering Chemistry Research, 43 (2004) 7683-7696.

[35] I.K. Konstantinou, T.A. Albanis, TiO_2-assisted photocatalytic degradation of azo dyes in aqueous solution: kinetic and mechanistic investigations - A review, Applied Catalysis B-Environmental, 49 (2004) 1-14.

[36] J.M. Herrmann, Heterogeneous photocatalysis: State of the art and present applications, Topics in Catalysis, 34 (2005) 49-65.

[37] A.V. Emeline, V. Ryabchuk, N. Serpone, Factors affecting the efficiency of a photocatalyzed process in aqueous metal-oxide dispersions - Prospect of distinguishing between two kinetic models, Journal of Photochemistry and Photobiology a-Chemistry, 133 (2000) 89-97.

[38] S. Brosillon, L. Lhomme, C. Vallet, A. Bouzaza, D. Wolbert, Gas phase photocatalysis and liquid phase photocatalysis: Interdependence and influence of substrate concentration and photon flow on degradation reaction kinetics, Applied Catalysis B-Environmental, 78 (2008) 232-241.

[39] K. Pirkanniemi, M. Sillanpaa, Heterogeneous water phase catalysis as an environmental application: a review, Chemosphere, 48 (2002) 1047-1060.

[40] Y. Paz, Preferential photodegradation - why and how?, Comptes Rendus Chimie, 9 (2006) 774-787.

[41] V. Brezova, S. Vodny, M. Vesely, M. Ceppan, L. Lapcik, Photocatalytic oxidation of 2-ethoxyethanol in a water suspension of titanium dioxide, Journal of Photochemistry and Photobiology a-Chemistry, 56 (1991) 125-134.

[42] T. Matsunaga, R. Tomoda, T. Nakajima, H. Wake, Photoelectrochemical sterilization of microbial cells by semiconductor powders, Fems Microbiology Letters, 29 (1985) 211-214.

[43] T. Matsunaga, R. Tomoda, T. Nakajima, H. Wake, Photoelectrochemical sterilization of microbial cells by semiconductor powders, Fems Microbiology Letters, 29 (1985) 211-214.

[44] A.T. Cooper, D. Yogi Goswami, S.S. Block, Solar photochemical detoxification and disinfection for water treatment in tropical developing countries, Journal of Advanced Oxidation Technologies, 3 (1998) 151-154.

[45] H.N. Pham, T. McDowell, E. Wilkins, Photocatalytically-mediated disinfection of water using tio2 as a catalyst and spore-forming Bacillus pumilus as a model, Journal of Environmental Science & Health Part A, 30 (1995) 627-636.

[46] D.M. Blake, P.C. Maness, Z. Huang, E.J. Wolfrum, J. Huang, W.A. Jacoby, Application of the photocatalytic chemistry of titanium dioxide to disinfection and the killing of cancer cells, Separation and Purification Methods, 28 (1999) 1-50.

[47] J.C. Sjogren, R.A. Sierka, Inactivation of phage MS2 by iorn-aided titanium-dioxide photocatalysis, Applied and Environmental Microbiology, 60 (1994) 344-347.
[48] R.J. Watts, S.H. Kong, M.P. Orr, G.C. Miller, B.E. Henry, Photocatalytic inactivation of coliform bacteria and viruses in secondary waste-water effluent, Water Research, 29 (1995) 95-100.

[49] D. Gerrity, H. Ryu, J. Crittenden, M. Abbaszadegan, Photocatalytic inactivation of viruses using titanium dioxide nanoparticles and low-pressure UV light, Journal of Environmental Science and Health Part a-Toxic/Hazardous Substances & Environmental Engineering, 43 (2008) 1261-1270.

[50] M. Soekmen, S. Degerli, A. Aslan, Photocatalytic disinfection of Giardia intestinalis and Acanthamoeba castellani cysts in water, Experimental Parasitology, 119 (2008) 44-48.

[51] T. Matsunaga, R. Tomoda, T. Nakajima, N. Nakamura, T. Komine, Continuous-sterilization system that uses photosemiconductor powder, Applied and Environmental Microbiology, 54 (1988) 1330-1333.

[52] T. Saito, T. Iwase, J. Horie, T. Morioka, Mode of photocatalytic bactericidal action of powdered semiconductor TiO_2 on mutans streptococci, Journal of Photochemistry and Photobiology B-Biology, 14 (1992) 369-379.

[53] K. Sunada, T. Watanabe, K. Hashimoto, Studies on photokilling of bacteria on TiO_2, Journal of Photochemistry and Photobiology A: Chemistry, 156 (2003) 227-233.

[54] L. Belhacova, J. Krysa, J. Geryk, J. Jirkovsky, Inactivation of microorganisms in a flow-through photoreactor with an immobilized TiO2 layer, Journal of Chemical Technology and Biotechnology, 74 (1999) 149-154.

[55] M. Cho, H. Chung, W. Choi, J. Yoon, Linear correlation between inactivation of E-coli and OH radical concentration in TiO2 photocatalytic disinfection, Water Research, 38 (2004) 1069-1077.

[56] M. Cho, H.M. Chung, W.Y. Choi, J.Y. Yoon, Different inactivation Behaviors of MS-2 phage and Escherichia coli in TiO2 photocatalytic disinfection, Applied and Environmental Microbiology, 71 (2005) 270-275.

[57] I.B. Ditta, A. Steele, C. Liptrot, J. Tobin, H. Tyler, H.M. Yates, D.W. Sheel, H.A. Foster, Photocatalytic antimicrobial activity of thin surface films of TiO2, CuO and TiO2/CuO dual layers on Escherichia coli and bacteriophage T4, Applied Microbiology and Biotechnology, 79 (2008) 127-133.

[58] C. Guillard, T.H. Bui, C. Felix, V. Moules, B. Lina, P. Lejeune, Microbiological disinfection of water and air by photocatalysis, Comptes Rendus Chimie, 11 (2008) 107-113.

[59] J.R. Guimaraes, A.S. Barretto, Photocatalytic inactivation of Clostridium perfringens and coliphages in water, Brazilian Journal of Chemical Engineering, 20 (2003) 403-411.

[60] N. Kashige, Y. Kakita, Y. Nakashima, F. Miake, K. Watanabe, Mechanism of the photocatalytic inactivation of Lactobacillus casei phage PL-1 by titania thin film, Current Microbiology, 42 (2001) 184-189.

[61] S. Lee, K. Nishida, M. Otaki, S. Ohgaki, Photocatalytic inactivation of phage Qβ by immobilized titanium dioxide mediated photocatalyst, Water Science and Technology, 35 (1997) 101-106.

[62] P.C. Maness, S. Smolinski, D.M. Blake, Z. Huang, E.J. Wolfrum, W.A. Jacoby, Bactericidal activity of photocatalytic TiO_2 reaction: Toward an understanding of its killing mechanism, Applied and Environmental Microbiology, 65 (1999) 4094-4098.

[63] G. Gottschalk, Biosynthesis of *Escherichia coli* Cells from Glucose, Bacterial Metabolism, Springer New York1986, pp. 37-95.

[64] K.S. Yao, D.Y. Wang, J.J. Yan, L.Y. Yang, W.S. Chen, Photocatalytic effects of TiO_2/Fe thin film irradiated with visible light on cellular surface ultrastructure and genomic DNA of bacteria, Surface & Coatings Technology, 201 (2007) 6882-6885.

[65] W.G. Wamer, J.J. Yin, R.R. Wei, Oxidative damage to nucleic acids photosensitized by titanium dioxide, Free Radical Biology and Medicine, 23 (1997) 851-858.

[66] K. Hirakawa, M. Mori, M. Yoshida, S. Oikawa, S. Kawanishi, Photo-irradiated titanium dioxide catalyzes site specific DNA damage via generation of hydrogen peroxide, Free Radical Research, 38 (2004) 439-447.

[67] Y. Wang, X. Yang, Photocatalytic effect on plasmid DNA damage under different UV irradiation time, Indoor Air 2005: Proceedings of the 10th International Conference on Indoor Air Quality and Climate, Vols 1-5, (2005) 2962-2965.

[68] G. Gogniat, S. Dukan, TiO_2 photocatalysis causes DNA damage via Fenton reaction-generated hydroxyl radicals during the recovery period, Applied and Environmental Microbiology, 73 (2007) 7740-7743.

[69] X.-C. Shen, Z.-L. Zhang, B. Zhou, J. Peng, M. Xie, M. Zhang, D.-W. Pang, Visible light-induced plasmid DNA damage catalyzed by a CdSe/ZnS-photosensitized nano-TiO_2 film, Environmental Science & Technology, 42 (2008) 5049-5054.

[70] M. Sokmen, F. Candan, Z. Sumer, Disinfection of E-coli by the Ag-TiO_2/UV system: lipidperoxidation, Journal of Photochemistry and Photobiology a-Chemistry, 143 (2001) 241-244.

[71] Y. Li, M. Ma, X. Wang, X. Wang, Inactivated properties of activated carbon-supported TiO2 nanoparticles for bacteria and kinetic study, Journal of Environmental Sciences-China, 20 (2008) 1527-1533.

[72] V.A. Nadtochenko, O.M. Sarkisov, V.V. Nikandrov, P.A. Chubukov, N.N. Denisov, Inactivation of pathogenic microorganisms in the photocatalytic process on nanosized TiO_2 crystals, Russian Journal of Physical Chemistry B, 2 (2008) 105-114.

[73] J.C. Ireland, P. Klostermann, E.W. Rice, R.M. Clark, Inactivation of Escherichia coli by titanium dioxide photocatalytic oxidation, Applied and Environmental Microbiology, 59 (1993) 1668-1670.

[74] Y. Kikuchi, K. Sunada, T. Iyoda, K. Hashimoto, A. Fujishima, Photocatalytic bactericidal effect of TiO_2 thin films: Dynamic view of the active oxygen species responsible for the effect, Journal of Photochemistry and Photobiology a-Chemistry, 106 (1997) 51-56.

[75] F.M. Salih, Enhancement of solar inactivation of Escherichia coli by titanium dioxide photocatalytic oxidation, Journal of Applied Microbiology, 92 (2002) 920-926.

[76] M. Cho, J. Yoon, Measurement of OH radical CT for inactivating Cryptosporidium parvum using photo/ferrioxalate and photo/TiO_2 systems, Journal of Applied Microbiology, 104 (2008) 759-766.

[77] C. Ogino, M.F. Dadjour, K. Takaki, N. Shimizu, Enhancement of sonocatalytic cell lysis of Escherichia coli in the presence of TiO2, Biochemical Engineering Journal, 32 (2006) 100-105.

[78] H. Takashima, Y. lida, K. Nakamura, Y. Kanno, Microwave Sterilization by TiO_2 Filter Coated with Ag Thin Film, Systems, Man and Cybernetics, 2006. SMC '06. IEEE International Conference on, 2006, pp. 1413-1418.

[79] MWH, Water Treatment: Principles and Design, 2 ed., Wiley2005.

[80] S.N. Frank, A.J. Bard, Heterogeneous photocatalytic oxidation of cyanide ion in aqueous solutions at titanium dioxide powder, Journal of the American Chemical Society, 99 (1977) 303-304.

[81] N. Clarke, G. Knowles, High purity water using hydrogen peroxide and ultraviolet radiation, Effluent & Water Treatment Journal, 22 (1982) 335-&.

[82] K. Tanaka, T. Hisanaga, K. Harada, Efficient photocatalytic degradation of chloral hydrate in aqueous semiconductor suspensions, Journal of Photochemistry and Photobiology a-Chemistry, 48 (1989) 155-159.

[83] S. Guittonneau, J. De Laat, J.P. Duguet, C. Bonnel, M. Doré, Oxidation of Parachloronitrobenzene in Dilute Aqueous Solution by O_3 + UV and H_2O_2 + UV : A Comparative Study, Ozone: Science & Engineering, 12 (1990) 73-94.

[84] F.J. Beltran, M. Gonzalez, J.F. Gonzalez, Industrial wastewater advanced oxidation .1. UV radiation in the presence and absence of hydrogen peroxide, Water Research, 31 (1997) 2405-2414.

[85] G.S. Wang, S.T. Hsieh, C.S. Hong, Destruction of humic acid in water by UV light - Catalyzed oxidation with hydrogen peroxide, Water Research, 34 (2000) 3882-3887.

[86] J.A.H. Melian, J.M.D. Rodriguez, A.V. Suarez, E.T. Rendon, C.V. do Campo, J. Arana, J.P. Pena, The photocatalytic disinfection of urban waste waters, Chemosphere, 41 (2000) 323-327.

[87] M. Otaki, T. Hirata, S. Ohgaki, Aqueous microorganisms inactivation by photocatalytic reaction, Water Science and Technology, 42 (2000) 103-108.

[88] T. Kato, H. Tohma, O. Miki, T. Shibata, M. Tamura, Degradation of Norovirus in Sewage Treatment Water by Photocatalytic Ultraviolet Disinfection, Nippon Steel Technical, 2005, pp. 41-44.

[89] S. Bounty, R.A. Rodriguez, K.G. Linden, Inactivation of adenovirus using low-dose UV/H2O2 advanced oxidation, Water Research, 46 (2012) 6273-6278.

[90] J.E. Lee, G. Ko, Norovirus and MS2 inactivation kinetics of UV-A and UV-B with and without TiO2, Water Research, 47 (2013) 5607-5613.

[91] S.P. Sherchan, S.A. Snyder, C.P. Gerba, I.L. Pepper, Inactivation of MS2 coliphage by UV and hydrogen peroxide: Comparison by cultural and molecular methodologies, Journal of Environmental Science and Health Part a-Toxic/Hazardous Substances & Environmental Engineering, 49 (2014) 397-403.

[92] V.S. Coker, A. Garrity, W.B. Wennekes, H.D.W. Roesink, R.S. Cutting, J.R. Lloyd, Cr(VI) and azo dye removal using a hollow-fibre membrane system functionalized with a biogenic Pd-magnetite catalyst, Environmental Technology, 35 (2014) 1046-1054.

[93] G.E. Romanos, C.P. Athanasekou, V. Likodimos, P. Aloupogiannis, P. Falaras, Hybrid Ultrafiltration/Photocatalytic Membranes for Efficient Water Treatment, Industrial & Engineering Chemistry Research, 52 (2013) 13938-13947.

[94] W. Li, T.T. Li, X.G. Ma, Y.L. Li, L.B. An, Z.M. Zhang, Electrospinning preparation of a H4SiW12O40/polycaprolactam composite nanofibrous membrane and its greatly enhanced photocatalytic activity and mechanism, Rsc Advances, 6 (2016) 12491-12496.

[95] G.L. Wang, S. Chen, H.T. Yu, X. Quan, Integration of membrane filtration and photoelectrocatalysis using a TiO_2/carbon/Al_2O_3 membrane for enhanced water treatment, Journal of Hazardous Materials, 299 (2015) 27-34.

[96] H. Choi, A.C. Sofranko, D.D. Dionysiou, Nanocrystalline TiO2 photocatalytic membranes with a hierarchical mesoporous multilayer structure: Synthesis, characterization, and multifunction, Advanced Functional Materials, 16 (2006) 1067-1074.

[97] H. Choi, E. Stathatos, D.D. Dionysiou, Photocatalytic TiO_2 films and membranes for the development of efficient wastewater treatment and reuse systems, Desalination, 202 (2007) 199-206.

[98] H. Zhang, H. Zhao, P. Liu, S. Zhang, G. Li, Direct growth of hierarchically structured titanate nanotube filtration membrane for removal of waterborne pathogens, Journal of Membrane Science, 343 (2009) 212-218.

[99] N. Ma, X. Fan, X. Quan, Y. Zhang, Ag-TiO_2/HAP/Al_2O_3 bioceramic composite membrane: Fabrication, characterization and bactericidal activity, Journal of Membrane Science, 336 (2009) 109-117.

[100] L. Liu, Z.Y. Liu, H.W. Bai, D.D. Sun, Concurrent filtration and solar photocatalytic disinfection/degradation using high-performance Ag/TiO2 nanofiber membrane, Water Research, 46 (2012) 1101-1112.

[101] R. Goei, T.-T. Lim, Ag-decorated TiO_2 photocatalytic membrane with hierarchical architecture: Photocatalytic and anti-bacterial activities, Water Research, 59 (2014) 207-218.

[102] R.A. Damodar, S.-J. You, H.-H. Chou, Study the self cleaning, antibacterial and photocatalytic properties of TiO_2 entrapped PVDF membranes, Journal of Hazardous Materials, 172 (2009) 1321-1328.

[103] S.S. Madaeni, N. Ghaemi, Characterization of self-cleaning RO membranes coated with TiO_2 particles under UV irradiation, Journal of Membrane Science, 303 (2007) 221-233.

[104] H. Yamashita, H. Nakao, M. Takeuchi, Y. Nakatani, M. Anpo, Coating of TiO_2 photocatalysts on super-hydrophobic porous teflon membrane by an ion assisted deposition method and their self-cleaning performance, Nuclear Instruments & Methods in Physics Research Section B-Beam Interactions with Materials and Atoms, 206 (2003) 898-901.

[105] K. Feng, L. Hou, B.B. Tang, P.Y. Wu, A self-protected self-cleaning ultrafiltration membrane by using polydopamine as a free-radical scavenger, Journal of Membrane Science, 490 (2015) 120-128.

[106] C. Xu, Y. Xu, J. Zhu, Photocatalytic Antifouling Graphene Oxide-Mediated Hierarchical Filtration Membranes with Potential Applications on Water Purification, Acs Applied Materials & Interfaces, 6 (2014) 16117-16123.

[107] V. Augugliaro, M. Litter, L. Palmisano, J. Soria, The combination of heterogeneous photocatalysis with chemical and physical operations: A tool for improving the photoprocess performance, Journal of Photochemistry and Photobiology C-Photochemistry Reviews, 7 (2006) 127-144.

[108] M.F.J. Dijkstra, H. Buwalda, A.W.F. de Jong, A. Michorius, J.G.M. Winkelman, A. Beenackers, Experimental comparison of three reactor designs for photocatalytic water purification, Chemical Engineering Science, 56 (2001) 547-555.

[109] R. Molinari, L. Palmisano, E. Drioli, M. Schiavello, Studies on various reactor configurations for coupling photocatalysis and membrane processes in water purification, Journal of Membrane Science, 206 (2002) 399-415.

[110] G. Mascolo, R. Comparelli, M.L. Curri, G. Lovecchio, A. Lopez, A. Agostiano, Photocatalytic degradation of methyl red by TiO_2: Comparison of the efficiency of immobilized nanoparticles versus conventional suspended catalyst, Journal of Hazardous Materials, 142 (2007) 130-137.

[111] S. Mozia, A.W. Morawski, Hybridization of photocatalysis and membrane distillation for purification of wastewater, Catalysis Today, 118 (2006) 181-188.

[112] S.U. Geissen, W. Xi, A. Weidemeyer, A. Vogelpohl, L. Bousselmi, A. Ghrabi, A. Ennabll, Comparison of suspended and fixed photocatalytic reactor systems, Water Science and Technology, 44 (2001) 245-249.

[113] J. Ryu, W. Choi, K.H. Choo, A pilot-scale photocatalyst-membrane hybrid reactor: performance and characterization, Water Science and Technology, 51 (2005) 491-497.

[114] J.F. Fu, M. Ji, Z. Wang, L.N. Jin, D.N. An, A new submerged membrane photocatalysis reactor (SMPR) for fulvic acid removal using a nano-structured photocatalyst, Journal of Hazardous Materials, 131 (2006) 238-242.

[115] S.S. Chin, T.M. Lim, K. Chiang, A.G. Fane, Hybrid low-pressure submerged membrane photoreactor for the removal of bisphenol A, Desalination, 202 (2007) 253-261.

[116] R. Thiruvenkatachari, T.O. Kwon, I.S. Moon, Application of slurry type photocatalytic oxidation-submerged hollow fiber microfiltration hybrid system for the degradation of bisphenol A (BPA), Separation Science and Technology, 40 (2005) 2871-2888.

[117] T.E. Doll, F.H. Frimmel, Cross-flow microfiltration with periodical back-washing for photocatalytic degradation of pharmaceutical and diagnostic residues-evaluation of the long-term stability of the photocatalytic activity of TiO_2, Water Research, 39 (2005) 847-854.

[118] K. Sopajaree, S.A. Qasim, S. Basak, K. Rajeshwar, An integrated flow reactor-membrane filtration system for heterogeneous photocatalysis. Part I: Experiments and modelling of a batch-recirculated photoreactor, Journal of Applied Electrochemistry, 29 (1999) 533-539.

[119] S.A. Tsarenko, V.M. Kochkodan, A.O. Samsoni-Todorov, V.V. Goncharuk, Removal of humic substances from aqueous solutions with a photocatalytic membrane reactor, Colloid Journal, 68 (2006) 341-344.

[120] D. Sun, T.T. Meng, T.H. Loong, T.J. Hwa, Removal of natural organic matter from water using a nano-structured photocatalyst coupled with filtration membrane, Water Science and Technology, 49 (2004) 103-110.

[121] S.A. Lee, K.H. Choo, C.H. Lee, H.I. Lee, T. Hyeon, W. Choi, H.H. Kwon, Use of ultrafiltration membranes for the separation of TiO_2 photocatalysts in drinking water treatment, Industrial & Engineering Chemistry Research, 40 (2001) 1712-1719.

[122] R. Molinari, M. Borgese, E. Drioli, L. Palmisano, M. Schiavello, Hybrid processes coupling photocatalysis and membranes for degradation of organic pollutants in water, Catalysis Today, 75 (2002) 77-85.

[123] R. Molinari, F. Pirillo, V. Loddo, L. Palmisano, Heterogeneous photocatalytic degradation of pharmaceuticals in water by using polycrystalline TiO_2 and a nanofiltration membrane reactor, Catalysis Today, 118 (2006) 205-213.

[124] V. Augugliaro, E. Garcia-Lopez, V. Loddo, S. Malato-Rodriguez, I. Maldonado, G. Marci, R. Molinari, L. Palmisano, Degradation of lincomycin in aqueous medium: Coupling of solar photocatalysis and membrane separation, Solar Energy, 79 (2005) 402-408.

[125] R. Molinari, F. Pirillo, M. Falco, V. Loddo, L. Palmisano, Photocatalytic degradation of dyes by using a membrane reactor, Chemical Engineering and Processing, 43 (2004) 1103-1114.

[126] J.H. Lehr, J. Keeley, Water encyclopedia: domestic, municipal, and industrial water supply and waste disposal, Water encyclopedia: domestic, municipal, and industrial water supply and waste disposal, (2005) xvi + 952 pp.-xvi + 952 pp.

[127] J.H. Tay, D. Chen, D.D. Sun, Removal of color substances using photocatalytic oxidation for membrane filtration processes, Water Science and Technology, 43 (2001) 319-325.

[128] P. Le-Clech, E.K. Lee, V. Chen, Hybrid photocatalysis/membrane treatment for surface waters containing low concentrations of natural organic matters, Water Research, 40 (2006) 323-330.

[129] H. Zhang, X. Quan, S. Chen, H. Zhao, Y. Zhao, Fabrication of photocatalytic membrane and evaluation its efficiency in removal of organic pollutants from water, Separation and Purification Technology, 50 (2006) 147-155.

[130] S.H. Kim, S.Y. Kwak, B.H. Sohn, T.H. Park, Design of TiO_2 nanoparticle self-assembled aromatic polyamide thin-film-composite (TFC) membrane as an approach to solve biofouling problem, Journal of Membrane Science, 211 (2003) 157-165.

[131] S.-J. You, G.U. Semblante, S.-C. Lu, R.A. Damodar, T.-C. Wei, Evaluation of the antifouling and photocatalytic properties of poly(vinylidene fluoride) plasma-grafted poly(acrylic acid) membrane with self-assembled TiO_2, Journal of Hazardous Materials, 237 (2012) 10-19.

[132] X.W. Zhang, D.K. Wang, D.R.S. Lopez, J.C.D. da Costa, Fabrication of nanostructured TiO2 hollow fiber photocatalytic membrane and application for wastewater treatment, Chemical Engineering Journal, 236 (2014) 314-322.

[133] M.J. Liu, L. He, X.N. Liu, C.B. Liu, S.L. Luo, Reduced graphene oxide and CdTe nanoparticles co-decorated TiO2 nanotube array as a visible light photocatalyst, Journal of Materials Science, 49 (2014) 2263-2269.

[134] X. Zhang, A.J. Du, P. Lee, D.D. Sun, J.O. Leckie, TiO_2 nanowire membrane for concurrent filtration and photocatalytic oxidation of humic acid in water, Journal of Membrane Science, 313 (2008) 44-51.

[135] X. Zhang, A.J. Du, P. Lee, D.D. Sun, J.O. Leckie, Grafted multifunctional titanium dioxide nanotube membrane: Separation and photodegradation of aquatic pollutant, Applied Catalysis B-Environmental, 84 (2008) 262-267.

[136] M.J. Benotti, B.D. Stanford, E.C. Wert, S.A. Snyder, Evaluation of a photocatalytic reactor membrane pilot system for the removal of pharmaceuticals and endocrine disrupting compounds from water, Water Research, 43 (2009) 1513-1522.

[137] Y.-F. Lin, K.-L. Tung, Y.-S. Tzeng, J.-H. Chen, K.-S. Chang, Rapid atmospheric plasma spray coating preparation and photocatalytic activity of macroporous titania nanocrystalline membranes, Journal of Membrane Science, 389 (2012) 83-90.

[138] H. Choi, E. Stathatos, D.D. Dionysiou, Sol-gel preparation of mesoporous photocatalytic TiO2 films and TiO2/Al2O3 composite membranes for environmental applications, Applied Catalysis B-Environmental, 63 (2006) 60-67.

[139] L. Liu, F. Chen, F. Yang, Stable photocatalytic activity of immobilized Fe-0/TiO_2/ACF on composite membrane in degradation of 2,4-dichlorophenol, Separation and Purification Technology, 70 (2009) 173-178.

[140] F. Rota, M. Cavassi, D. Niego, R. Gorlani, L. Vianelli, L. Tatti, P. Bruzzi, A. Moroni, I.R. Bellobono, M. Bianchi, H. Muntau, Mathematical modelling of photomineralization of phenols in aqueous solution, by photocatalytic membranes immobilizing titanium dioxide, Chemosphere, 33 (1996) 2159-2173.

[141] G.E. Romanos, C.P. Athanasekou, F.K. Katsaros, N.K. Kanellopoulos, D.D. Dionysiou, V. Likodimos, P. Falaras, Double-side active TiO_2-modified nanofiltration membranes in continuous flow photocatalytic reactors for effective water purification, Journal of Hazardous Materials, 211 (2012) 304-316.

[142] H.-J. Hong, S.K. Sarkar, B.-T. Lee, Formation of TiO_2 nano fibers on a micro-channeled Al_2O_3-ZrO_2/TiO_2 porous composite membrane for photocatalytic filtration, Journal of the European Ceramic Society, 32 (2012) 657-663.

[143] A.A. Taha, Direct synthesis of mesostructured carbon nanofibers decorated with silver-nanoparticles as a multifunctional membrane for water treatment, Advances in Natural Sciences-Nanoscience and Nanotechnology, 6 (2015).

[144] R. Goei, T.-T. Lim, Ag-decorated TiO2 photocatalytic membrane with hierarchical architecture: Photocatalytic and antibacterial activities, Water Res., 59 (2014) 207-218.

[145] N. Ma, X. Fan, X. Quan, Y. Zhang, Ag–TiO2/HAP/Al2O3 bioceramic composite membrane: Fabrication, characterization and bactericidal activity, J. Membr. Sci., 336 (2009) 109-117.

[146] X. Zheng, Q. Wang, L. Chen, J. Wang, R. Cheng, Photocatalytic membrane reactor (PMR) for virus removal in water: Performance and mechanisms, Chemical Engineering Journal, 277 (2015) 124-129.

CHAPTER 2. VIRUS REMOVAL AND INACTIVATION IN A HYBRID MICROFILTRATION-UV PROCESS WITH A PHOTOCATALYTIC MEMBRANE

2.1 Introduction

Photocatalytic membrane reactors (PMRs) combine membrane separation and photocatalysis in one hybrid process [1, 2]. PMR is a highly versatile technology due to the range of engineering designs it affords and the realm of possible applications. Water treatment is a salient example of such application area. Since 1985 when Matsunaga et al. [3] used Pt-loaded TiO_2 for catalytic inactivation of three types of bacteria, applications of photocatalysis to water disinfection have been growing [4]. Indeed, there is a large body of literature on the use of photocatalysis for inactivating microorganisms in water [5, 6]. Notably, photocatalytic treatment can be highly effective with respect to viruses (e.g. [7-10]). Most of the PMR-based water treatment work, however, has focused on chemical pollutants. To our knowledge, there have been only five reports on the application of photocatalytic membranes to water disinfection [11-15]. All five studies were on *E. Coli* control and three of the five [13-15] also used silver, a known bactericide, as a component of photocatalytic membranes. Several studies (e.g. [16]) also explored how an added photocatalytic function can help improve membrane's resistance to biofouling.

Various PMRs have been implemented that employ different types of light sources and membranes. UV lamps have been the most common choice of the source of photons although new visible light catalyst materials make using visible light possible [17]. Because of the ability to support oxidation reaction, ceramic membranes have been used much more commonly than their polymeric and nanocomposite counterparts [18]. Many different photocatalytic materials have been explored as well, with TiO_2 being by far the most studied and applied photocatalyst [17, 19].

PMRs can be categorized into two major groups: a) PMRs with the catalyst materials suspended in the bulk of the feed solution and b) reactors where the catalyst is immobilized on the membrane surface. In the latter case, typically it is the feed surface of the membrane that supports the catalyst. By illuminating such surface with UV light, photocatalysis occurs in the immediate vicinity of the separation layer bringing about potential additional advantages of fouling control and retentate disinfection. This PMR configuration, however, couples separation and catalytic properties of the membrane making their optimization more challenging.

An alternative configuration is when it is the membrane support layer (i.e. permeate side of the membrane) that is photocatalytic. To our knowledge, the only study that explored such configuration is the work by Bosc et al. [20]. One major benefits of such approach is the possibility of an independent control of the separation and photocatalytic functions. Another benefit is an extension of the first: by regulating what materials are retained by the membrane, one can control the make-up of the permeate solution to improve the photocatalytic function. For example, catalyst poisons or particulates capable of shielding UV light may be removed at the feed-membrane interface to make photocatalysis on the permeate side more efficient. The choice of PMRs configuration has implications for the design of the catalytic layer. Because most practicable membranes are asymmetric, the feed and permeate faces of membranes have dramatically different morphologies. The membrane “skin” (i.e. the feed side) has much smaller pores and typically a much smoother surface than the permeate side. This implies that different coating strategies might be needed to form photocatalytic layers on these supports.

The goal of this work is to extend the PMR design concept proposed by Bosc et al. [20] to tubular

membranes and to apply such PMR to photocatalytic disinfection of viruses. We employ P22 bacteriophage as a model virus and compare the performance of the proposed PMR against that of its constituent processes – UV disinfection and microfiltration. To our knowledge, this is the first application of photocatalytic membranes to virus removal or inactivation.

2.2 Experimental

2.2.1 Reagents

Aeroxide TiO_2 P25 powder was provided by Evonik Industries. Lysozyme (from chicken egg white), ethylenediaminetetraacetic acid (EDTA) and phosphoric acid were purchased from Sigma-Aldrich. Trypticase soy broth (TSB), trypticase soy agar (TSA) and Bacto agar were purchased from Becton, Dickinson and Co. Glycerol and sodium hydroxide were obtained from Avantor Performance Materials. KI/KIO_3 solution was a mixture of 0.6 M potassium iodide (Jade Scientific) and 0.1 M iodate (EM Industries) in 0.01 M borate buffer (Sigma-Aldrich). Ultrapure water (~ 17 MΩ/cm) was produced by a Barnstead E-pure water purification system (Thermo Fisher Scientific). The bacteriophage was propagated by inoculating 25 mL trypticase soy broth with Salmonella enterica serovar Typhimurium LT2 and allowing for growth at 37°C.

2.2.2 Bacteriophage propagation and preparation of feed suspension

To evaluate virus removal and inactivation efficiency of the hybrid photocatalytic UV-MF process, bacteriophage P22 was used as a model virus. P22 is a dsDNA virus [21-25] that has been used as a surrogate for human viruses to study their attenuation [25] and their fate in sewage [26]. The bacteriophage was propagated by inoculating 25 mL trypticase soy broth with Salmonella enterica serovar Typhimurium LT2 and allowing for growth at 37 °C. After overnight incubation, 0.1 mL of lysozyme (50 mg/mL) and 0.75 mL of 0.5 M EDTA were added to lyse host bacterial cells. The culture was then centrifuged at 4000 rpm for 10 min and the supernatant was filtered through a 0.45 μm sterile syringe filter unit (EMD Millipore). The resulting P22 stock suspension had P22 concentration of $5 \cdot 10^9$ PFU/mL and was maintained at 4 °C. The P22 bacteriophage feed

suspension used in all disinfection and filtration experiments was prepared by diluting 300 µL of P22 stock in 3 L of ultrapure water and thus had P22 concentration of ~ $5 \cdot 10^5$ PFU/mL.

2.2.3 Membranes and deposition of photocatalytic coating on their surface

Membranes used in all tests were TiO_2 tubular ceramic microfilters (TAMI Industries) with a nominal pore size of 0.8 µm, 25 cm in length, outer diameter of 1 cm and the inner diameter of 0.6 cm. The permeate side of the membrane was coated with commercial Aeroxide TiO_2 P25 powder (50 ± 15 m^2/g, 78-85% anatase and 14-17% rutile [27], mean particle size of 21 nm) by dip-coating the membrane with a 10 wt% TiO_2 solution prepared following the procedure described by Wang et al. [28]. Prior to its use in the dip-coating procedure, the TiO_2 suspension was stirred and sonicated for 24 h. The tubular ceramic membrane with both ends sealed by Parafilm (to avoid coating the internals walls of the membrane channel) was vertically dipped into the TiO_2 suspension, maintained submerged for 30 s, and then withdrawn at a constant speed of 4.7 cm/min. The dip-coating instrument was constructed in-house using a syringe pump (55-2219, Harvard apparatus). The entire procedure included 10 coating cycles with 5 min drying at 80°C after the deposition of each coat. After the tenth coating cycle, the membrane was dried at 80°C for 24 h, and then calcined in a furnace (RHF 15/3, Carbolite Ltd). The furnace temperature was programmed to increase to 500 °C with a ramp rate of 4.0 °C/min, stay constant for 45 min, and finally decrease to the room temperature at a rate of 4.0 °C/min.

2.2.4 Membrane cleaning

Prior to each filtration experiment, the membrane was cleaned by following the procedure recommended by the membrane supplier: the membrane was first soaked in 20 g/L NaOH at 85

°C for 30 min, rinsed with ultrapure water to bring pH to 7, soaked in 75% H_3PO_4 at 50 °C for 15 min, and then again rinsed with DI water to bring pH to 7. The efficacy of cleaning was verified by performing a pure water flux test and comparing membrane resistances before and after cleaning.

2.2.5 Hybrid UV-membrane filtration unit: Design and operation

Figure 2.1 shows the schematic of the hybrid MF-UV disinfection unit used in all filtration experiments. The membrane and the UV lamp were placed in the foci of two alumina parabolic reflectors (Fig. 2.2) positioned to face each other at a distance that could be adjusted to regulate UV fluence on the membrane surface. The parabolic design ensured that the outer surface of the membrane was evenly irradiated by the UV light. UV-C irradiation was generated by a preheated germicidal UV lamp (16 W, model GPH330T5L/4, Atlantic Ultraviolet Corp.) The crossflow was provided by a peristaltic pump (model 621 CC, Watson-Marlow) equipped with a pulsation dampener (AD-10 PS, Yamada America). Transmembrane pressure was measured by pressure gauges (0 to 15 psi range, Ashcroft) installed on the feed and retentate sides of the membrane unit. The crossflow flux was measured using a flowmeter (model 101-8, McMillan). Permeate was collected on an electronic mass balance (Adventurer Pro AV8101C, Ohaus) interfaced with a data acquisition system (model NI PCI-6221, National Instruments).

All filtration tests were performed in a constant pressure mode with the average transmembrane pressure of 2.8 ± 0.2 psi (19.4 ± 1.5 psi). Average pressure values in filtration tests of different types were 2.67 ± 0.14 psi, 2.83 ± 0.14 psi, and 2.95 ± 0.30 psi in experiments on MF only, UV +MF with non-catalytic membranes, and UV + MF photocatalytic membrane, correspondingly

(see Appendix A, Table A1). The membrane, which was operated in an inside-out flow geometry, was housed in a quartz sleeve (160 mm in length, 20.5 mm in outer diameter) to allow for both illumination of the permeate side of the membrane by UV light and permeate collection. At the membrane ends, the space between the membrane and the quartz sleeve was sealed using two silicone stoppers (Fig. 2.2). The permeate was allowed to leave the quartz sleeve through a syringe needle into the permeate collection tube and the permeate mass flow rate was recorded at 1 s intervals. The average crossflow rate was 1.06 ± 0.09 L/min translating into the average crossflow velocity of 0.62 ± 0.05 m/s. Average crossflow rate values in filtration tests of different types were 1.1 ± 0.0 L/min, 1.0 ± 0.1 L/min, and 1.1 ± 0.0 L/min in experiments on MF only, UV +MF with non-catalytic membranes, and UV + MF photocatalytic membrane, correspondingly (see Appendix, Table A1).

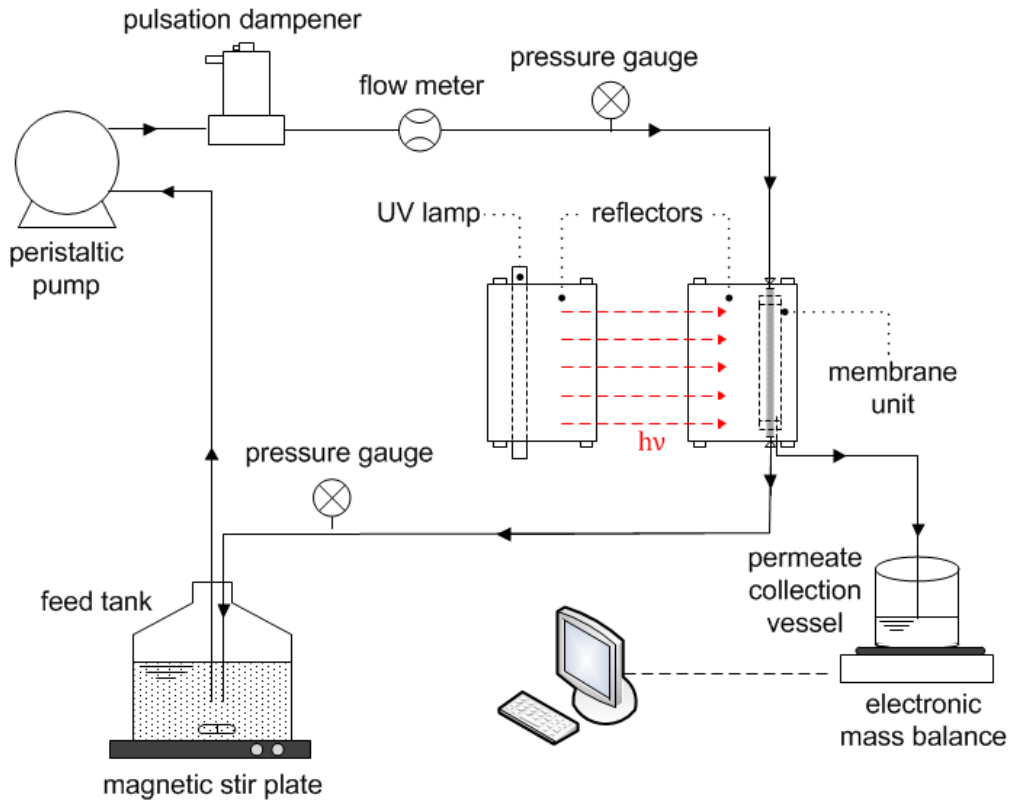

Figure 2.1 Schematic diagram of the hybrid membrane filtration-UV treatment system

Temperature of the permeate as a function of filtration time and UV exposure was measured in real time in a separate crossflow test with the membrane tilted at an angle to fasten permeate collection and minimize heat loss prior to the measurement. The samples of permeate were collected in a 2 mL vial (2 mL) periodically for 2 h. The temperature of the solution was measured with a digital thermometer (model S407993; Fisher Scientific: accuracy: ±1°C).

2.2.6 Sample collection and storage

Samples of the feed solution were withdrawn from the feed tank before and after each filtration experiment. In each filtration test, permeate samples were collected immediately after the start of filtration as well as 10, 20, 30, 45 and 60 min into the experiment. Each sample was divided into two aliquots. One aliquot was placed in a glass vial with a plastic cap, wrapped in foil, and stored at 4 °C. The second aliquot was frozen in a 5mL cryogenic vial at -80°C as a backup. The cryoprotectant (20% glycerol) to sample volume ratio was 1:1.

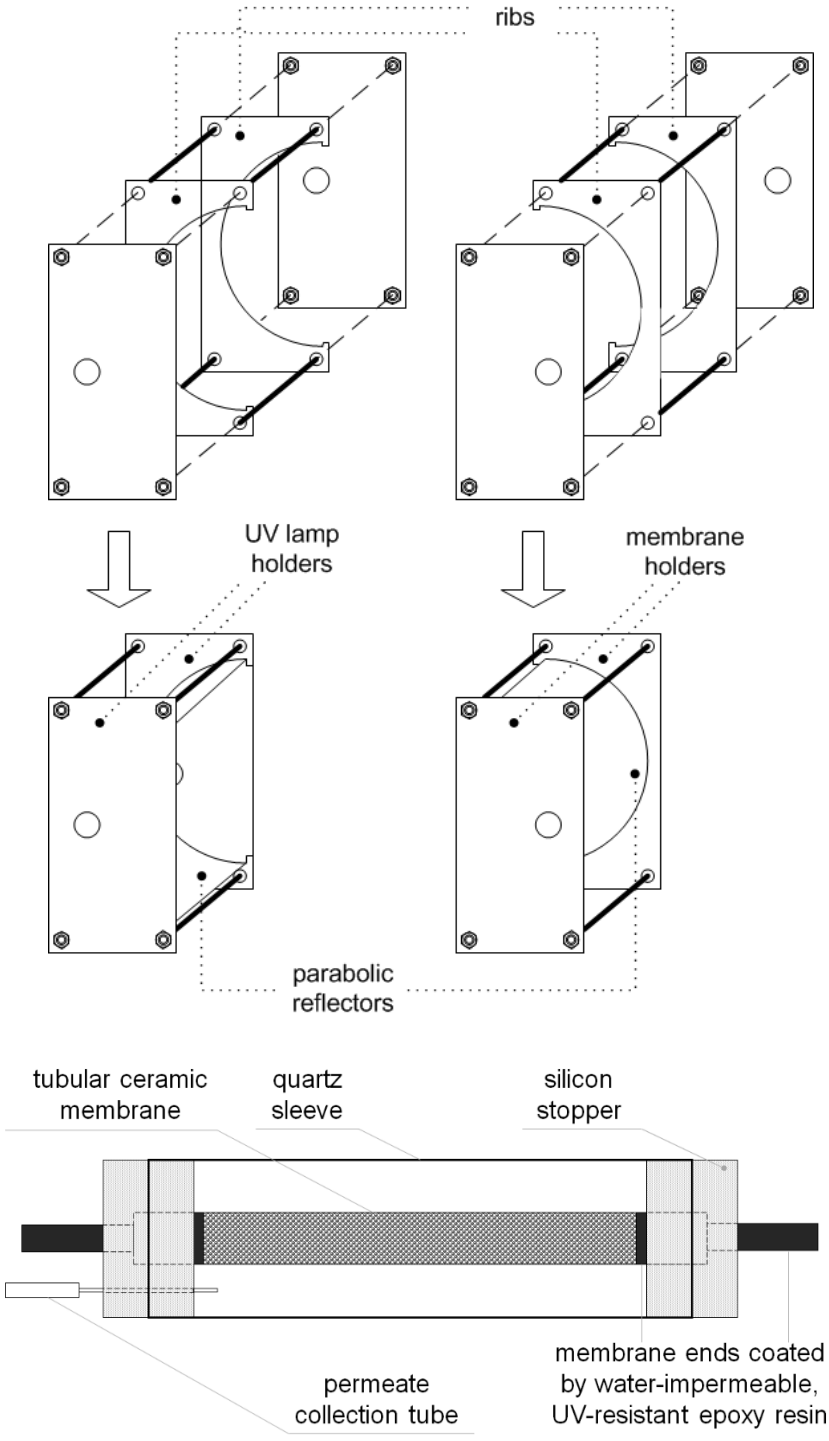

Figure 2.2 Design of custom-made parabolic UV light reflectors and the membrane housing unit

Note: The membrane housing unit is drawn not to scale. Membrane's length and outer diameter are 0.25 m and 0.01 m, respectively.

2.2.7 UV dose quantification

Chemical actinometry [29-31] was used to measure UV fluence by determining the UV absorbance of KI/KIO_3 solution. The exposure of the KI/KIO_3 solution to UV light results in the formation of triiodide, the concentration of which can be determined spectrophotometrically at 352 nm (MultiSpec 1501, Shimadzu). For each measurement, the absorbance of the KI/KIO_3 solution in dark was used as a baseline. To determine the quantum yield Φ (mole of product formed per mole of photons absorbed), the concentration of KI was first measured by recording KI absorbance at 300 nm and applying the Beer-Lambert law: $C_{KI} = \frac{1}{\ell}\frac{A_{300}}{\varepsilon_{300}}$, where A_{300} and ε_{300} =1.061 M^{-1} cm^{-1} are the absorbance of KI at 300 nm and the extinction coefficient of KI at 300 nm, respectively [32], and ℓ = 1 cm is the optical path length of the spectrophotometer cell. With C_{KI} known, Φ was computed as: $\Phi = 0.75(1 + (T - 20.7))(1 + (C_{KI} - 0.577))$, where T is the solution temperature in °C.

Fluence F (mJ/cm^2) is given by [32]

$$F = \frac{n}{\Phi}\frac{\Delta A_{352}}{\varepsilon_{352}\ell}\frac{V_s}{S_s} \quad (1)$$

where n = $4.72 \cdot 10^5$ ($J \cdot E^{-1}$) is a conversion factor for 254 nm wavelength, ε_{352} = 27,600 $M^{-1}cm^{-1}$ is the extinction coefficient of triiodide at 352 nm [33], V_s (mL) is the total volume of solution in the quartz sleeve, and S_s = 96.6 cm^2 is the surface area of the quartz sleeve exposed to UV light.

2.2.8 Quantifying the efficacy of disinfection by direct UV only

The disinfection efficacy of UV light in the crossflow system in the absence of photocatalyst could not be measured because the possibility of a photocatalytic effect could not be eliminated. Instead, to quantify virus inactivation due to UV only we employed the following multistep procedure:

Step 1: Measuring the permeate retention time in the quartz sleeve. Based on the measured values of the permeate mass flow rate, $\dot{m}_p$, and the mass of the residual permeate solution, m_r, in the quartz sleeve, the retention time of permeate solution was calculated as $\mathrm{t} = \frac{\mathrm{L}}{\mathrm{v}}$, where L is the length of the quartz sleeve (L = 15 cm); $v = \frac{\dot{m}_p}{\rho \cdot A_r}$ is the flux of permeate solution in quartz sleeve, ρ is the density of permeate solution and $A_r = \frac{m_r}{\rho \cdot L}$ is the cross-sectional area of the residual permeate solution in the sleeve.

Step 2: Relating UV fluence to permeate retention time. This was done by placing the KI/KIO_3 indicator solution in the permeate chamber (the quartz sleeve) of the hybrid UV- MF unit, without applying any pressure or crossflow and exposing the solution to UV. Because the permeate retention time values calculated at Step 1 did not exceed 30 s in any of the experiments, the KI/KIO_3 solution was exposed to UV irradiation for 5, 10, 20 and 30 s. Based on these measurements, the dependence of UV fluence on retention time was established.

Step 3: Determining P22 inactivation as a function of UV fluence. To determine the dependence of P22 inactivation efficiency on UV fluence, P22 suspensions were exposed to UV for 5, 10, 15, 20 and 30 s in a sequence of separate tests. The obtained values of P22 inactivation (see section 2.10) were related to UV fluence using the relationship established at step 2.

Following the above three steps, the P22 removal efficacy was related to the mass flow rate. Thus, in each test of the hybrid microfiltration-UV process, the contribution of direct UV to virus inactivation could be determined.

2.2.9 Electron microscopy of the membrane surface

Scanning electron microscopy (SEM) images of the tubular membrane surface as well as the membrane's cross-section were recorded (JEOL 6610LV SEM) under magnifications of ×700 and ×1000. Membrane samples for SEM imaging were obtained by breaking the membrane, mounting a piece with membrane's cross-section exposed onto an aluminum stub and coating the mounted sample with ~ 20 nm thick layer of gold (Emscope Sputter Coater, model SC 500, Quorum Technologies).

2.2.10 Quantification of the viable bacteriophage

The concentration of viable P22 bacteriophage was quantified by plaque assaying. TSA plates (1.5%) and 1% top agar tubes were prepared according to the standard method [34]. On the same day as the experiment, the *Salmonella enterica serovar Typhimurium LT2* stock was removed from -80 ºC and defrosted. One milliliter of the defrosted stock was introduced into 10 mL TSB media under sterile conditions and placed in a 37 °C incubator. After overnight incubation, 1 mL *Salmonella enterica serovar Typhimurium LT2* culture was transferred to 30 mL TSB at 37 °C for 3 h to reach the log phase of growth. The concentrations of viable P22 in feed solution and filtrate samples were determined by the double agar layer method [34]. First, top agar tubes were boiled and then placed in a 45-48 °C water bath. A series of dilutions (10^1 to 10^4) was prepared for each sample and each diluted sample was analyzed in triplicate. Second, one top agar tube was removed

from the water bath, 0.3 mL of log phase *Salmonella enterica serovar Typhimurium LT2* culture and 1 mL of sample were sequentially added. Then, the mixture was gently agitated and poured on a 1.5% TSA bottom agar plate. Slight shaking and swirling was applied to distribute the agar evenly on the plate. After the top agar hardened at room temperature, the plates were inverted and incubated for 16 to 18 h at 37 °C. Finally, the number of circular clear spots in each lawn of host bacteria was counted to determine plaque-forming units (PFU/mL) for each sample.

2.2.11 Quantification of the total bacteriophage

The total P22 bacteriophage count, which includes both the viable (infective) and non-viable (non-infective) virus, was determined by qPCR. Within 24 h of the filtration experiment, DNA of the bacteriophage was extracted using a MagNA Pure automatic extraction machine and MagNA Pure Compact Nucleic Acid Isolation Kit (Roche Diagnostics Corp). Samples (390 µL each) were extracted with 10 µL carrier RNA (1 µg/µL, Qiagen) to obtain 100 µL eluates. Carrier RNA was added to prevent DNA adsorption on the surfaces of the extraction kit. The nucleic acid eluents were stored at −20 °C. Each eluate was analyzed by real-time qPCR in triplicate following the procedure described by Masago et al. [25] (also see Appendix; Table A2). Each sample that was subjected to qPCR analysis consisted of 5 µL nucleic acid eluates, 10 µl of qPCR master mix (LightCycler 480 Probes, Roche), 2 µL of each forward and reverse primers (5 µmol/µL, Integrated DNA Technologies), 0.3 µL of Taqman Probe (10 µmol/L, Eurofins MWG Operon) and 0.7 µL of PCR-grade water (Qiagen). This study used same sequences of primers and probe as in Masago et al. [25]. The qPCR analysis started with 95°C for 15 min then followed by 45 amplification cycles at 95 °C for 10 s, 60 °C for 20 s and 72 °C for 10 s and finally cooling at 40°C for 30 s. To

relate the crossing-point (C_p) values to the numbers of P22 DNA copies, a standard curve developed in our laboratory was used.

2.3 Results and Discussion

2.3.1 Hybrid membrane filtration-UV process: The concept and a brief rationale

UV disinfection is effective against a broad range of microorganisms and has unique advantages over other disinfection processes. As a unit operation, UV disinfection does not involve addition of chemicals and does not generate harmful disinfection by-products typical for chemical disinfection unit processes such as chlorination and ozonation.

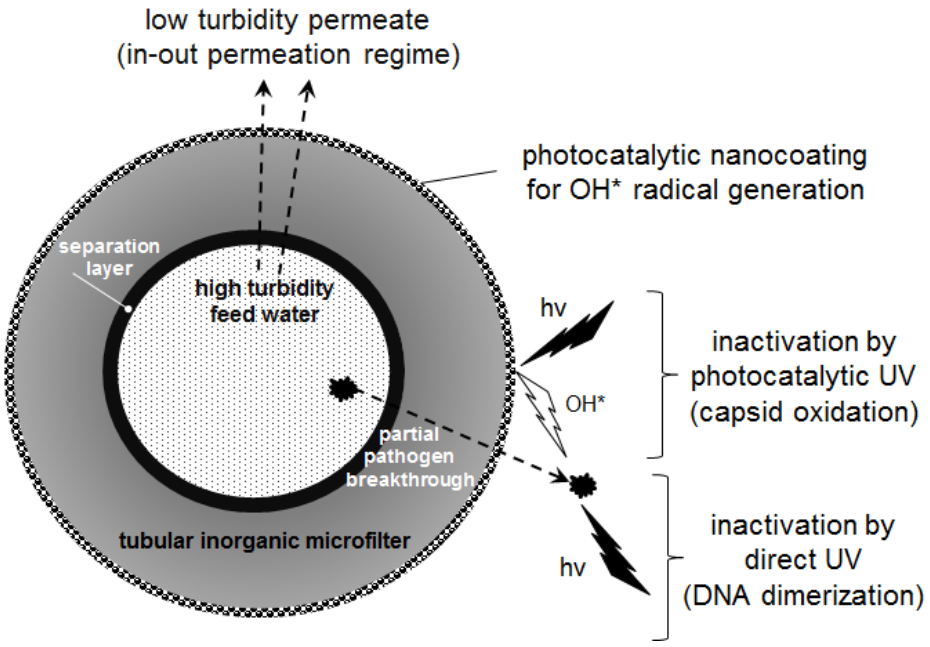

Figure 2.3 Conceptual illustration of the hybrid membrane filtration-UV disinfection process

UV light is also effective for inactivating chlorine-resistant pathogens such as *Cryptosporidium* and *Giardia* protozoa (e.g. [35, 36]). A fundamental limitation of UV disinfection is that RNA-based microorganisms – a group that includes many EPA-regulated viruses such as enteroviruses, hepatitis A virus, and caliciviruses – are resistant to UV. Furthermore, some pathogens can repair

UV-induced damage to their DNA. Another challenge is presented by water turbidity. Turbidity, when present at high levels, limits UV light access to microorganisms and is known to diminish the efficacy of UV disinfection [37, 38].

The proposed novel approach combines microfiltration and UV disinfection into a hybrid photocatalytic process (Fig. 2.3) to overcome the above two challenges. The ultra- or microfiltration membrane operated in an inside-our geometry removes turbidity so that the UV irradiation is applied to a relatively turbidity-free permeate stream. The degree of turbidity removal is controlled by an appropriate choice of the membrane pore size.

At the same time, the membrane serves as a support for photocatalytic nanoparticles immobilized on the outer (i.e. permeate) membrane surface exposed to the UV light. The catalytic enhancement of UV disinfection is due to non-specific chemical oxidation by reactive oxygen species (ROS) catalytically generated at the membrane surface. The oxidation complements direct UV to pose a "dual threat" to pathogens with direct UV targeting microorganism's DNA and ROS damaging cellular membrane (in cases of bacteria and protozoa) or viral capsid (in case of viruses). These and several other advantages of the proposed hybrid process are summarized in Table 2.1.

Table 2.1 Rationale for the proposed UV-microfiltration hybrid process

Technology and its benefits		**Challenges**	**How the challenge is addressed in a hybrid process**
Photocatalytic UV disinfection	Photocatalytic UV is effective against a wide range of microbial pathogens.	Some pathogens are resistant to UV or can repair UV-induced damage	Catalytic oxidation at the membrane surface by ROS complements the physical effect of the direct UV.
	Chemicals demand and harm to receiving waters are minimal	Catalyst needs to be recovered	Membrane-supported catalyst is immobilized and does not need to be recovered.
	UV disinfection is catalytically enhanced	Efficiency is limited when turbidity is present	Turbidity is removed by the microfilter "upstream" from the UV reactor
Membrane filtration	Membranes provide absolute barrier to pathogens	Lower pore size for removal of smaller pathogens results in lower permeate fluxes	Redundancy introduced with catalytic UV disinfection enables trade-offs in pore sizes and product water fluxes

2.3.2 Efficacy of disinfection by direct UV irradiation

First, batch experiments were conducted to determine UV fluence as a function of UV exposure time by using KI/KIO_3 solution as an indicator. Following the procedure described in section 2.7 (see eq. (1)), values of UV fluence were calculated (see Appendix, Fig. A1). The exposure time was considered to be equal to the retention time of permeate solution in the quartz sleeve. The

results show that fluence increased linearly with exposure time (see SI). Second, the log removal (LRV) of viable P22 was measured as a function of UV fluence LRV is defined as

$$LRV(t) = -log\left(\frac{N}{N_0}\right) \tag{2}$$

where N_0 and N are P22 concentrations in the batch reactor at time 0 and time t into the reaction, respectively. The kinetics of P22 inactivation by UV light could be approximated (Fig. 2.4) by the Collins-Selleck model [39, 40]:

$$ln\left(\frac{N}{N_0}\right) = -\Lambda_{CS}[ln(\Phi) - \ln(b)] \tag{3}$$

where Λ_{CS} is Collins-Selleck coefficient of specific lethality and b is the lag coefficient. Based on the fit of experimental data to eq. (3), the following values of these two coefficients were determined: Λ_{CS} = 1.972; b = 0.376 mW·s/cm^2. With $\Phi(t)$ and $LRV(\Phi)$ dependencies determined, the dependence of the efficacy of disinfection (expressed in terms of LRV) by direct UV irradiation on the UV exposure time was established. The small negative "lag" described by b (i.e. non-zero extrapolated value of P22 inactivation based on the fit given by eq. (3)) is attributed to an experimental error.

The decelerating kinetics described by the Collins-Selleck model could be a consequence of P22's being shielded from the UV light by residual components of the virus growth media.

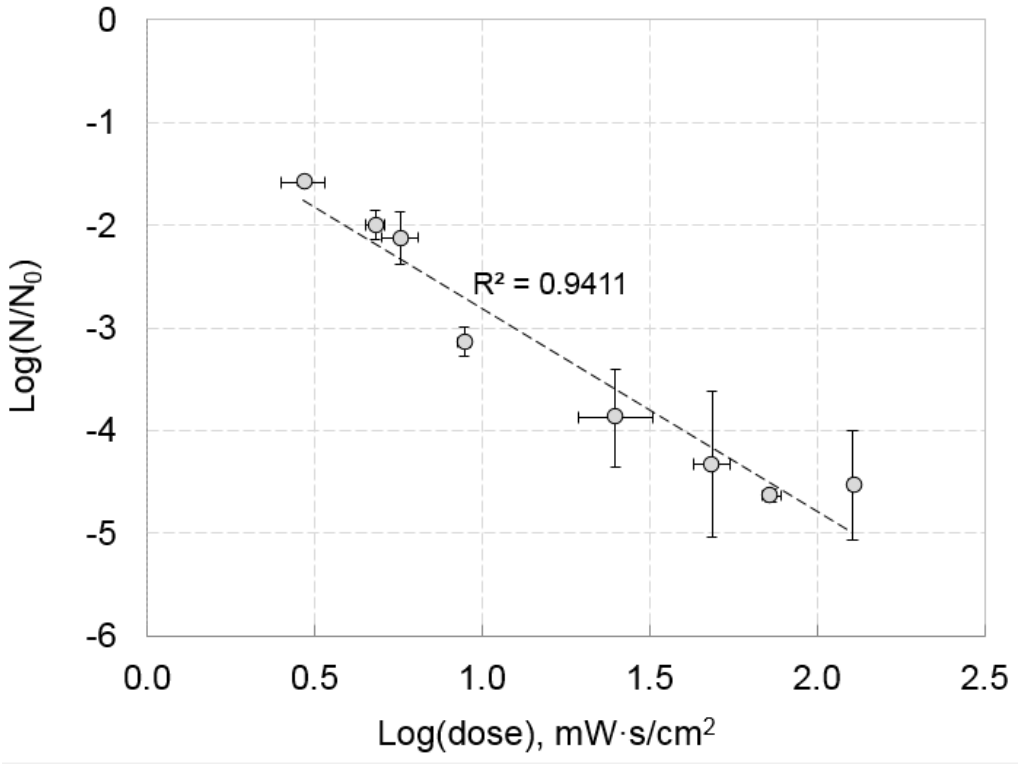

Figure 2.4 Log removal of viable P22 bacteriophage as a function of UV fluence

Note: Each data point is based on a triplicate measurement. Error bars represent standard deviations (n=3).

2.3.3 Characterization of the tubular ceramic membrane

SEM images of the as-received tubular ceramic membrane and the same membrane coated with TiO_2 P25 nanocatalyst are presented in Fig. 2.5. The separation layer of this 0.8 µm nominal pore size membrane is on the inner wall of the membrane channel making the membrane suitable for use in the inside-out flow geometry only.

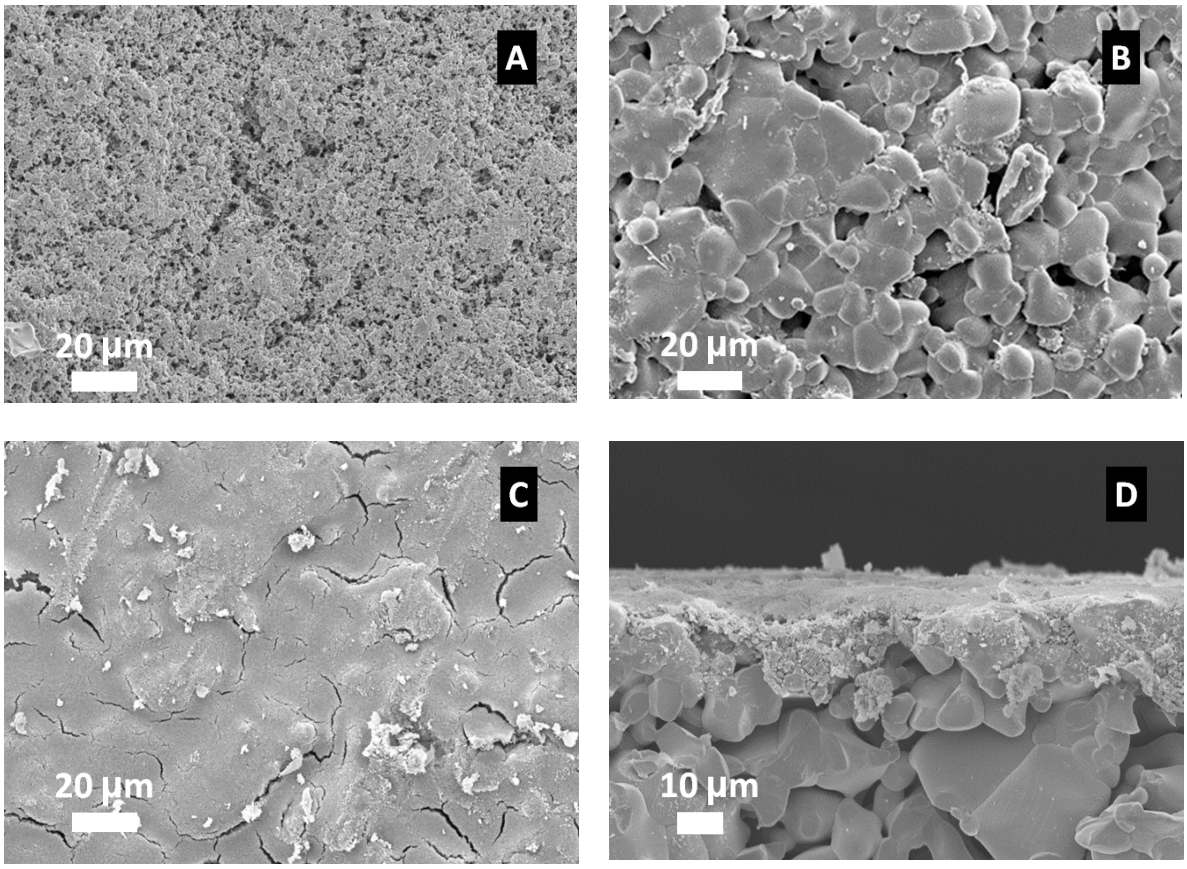

Figure 2.5 Scanning electron micrographs of the tubular ceramic membrane

Note: A) planar view of the inner surface, B) planar view of the uncoated outer surface, C) planar view of the TiO2-coated outer surface, and D) the cross-sectional view of the coated outer surface of the tubular ceramic membrane.

Accordingly, the inner (feed) surface of the membrane has a finer pore structure (Fig. 2.5A) than the more porous and rough outer (permeate) surface composed of larger TiO_2 grains (Fig. 2.5B). The coating-induced morphological changes of the outer membrane surface could be clearly observed: the 10-layer coating covered the outer surface of the membrane with a layer of TiO_2 P25 that is relatively smooth but cracked (Fig. 2.5C). The cracking might be due to the high roughness of the underlying membrane surface, which could lead to an uneven tensile stress in the coating

[41, 42]. The coating was not homogeneous over the entire membrane surface with some portions of the membrane coated with a denser catalyst layer. The reasons were not clear and an additional study would be required to optimize the coating process.

Coating the permeate surface with a TiO_2 layer led to ~ 40% decline in the permeability of the membrane. Figure 2.6A illustrates how the specific permeate flux, J , of uncoated and coated membranes changed with the time of filtration of ultrapure water first in the absence of UV and then after exposed to UV irradiation. In the absence of UV (i.e. during the first 60 min of the filtration test) the specific permeate flux through an uncoated membrane declined by ~ 17.5%. A declining trend for pure water permeate flux for ceramic membranes has been reported in the past [43-45] and attributed by Mendret et al [45] to the very slow hydration of the membrane surface. However, given the very large nominal pore size (0.8 μm) of the membrane employed in our study, hydration shell should be much thinner than the pore size so that hydration can be eliminated as the reason for flux decline. A part of the reason for this flux behavior is the change in water temperature (Fig. 2.6B) as it decreased throughout the first 60 min of the test from its initial value ($23\ ^0C$) towards the lower temperature of the ambient air ($20.3\ ^\circ C$). When the temperature induced changes were factored out by normalizing values of the specific permeate flux by viscosity, the resulting time dependence of membrane permeability still showed a 16.5% decline (Fig. 2.6C). Tentatively, we attribute the observed flux behavior to the re-arrangement of loosely affixed TiO_2 particles due to permeate flow.

A)

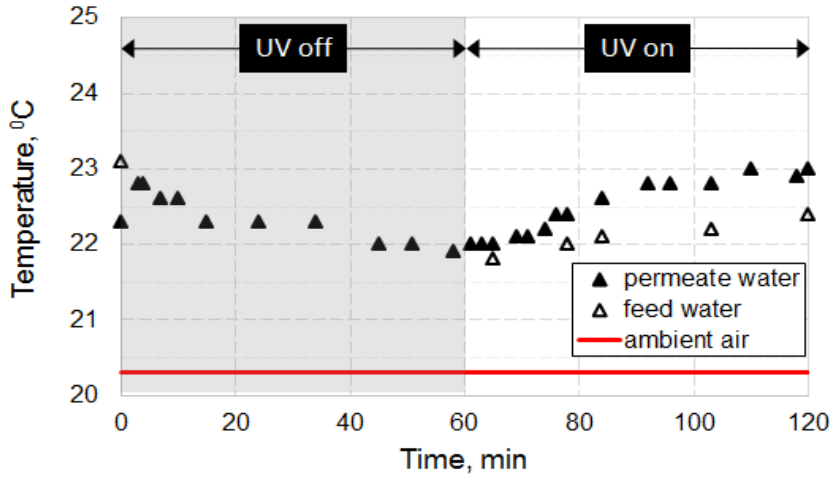

B)

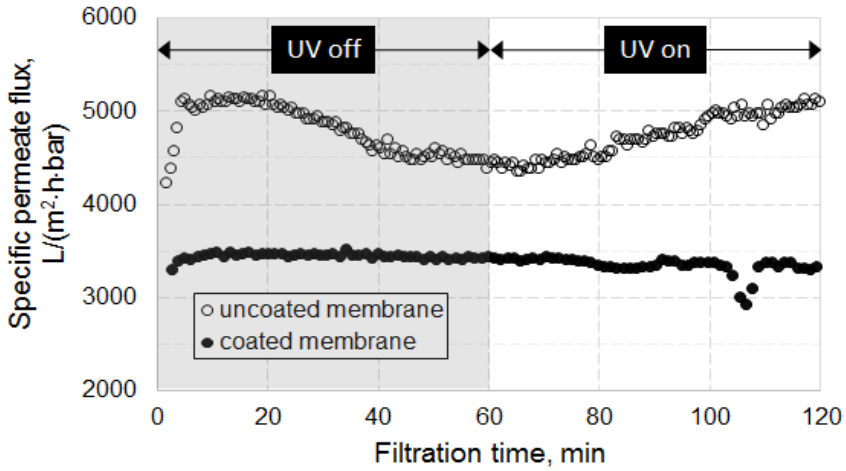

C)

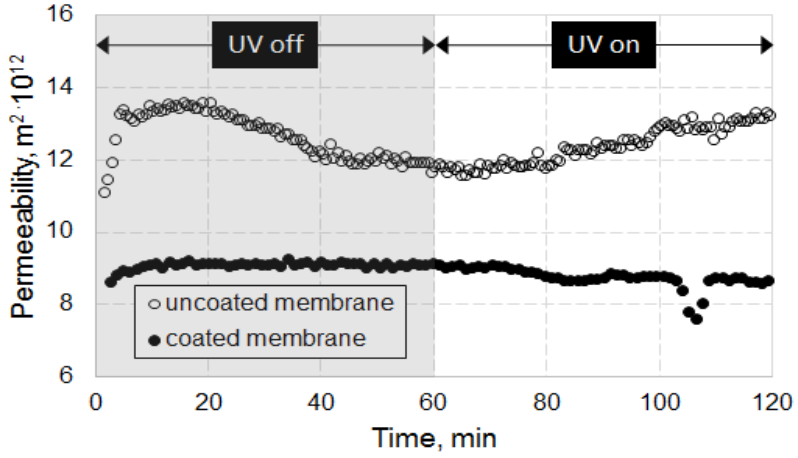

Figure 2.6 Specific permeate flux of ultrapure water

Note: (A) temperature of ambient air, feed water and permeate water, (B) and membrane permeability, (C) as functions of filtration time for uncoated and TiO2 P25-coated membranes.

When the outer membrane surface was illuminated by the UV light the permeate flux (Fig. 2.6A) started to increase. We attribute this increase to higher temperature (Fig. 2.6B) and resulting lower viscosity of the permeating water due to membrane heating by the UV light. The temperature effect could not fully explain away the increase in flux - the permeability still increased with time (Fig. 2.6C) in the presence of UV. We attribute this fact to errors in temperature measurements: collecting a sample for temperature measurements takes time during which the water in the sample can cool down.

Mendret et al [45] reported similar UV-induced increases in permeate flux and explained them as stemming from photoinduced hydrophilicity [46, 47]. In our case though it was the porous permeate side of the membrane, and not the permeability-controlling separation layer, that was exposed to UV irradiation (Fig. 2.3). Because the membrane is not transparent to UV, only a thin sublayer of the membrane on its permeate side could have experienced photoinduced changes in surface hydrophilicity. The resulting improved wettability of this part of porous structure could not have been responsible for the observed increase in the overall permeability of the membrane.

Notably, the coated membrane did not show a similar dependence on filtration time on the absence of UV light nor did it show a response to the UV irradiation. This behavior can be rationalized by posing that a) loose particles in the membrane are stabilized during the coating and sintering procedures, and b) energy of the UV irradiation is absorbed by the coating and not dissipated as heat that can increase the temperature of the permeating solution.

2.3.4 Removal and inactivation of bacteriophage P22

Separate experiments were performed on the removal and inactivation of P22 bacteriophage in three treatment processes: 1) MF only, 2) hybrid UV-MF process with an uncoated membrane, and 3) hybrid UV-MF process with a TiO_2-coated membrane. Figure 2.7 summarizes LRV data for viable P22 by the four processes for six different times into the filtration process (also see Appendix, Table A3):

1) Among all processes tested, microfiltration, applied alone, was the least effective in removing viable P22 (LRV = 0.5 ± 0.5). The low removal rate was due to the large nominal pore size of the microfilter (0.8 μm) relative to the hydrodynamic diameter of P22 bacteriophage (d_p = 68.8 nm) [48]. The overall removal of viable P22 by the membrane can be attributed to a combination of adsorption, size exclusion, and inactivation upon contact with the membrane surface. Despite the mismatch between the pore size and virus diameter, size exclusion may still be possible because the membrane pore size distribution is of finite width and may include very small pores.

2) The estimated (see section 2.8) inactivation by direct UV was very stable throughout the entire 60 min of filtration with an average LRV of 1.6 ± 0.1. The contribution of the UV process to bacteriophage inactivation is due to UV's germicidal effect, which reduces the number of infective viruses but not the total number of viral particles.

3) Averaged over filtration time, the LRV removal of viable P22 by the hybrid UV-MF process with an uncoated MF membrane (2.3 ± 0.2) was not statistically different from the arithmetic sum

of LRVs achieved by the two constituent processes, UV and MF with uncoated membrane - applied separately.

4) By contrast, the hybrid UV-MF process with a membrane coated with TiO_2 photocatalyst resulted in an average LRV of 5.0 ± 0.7, which was more than two times higher than the corresponding value for the hybrid UV-MF test with uncoated membranes.

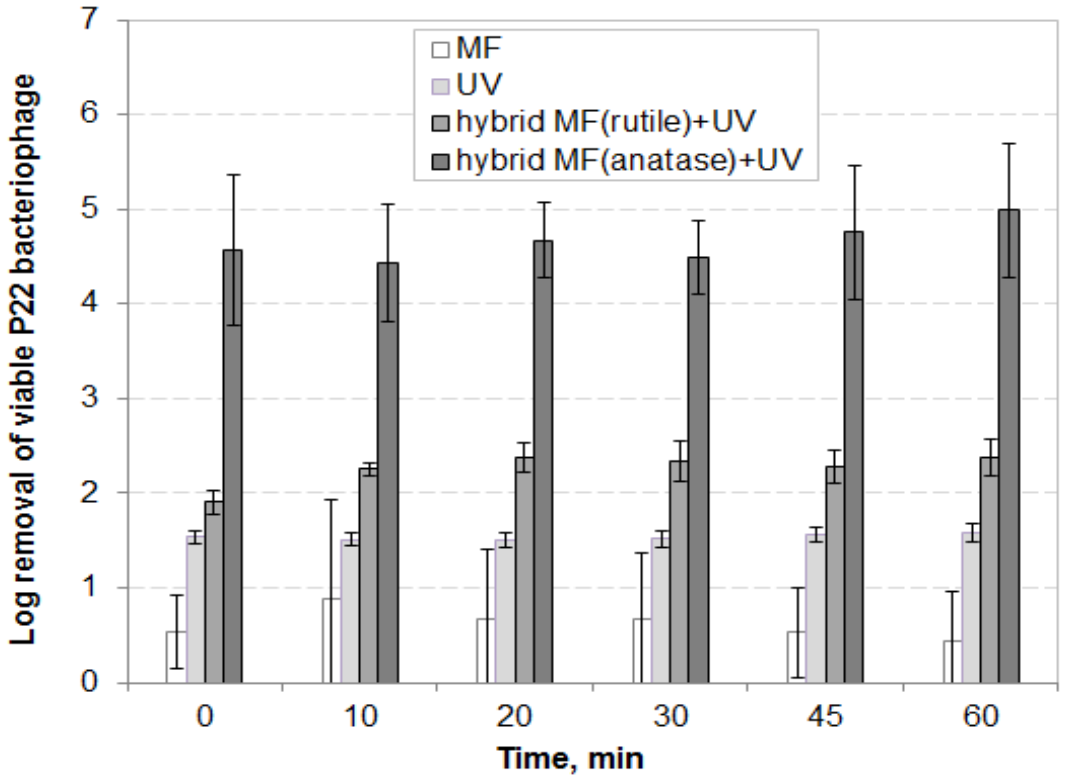

Figure 2.7 Inactivation and/or removal of viable P22 bacteriophage

Note: 1) direct UV only 2) microfiltration only, 3) non-photocatalytic hybrid UV-MF process, and 4) photocatalytic hybrid UV-MF process. Error bars represent standard deviations (n=3).

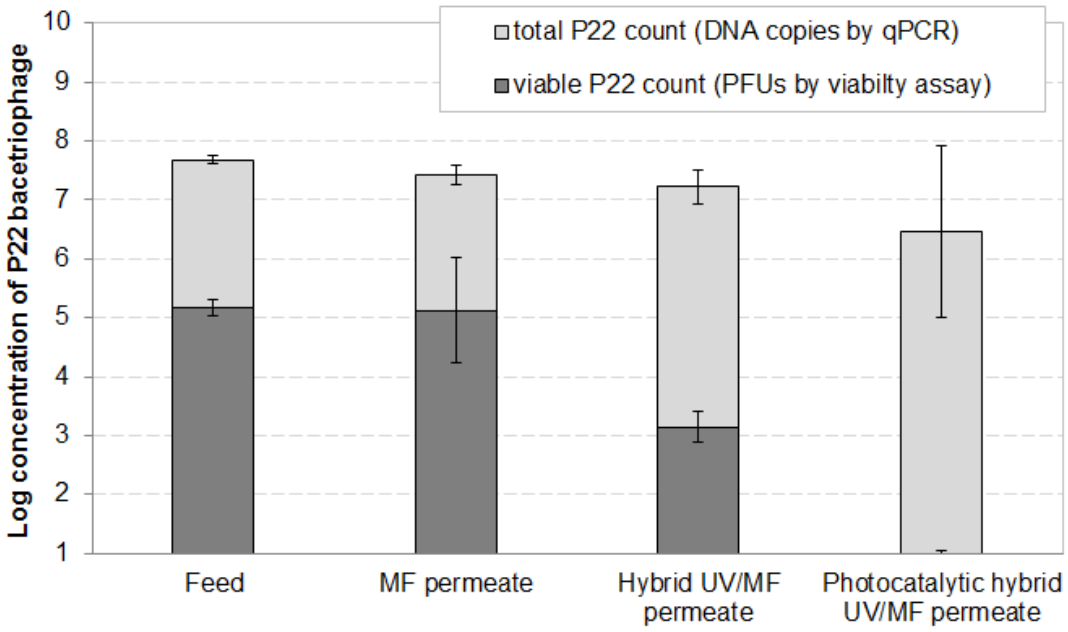

Figure 2.8 Log concentration of viable and total bacteriophage P22 in the feed solution and in the permeate 30 min into the filtration process

The synergistic effect was due to the membrane-based photocatalysis, wherein reactive oxygen species (ROS) generated at the surface of TiO_2 nanoparticles of the coating provide non-specific oxidation that complemented the effect of direct UV. While direct UV inactivates viruses by dimerizing their DNA [49], ROS contribute to disinfection by oxidizing the protein capsid of viruses. As mentioned earlier, this contribution of photocatalysis to the overall removal of viable viruses is especially important because, in contrast to direct UV, it can inactivate RNA viruses.

Figure 2.8 provides absolute values of the total concentration of P22 and the concentration of viable P22 in the effluent after 30 min of operation of each of the three treatment processes. The total virus count (i.e. viable and non-infective fractions together) in feed and permeate samples was estimated based on DNA copy counts measured by qPCR. The data show that the

photocatalytic UV-MF process is effective in inactivating viable P22 even though the reduction of the total virus is not significant. The large value of the LRV recorded for the hybrid process points to the possibility of employing membranes with even larger pore size to enable higher flow rates.

2.3.5 Potential applications in water treatment

The proposed hybrid process can mitigate two salient disadvantages of UV disinfection: resistance of certain environmentally important pathogens to UV disinfection and low efficacy of UV light when applied to highly turbid waters. Coupling microfiltration with photocatalytic UV process can make disinfection of highly turbid or large flow rate streams (e.g. ballast and storm water) more efficient in terms of the required UV dose for a given level of disinfection. This improvement, however, would likely come at the expense of membrane fouling and, therefore, a higher cost of membrane operation.

A possible application for the proposed hybrid process and an important environmentally-relevant example of a high flow rate operation requiring disinfection is ballast water treatment. Recent International Marine Organization D2 regulations impose limits on the concentration of microbes in ballast water. According to these regulations, all vessels built after January 1, 2016 must comply with the U.S. Coast Guard Discharge Standards Phase 2 that require that no more than 10^3 bacteria and 10^4 viruses are present in 100 mL of treated ballast water. Given the very small size of microorganisms and the large flow rates typical for ballast water treatment, complete physical removal of bacteria and especially viruses is unlikely, which makes disinfection a critical second barrier. It is now recognized that no single process efficiently removes the wide range of potential invasive species in ballast water and that a combination of technologies must be considered [50].

A combination of filtration and subsequent disinfection has been identified as the best available treatment [51]. To date, UV disinfection has been applied as a stand-alone unit [52-56] and in combination with physical separation methods that use filters [57, 58] and hydrocyclones [59, 60]. The prior history of adoption of these technologies by the shipping industry bodes well for the application of new hybrid technologies that combine filtration and UV light

Innovative reflector designs can further facilitate field applications of the proposed photocatalytic membrane reactor. For example, we envision a reflector with a parabolic profile of corrugation as a large surface area lens that focuses incident light on tubular filters positioned in foci of the parabolas. Finally, membranes can support a broad range of photocatalytic materials including high efficiency UV and visible-light photocatalysts that tap into solar energy and may enable low cost disinfection.

2.4 Conclusions

We report on the first application of photocatalytic membranes for virus removal and inactivation. In the proposed hybrid technology, UV light is focused on a TiO_2-coated outer surface of a tubular ceramic membrane operated in an inside-out geometry. The hybrid process is evaluated with respect to removal and inactivation of P22 bacteriophage, a model virus. The kinetics of P22 inactivation by direct UV was first evaluated in a separate set of tests in a batch UV reactor and found to fit Collins-Selleck model. To gauge the performance of the hybrid UV-microfiltration process, a number of crossflow filtration tests were performed with and without UV light as well as with and without photocatalytic coating on the membrane. Compared to stand-alone microfiltration, stand-alone UV disinfection and UV-microfiltration with a non-photocatalytic membrane, the hybrid photocatalytic UV-microfiltration process was considerably more effective in inactivating the virus. Average values of log removal of viable P22 by these four processes were 0.5 ± 0.5, 1.6 ± 0.1, 2.3 ± 0.2, and 5.0 ± 0.7, respectively. The proposed hybrid process can mitigate two salient disadvantages of disinfection by direct UV: resistance of certain environmentally important pathogens to UV and low efficacy of UV disinfection when applied to highly turbid waters. Virus removal and inactivation can be regulated by the choice of the membrane pore size, design of the photocatalytic coating, and by controlling UV fluence applied to the permeate stream. Potential applications of the hybrid UV-microfiltration technology include treatment of turbid, high fouling potential and high flow rate streams that cannot be cost-effectively disinfected by other means.

APPENDICES

Appendix A: Supporting information

Table A.1 Sequences of Primers and Taqman probe

Primers/probe	Sequence
Reverse	CTT AAC AAG CTC TGA CTG CTC ATC A
Forward	CCA TCG CCT GTG ACT CGA T
Taqman Probe	FAM-TCG CAA CGA TGC AGA ACG ACT CG-TAMRA

Note: Reference [29].

Table A.2 Log removal of viable P22 in different treatment processes as determined by plaque assay analysis

Treatment process	Filtration time, min					
	0	10	20	30	45	60
UV	1.54 ± 0.07	1.51 ± 0.07	1.51 ± 0.08	1.52 ± 0.09	1.56 ± 0.08	1.58 ± 0.09
MF (uncoated membrane)	0.54 ± 0.40	0.88 ± 1.05	0.67 ± 0.74	0.67 ± 0.70	0.53 ± 0.47	0.44 ± 0.51
UV + MF	2.08 ± 0.40	2.39 ± 1.05	2.18 ± 0.74	2.19 ± 0.70	2.10 ± 0.48	2.03 ± 0.52
Hybrid UV-MF process (uncoated membrane)	1.91 ± 0.13	2.25 ± 0.07	2.38 ± 0.15	2.33 ± 0.22	2.29 ± 0.18	2.38 ± 0.19
Hybrid UV-MF process Hybrid UV-MF process (coated membrane)ne)MF process (coated membrane)	4.57 ± 0.80	4.43 ± 0.61	4.67 ± 0.39	4.49 ± 0.38	4.75 ± 0.71	4.99 ± 0.70

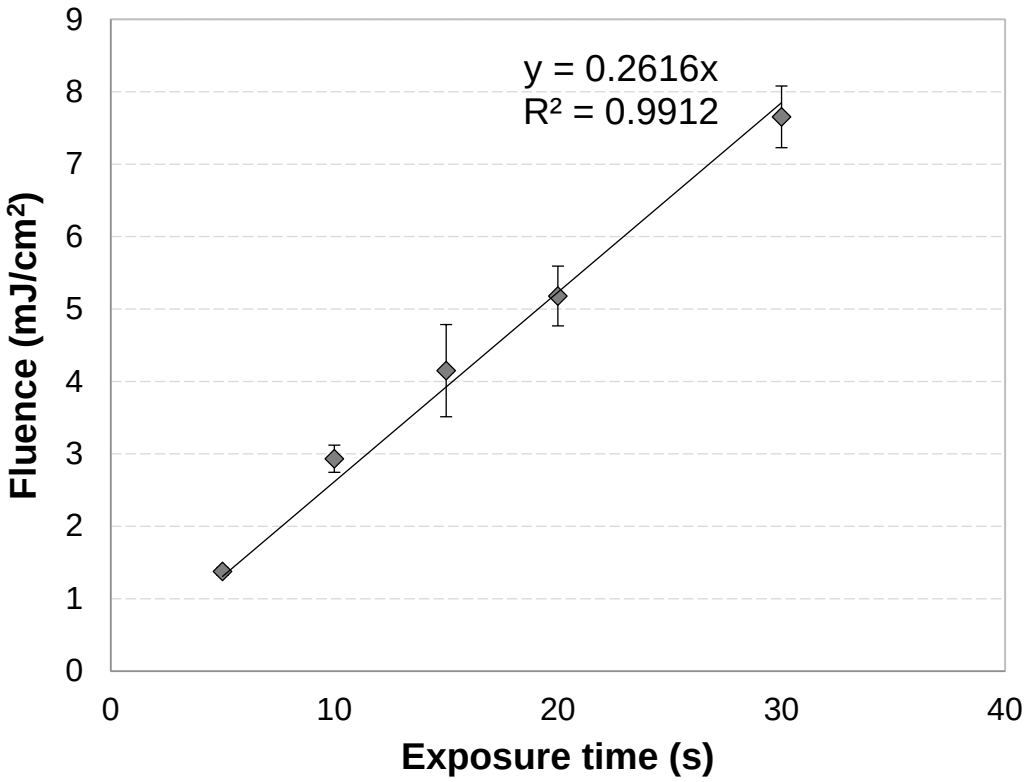

Figure A.1 UV fluence as a function of the exposure time

Note: Each data point is based on a triplicate measurement. Error bars correspond to standard deviations.

Appendix B. Photocatalytic coating on borosilicate glass slides

Borosilicate glass slides with the dimension of 24 mm×60 mm were purchased form VWR (catalog number 16004-096) and used to optimize the number of TiO_2 coating layers for the preparation of a photocatalytic ceramic membrane.

Borosilicate glasses are known to have a very low coefficient of thermal expansion (~3×10^{-6} K^{-1} at 20 °C). Therefore they show very good thermal resistance which allows for the use of temperatures up to 500 º C or even 550 º C for a short period of time [1]. Moreover, borosilicate glasses also possess excellent chemical resistance and flatness. In addition, the borosilicate glasses do not fluoresce under UV light [2].

B.1 Borosilicate glass slides cleaning procedure

Prior to coating, new borosilicate glass slides were carefully cleaned to eliminate the potential alkaline nature of new glass products and the interference of grease and/or organic matter [3]. First, borosilicate glass slides were soaked in 1% hydrochloric acid for 2 to 3 hours and rinsed with DI water [3]. Second, borosilicate glass slides were ultrasonically cleaned with detergent for 15 min and again rinsed with DI water. Third, borosilicate glass slides were ultrasonicated in acetone and ethanol solution for 15 min, respectively [4, 5]. Finally, borosilicate glass slides were rinsed with DI water and dried at ~30°C overnight prior to use.

B.2 Borosilicate glass slides coated with TiO_2 catalysts

Borosilicate glass slides were coated with TiO_2 using the dip-coating method. Suspension of TiO_2 particles with the concentration of 10 wt% was prepared by adding 100 g of P-25 TiO_2 powder into 900 g of distilled deionized water (DDI) with the addition of 0.02 g of dioctyl sulfosuccinate as a dispersant [6]. Then, the suspension was stirred for 24 h and ultrasonicated for a24 h before use. At the same time, all the glass containers were cleaned using 10% hydrochloric acid (detergent or 70% ethanol if needed) and rinsed with DI water. To evaluate the amount of TiO_2 deposited on glass slides during coating, each glass slide was weighed before and after the coating procedure.

Table B.1 shows major parameters of the dip-coating method. In all referenced studies TiO_2 was used as the only catalyst and glass was used as the substrate. Based on the analysis and comparison of the references, we developed our own coating procedure, which includes the following steps:

1. Cleaned borosilicate glass slide was immersed into TiO_2 solution at the speed of 4.7 cm/min.
2. After 30 s of immersion, the glass slide was withdrawn at the same speed of 4.7 cm/min.
3. TiO_2 coated glass slide was dried in oven at 80°C for 3-5 min after each coating. The desired number of coating layers was achieved by repeating the above steps.
4. After the last coating layer is deposited, the glass slide was dried in an oven at 80°C overnight and then sintered at 773K (~500°C) for 45 min.

In total, seven different borosilicate glass slides were coated with 1, 2, 5, 8, 10, 15 and 20 TiO_2 coating layers, respectively. Table B.2 shows the scanning electron microscope (SEM) images of the seven TiO_2 coated glass slides under different magnifications.

Table B.1 Summary of dip coating parameters from selected representative references

Substrate	Components	Concentration	Speed	Coating layers	Drying process	Sintering	TiO_2 amount	Sources
Glass	TTIP in *i*-prOH	0.5 mol/L	20.4cm/min	Several	dried at 150 °C during 1 h	450 °C	3 mg/cm^2	Guillard et. al. [7]
Conducting glass	TTIP in acetic acid solution in an ice/water	10mL/100mL acid solution	-	1	-	450 °C for 1 h	0.5 mg/cm^2	Yang et. al. [8]
Glass	Degussa P25 particles	4 g/l	-	4	dried at 100 °C for 1 h	450 °C	0.28 mg/cm^2	Alinsafi et. al. [9]
Glass beads	TTIP in *i*-prOH and DEA Degussa P-25 TiO_2 powder	0.5 M	12.8 cm/min	Several	125 °C for 24 h	100 °C for 1 h, then 600 °C for 1 h.	-	Balasubramanian et. al. [10]
Borosilicate Petri dish	TTIP and nitric acid in deionized water	15mL/150mL water	Evenly applied	1	75 °C for 24 h	400 °C for 2 h	~0.11 mg/cm^2	Ao et. al. [11]
Borosilicate glass	TTIP in ethanol and HCl (37%)	10mL/50mL ethanol	11.5 cm/min	Several to get tens of nm	dried at 70 °C during 5 min	80 °C for 12 h and then calcinated at 450 °C in air during 2 h	-	Ghazzal et. al. [12]

Note: TTIP—titanium isopropoxide; *i*-prOH— isopropanol; DEA— diethanolamine; HCl—hydrogen chloride.

Layers	Overall view	With magnification of ×1,500	With magnification of ×10,000
1	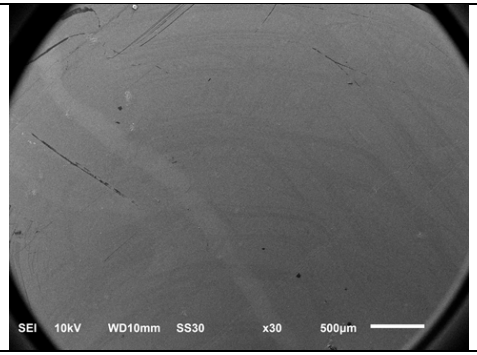	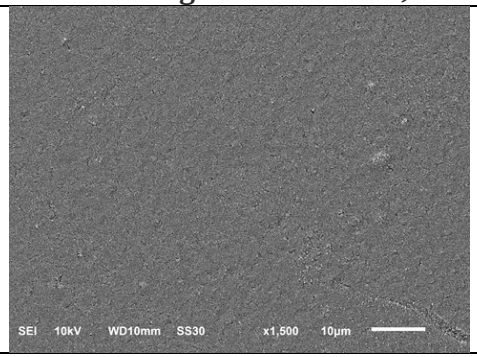	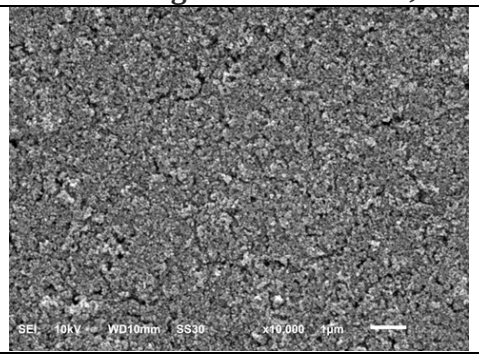
5	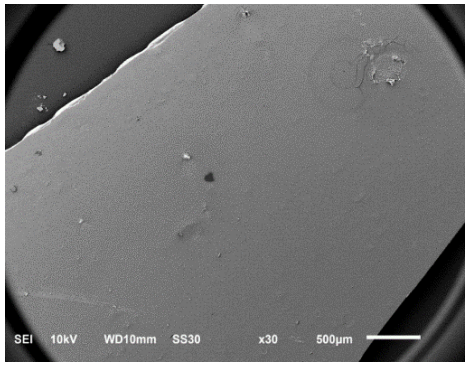	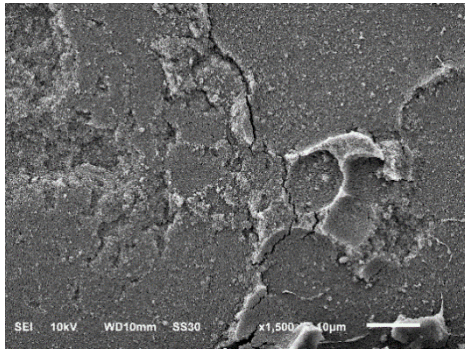	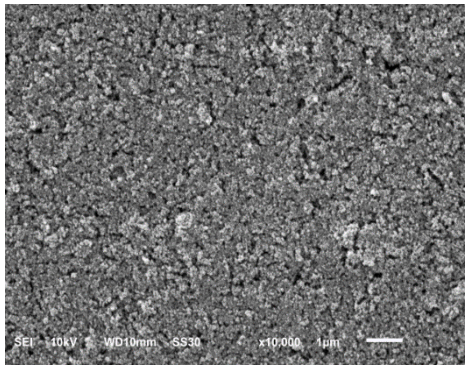
8	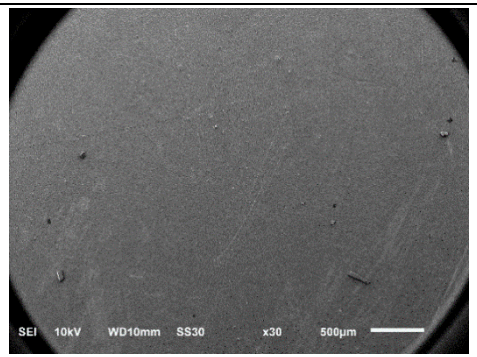	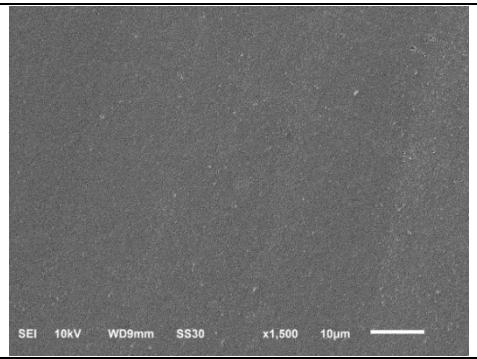	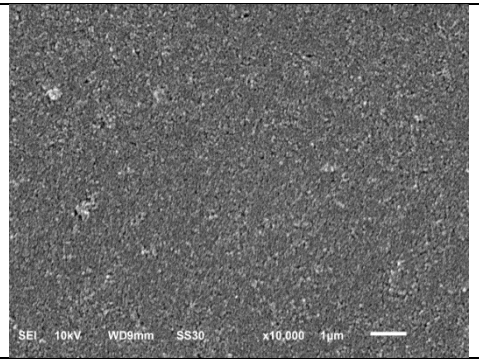

Figure B.1 SEM images of different coating layers on borosilicate glass slides under various magnifications

Figure B.1 (cont'd)

10	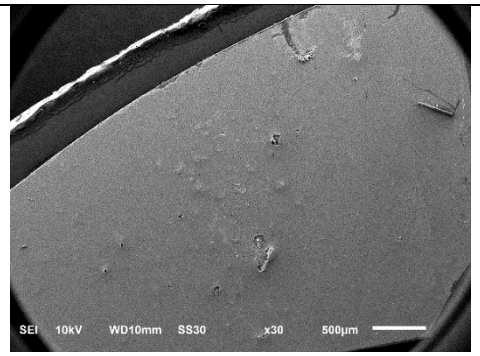	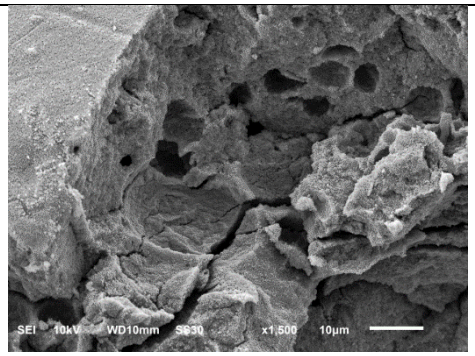	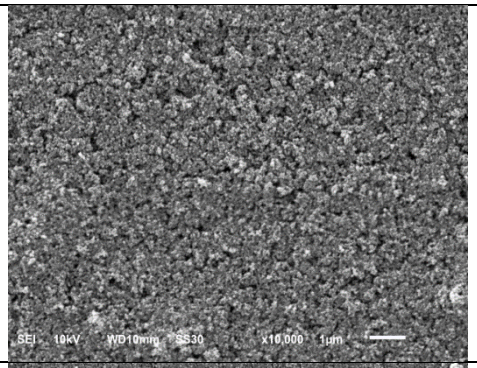
15	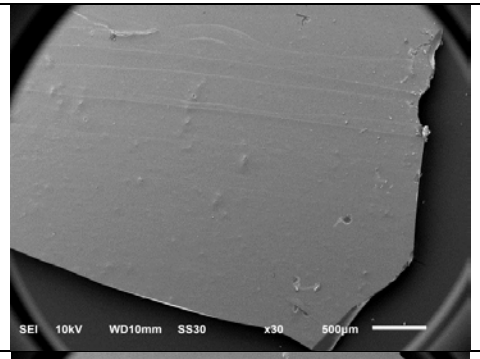	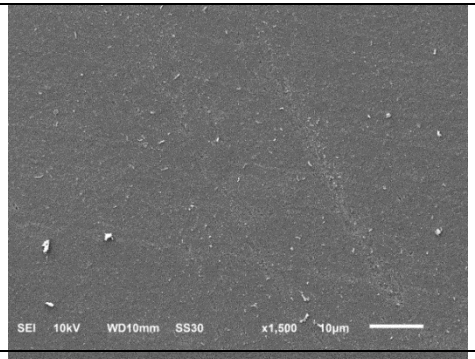	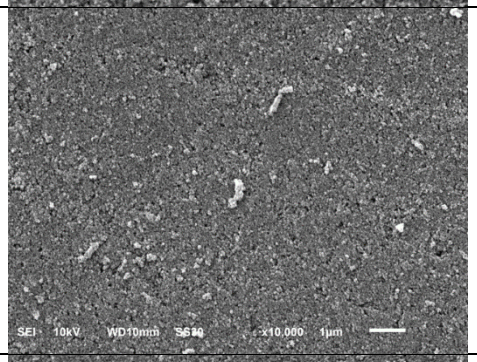
20	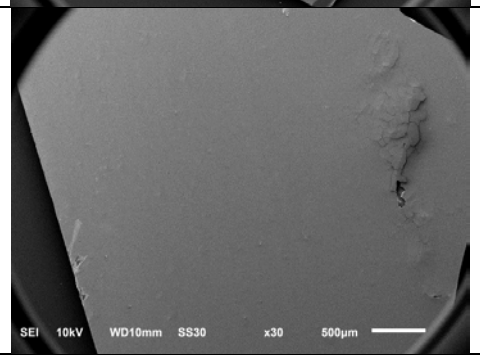	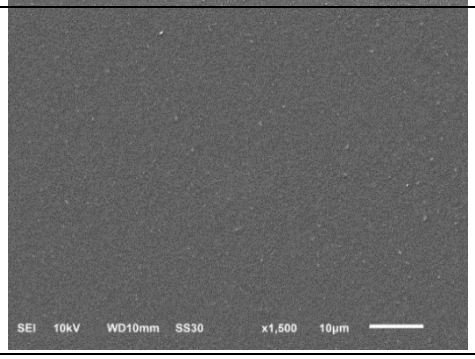	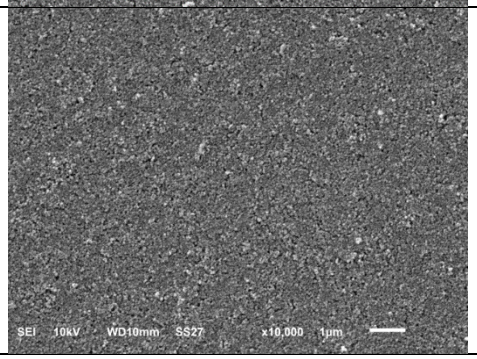

Appendix C. Photodegradation test of TiO2 coated borosilicate glass slides

To evaluate photocatalytic properties performance of the catalyst-coated borosilicate glass slides, methylene blue (MB) dye was adopted as an indicator compound and used in all photodegradation tests. All tests were conducted in batch. For each test, 200 mL MB solution with the concentration of 2 mg/L was prepared in a 250 mL glass beaker. After sufficient mixing, the coated glass slide was immersed in the beaker for 30 min to reach the adsorption and desorption balance prior to the photodegradation test. Meanwhile, UV lamp was preheated. Uncoated glass slides were used in control experiments.

The first sample was collected before the MB solution was exposed to UV and this sample was used to calculate the initial concentration of the MB in the solution. Then with the UV irradiation, 1 mL of the MB solution was sampled from the beaker at 10 min intervals during the first 1 h; samples were collected every 30 min during the 2^{nd} hour of the test. The whole experiment lasted for 2 h and the total of nine samples were collected. The MB concentration in each sample was measured using UV spectrophotometer. According to Beer-Lambert law, the concentration of MB is directly proportional to its absorbance. Thus, the degradation efficiency of the TiO_2 coated glass slide, which is usually expressed as a ratio of degraded concentration to initial concentration, can be calculated from the values of MB solution absorbance.

Figure C.1 shows the photodegradation performance of different coating layers. For coatings with fewer than five TiO_2 layers, MB degradation performance increased with an increase in the number of coats/layers. However, when coating included more than eight layers, the MB degradation

efficiencies were similar and the maximum degradation efficiencies were observed in tests with 10 layers. Thus 10 layers coating was selected as optimal.

Figure C.2 demonstrates the change of degradation rate with the increased amount of catalyst. At the initial stage, degradation rate improved with the increased amount of catalyst. Nevertheless, for the tests with the glass slides of more than 10 layers coatings, although more catalysts were deposited on the glass slides, the degradation efficiency remained stable. This trend indicated that the increased amount of catalysts contributed to the increase of the coating thickness but not the available area for photoactivity. In summary, according to the analysis on the photodegradation of MB in batch, 10 layers coating was selected.

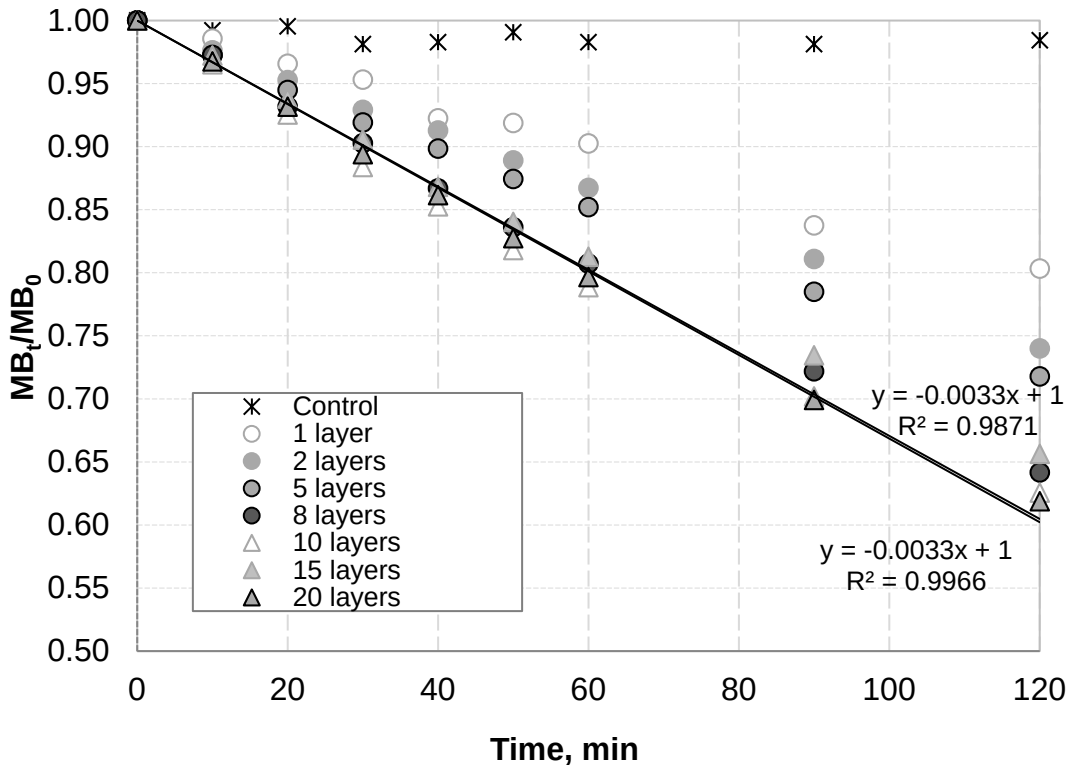

Figure C.1 Photodegradation of MB using borosilicate glass slides with different coating layers

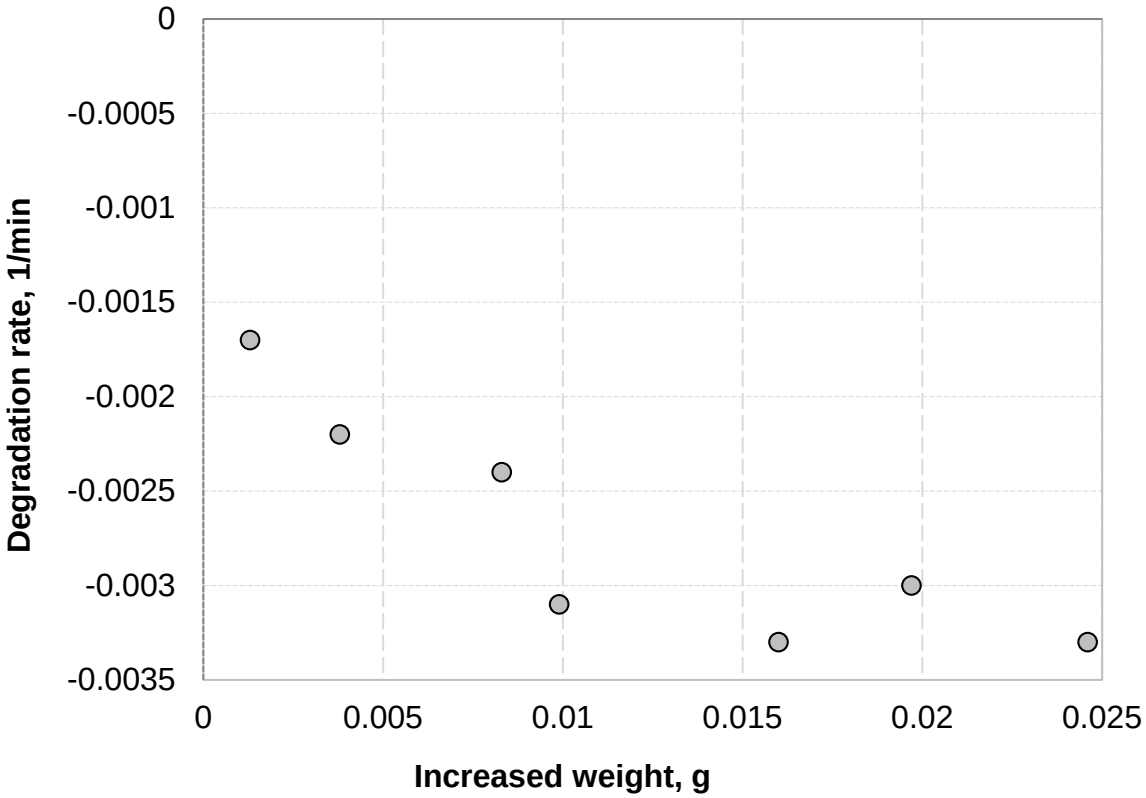

Figure C.2 The change of degradation rate with the increased amount of TiO_2 catalysts

REFERENCES

REFERENCES

[1] A. Zakersalehi, H. Choi, J. Andersen, D.D. Dionysiou, Photocatalytic ceramic membranes, in: E.M.V. Hoek, V.V. Tarabara (Eds.) Encyclopedia of Membrane Science and Technology, John Wiley & Sons, 2013.

[2] S. Leong, A. Razmjou, K. Wang, K. Hapgood, X. Zhang, H. Wang, TiO2 based photocatalytic membranes: A review, J. Membr. Sci., 472 (2014) 167-184.

[3] T. Matsunaga, R. Tomoda, T. Nakajima, H. Wake, Photoelectrochemical sterilization of microbial cells by semiconductor powders, FEMS Microbiol. Lett., 29 (1985) 211-214.

[4] M.N. Chong, B. Jin, C.W.K. Chow, C. Saint, Recent developments in photocatalytic water treatment technology: A review, Water Res., 44 (2010) 2997-3027.

[5] O.K. Dalrymple, E. Stefanakos, M.A. Trotz, D.Y. Goswami, A review of the mechanisms and modeling of photocatalytic disinfection, Appl. Catal. B, 98 (2010) 27-38.

[6] S. Pigeot-Remy, F. Simonet, E. Errazuriz-Cerda, J.C. Lazzaroni, D. Atlan, C. Guillard, Photocatalysis and disinfection of water: Identification of potential bacterial targets, Appl. Catal. Environ., 104 (2011) 390-398.

[7] J.C. Sjorgen, R.A. Sierka, Inactivation of phage MS2 by iron-aided titanium dioxide photocatalysis, Appl. Environ. Microbiol. , 60 (1994) 344-347.

[8] Q. Li, M.A. Page, B.J. Marinas, J.K. Shang, Treatment of coliphage MS2 with palladium-modified nitrogen-doped titanium oxide photocatalyst illuminated by visible light, Environ. Sci. Technol., 42 (2008) 6148-6153.

[9] J. Lee, K. Zoh, G. Ko, Inactivation and UV disinfection of murine norovirus with TiO2 under various environmental conditions, Appl. Environ. Microbiol., 74 (2008) 2111-2117.

[10] D. Gerrity, H. Ryu, J. Crittenden, M. Abbaszadegan, Photocatalytic inactivation of viruses using titanium dioxide nanoparticles and low-pressure UV light, J. Environ. Sci. Health A, 43 (2008) 1261-1270.

[11] H. Choi, M.G. Antoniou, A.A. de la Cruz, E. Stathatos, D.D. Dionysiou, Photocatalytic TiO2 films and membranes for the development of efficient wastewater treatment and reuse systems, Desalination, 202 (2007) 199-206.

[12] H. Zhang, H. Zhao, P. Liu, S. Zhang, G. Li, Direct growth of hierarchically structured titanate nanotube filtration membrane for removal of waterborne pathogens, J. Membr. Sci., 343 (2009) 212-218.

[13] N. Ma, X. Fan, X. Quan, Y. Zhang, Ag–TiO2/HAP/Al2O3 bioceramic composite membrane: Fabrication, characterization and bactericidal activity, J. Membr. Sci., 336 (2009) 109-117.

[14] L. Liu, Z.Y. Liu, H.W. Bai, D.D. Sun, Concurrent filtration and solar photocatalytic disinfection/degradation using high-performance Ag/TiO2 nanofiber membrane, Water Res., 46 (2012) 1101-1112.

[15] R. Goei, T.-T. Lim, Ag-decorated TiO2 photocatalytic membrane with hierarchical architecture: Photocatalytic and antibacterial activities, Water Res., 59 (2014) 207-218.

[16] R.A. Damodar, S.-J. You, H.-H. Chou, Study the self cleaning, antibacterial and photocatalytic properties of TiO2 entrapped PVDF membranes, J. Hazard. Mater., 172 (2009) 1321-1328.

[17] M. Pelaez, N.T. Nolan, S.C. Pillai, M.K. Seery, P. Falaras, A.G. Kontos, P.S.M. Dunlop, J.W.J. Hamilton, J.A. Byrne, K. O'Shea, M.H. Entezari, D.D. Dionysiou, A review on the visible light active titanium dioxide photocatalysts for environmental applications, Appl. Catal. Environ., 125 (2012) 331-349.

[18] A. Julbe, D. Farrusseng, C. Guizard, Porous ceramic membranes for catalytic reactors—overview and new ideas, J. Membr. Sci., 181 (2001) 3-20.

[19] K. Nakata, A. Fujishima, TiO2 photocatalysis: Design and applications, J. Photochem. Photobiol. C, 13 (2012) 169- 189.

[20] F. Bosc, A. Ayral, C. Guizard, Mesoporous anatase coatings for coupling membrane separation and photocatalyzed reactions, J. Membr. Sci., 265 (2005) 13-19.

[21] C.M. Teschke, K.N. Parent, 'Let the phage do the work': Using the phage P22 coat protein structures as a framework to understand its folding and assembly mutants, Virology, 401 (2010) 119-130.

[22] K.N. Parent, R. Khayat, L.H. Tu, M.M. Suhanovsky, J.R. Cortines, C.M. Teschke, J.E. Johnson, T.S. Baker, P22 Coat Protein Structures Reveal a Novel Mechanism for Capsid Maturation: Stability without Auxiliary Proteins or Chemical Crosslinks, Structure, 18 (2010) 390-401.

[23] K.N. Parent, R.S. Sinkovits, M.M. Suhanovsky, C.M. Teschke, E.H. Egelman, T.S. Baker, Cryo-reconstructions of P22 polyheads suggest that phage assembly is nucleated by trimeric interactions among coat proteins, Physical Biology, 7 (2010).

[24] J.R. Cortines, P.R. Weigele, E.B. Gilcrease, S.R. Casjens, C.M. Teschke, Decoding bacteriophage P22 assembly: Identification of two charged residues in scaffolding protein responsible for coat protein interaction, Virology, 421 (2011) 1-11.

[25] Y. Masago, T. Shibata, J.B. Rose, Bacteriophage P22 and Staphylococcus aureus attenuation on nonporous fomites as determined by plate assay and quantitative PCR, Appl. Environ. Microbiol., 74 (2008) 5838-5840.

[26] C.P. Shen, M.S. Phanikumar, T.T. Fong, I. Aslam, S.P. McElmurry, S.L. Molloy, J.B. Rose, Evaluating bacteriophage P22 as a tracer in a complex surface water system: The Grand River, Michigan, Environ. Sci. Technol., 42 (2008) 2426-2431.

[27] B. Ohtani, O.O. Prieto-Mahaney, D. Li, R. Abe, What is Degussa (Evonik) P25? Crystalline composition analysis, reconstruction from isolated pure particles and photocatalytic activity test, J. Photochem. Photobiol. A, 216 (2010) 179-182.

[28] W.Y. Wang, A. Irawan, Y. Ku, Photocatalytic degradation of Acid Red 4 using a titanium dioxide membrane supported on a porous ceramic tube, Water Res., 42 (2008) 4725-4732.

[29] R.O. Rahn, P. Xu, S.L. Miller, Dosimetry of room-air germicidal (254 nm) radiation using spherical actinometry, Photochem. Photobiol., 70 (1999) 314.

[30] R.O. Rahn, J. Bolton, M.I. Stefan, The iodide/iodate actinometer in UV disinfection: Determination of the fluence rate distribution in UV reactors, Photochem. Photobiol., 82 (2006) 611-615.

[31] R.O. Rahn, S. Echols, Iodide/iodate chemical actinometry using spherical vessels for radiation exposure as well as for monitoring absorbance changes, Photochem. Photobiol., 86 (2010) 990-993.

[32] R.O. Rahn, Potassium iodide as a chemical actinometer for 254 nm radiation: Use of iodate as an electron scavenger, Photochem. Photobiol., 66 (1997) 450-455.

[33] R.O. Rahn, M.I. Stefan, J.R. Bolton, E. Goren, P.S. Shaw, K.R. Lykke, Quantum yield of the iodide-iodate chemical actinometer: Dependence on wavelength and concentration, Photochem. Photobiol., 78 (2003) 146-152.

[34] EPA, Method 1602: Detection of male-specific (F+) and somatic coliphage in water by single agar layer (SAL) procedure, in: Office of Water, Engineering and Analysis Division, Washington, DC, 2001.

[35] Z. Bukhary, J. Hargy, B. Bolton, B. Dussert, J. Clancy, Inactivation of Cryptosporidium parvum oocysts using medium=pressure ultraviolet light, in: Proceedings of AWWA annual conference, Dallas, TX, 1998.

[36] K.G. Linden, G.-A. Shin, G. Faubert, W. Cairns, M.D. Sobsey, UV disinfection of Giardia lamblia cysts in water, Environ. Sci. Technol., 36 (2002) 2519-2522.

[37] F. Loge, K. Bourgeous, R. Emerick, J. Darby, Variations in wastewater quality parameters influencing UV disinfection performance: Relative impact of filtration, J. Environ. Eng. ASCE, 127 (2001) 832-837.

[38] J. Oppenheimer, T. Gillogly, G. Stolarik, R. Ward, Comparing the efficiency of low and medium pressure UV light for inactivating Giardia muris and Cryptosporidium parvum in waters with low and high levels of turbidity, in: Annual Conference and Exhibition of the American Water Works Association, New Orleans, LA, 2002.

[39] H. Collins, R. Selleck, G.C. White, Problems in obtaining adequate sewge dinsinfection, J. San. Eng. Div. ASCE, 97 (1971) 549-562.

[40] R. Selleck, B. Saunier, Kinetics of bacterial deactivation with chlorine, J. Environ. Eng. ASCE, 104 (1978) 1197-1212.

[41] C.J. Brinker, T.L. Ward, R. Sehgal, N.K. Raman, S.L. Hietala, D.M. Smith, D.W. Hua, T.J. Headley, Ultramicroporous silica-based supported membranes, J. Membr. Sci., 77 (1993) 165-179.

[42] J.H. Park, W.S. Kim, D.-H. Jo, J.S. Kim, J.M. Park, Effect of Ce conversion underlayer coating on the photo-catalytic activity of TiO2 sol-gel film deposited on hot-dip GI, J. Ind. Eng. Chem., 20 (2014) 1965-1972.

[43] H. Zhang, X. Quang, S. Chen, H. Zhao, Y. Zhao, Fabrication ofphotocatalytic membrane and evaluation its efficiencyinremoval oforganic pollutants from water, Separ. Purif. Technol., 50 (2006) 147-155.

[44] E. Chevereaua, N. Zouaouib, L. Limousya, P. Dutourniéa, S. Déonc, P. Bourseaud, Surface properties of ceramic ultrafiltration TiO2 membranes: Effects of surface equilibriums on salt retention, Desalination, 255 (2010) 1-8.

[45] J. Mendret, M. Hatat-Fraile, M. Rivallin, S. Brosillon, Hydrophilic composite membranes for simultaneous separation and photocatalytic degradation of organic pollutants, Separ. Purif. Technol., 111 (2013) 9-19.

[46] R. Wang, K. Hashimoto, A. Fujishima, M. Chikuni, E. Kojima, A. Kitamura, M. Shimohigoshi, T. Watanabe, Light-induced amphiphilic surfaces, Nature, 388 (1997) 431-432.

[47] R. Wang, K. Hashimoto, A. Fujishima, M. Chikuni, E. Kojima, A. Kitamura, M. Shimohigoshi, T. Watanabe, Photogeneration of highly amphiphilic TiO2 surfaces, Adv. Mater., 10 (1998) 135-138.

[48] E.V. Pasco, H. Shi, I. Xagoraraki, S.A. Hashsham, K.N. Parent, M.L. Bruening, V.V. Tarabara, Polyelectrolyte multilayers as anti-adhesive membrane coatings for virus concentration and recovery, J. Membr. Sci., 469 (2014) 140-150.

[49] W. Kowalski, UVGI for air and surface disinfection, in: Ultraviolet Germicidal Irradiation Handbook, 2009.

[50] E. Tsolaki, E. Diamadopoulos, Technologies for ballast water treatment: A review, J. Chem. Technol. Biotechnol., 85 (2010) 19-32.

[51] A.N. Perakis, Z. Yang, Options for nonindigenous species control and their economic impact on the Great Lakes and St. Lawrence seaway: A survey. , Mar. Technol., 40 (2003) 34-41.

[52] S. Montani, L. Mksumpun, K. Ichimi, Chemical and physical treatments for destruction of phytoflagellate cysts, J. Mar. Biotechnol., 2 (1995) 179-181.

[53] A.A. Cangelosi, I.T. Knight, M. Balcer, D. Wright, R. Dawson, C. Blatchley, The Great Lakes Ballast Technology Demonstration project: Biological effectiveness test program (including MV Regal Princess trials), in: International Maritinme Organization 1st International Ballast Water Treatment R&D Symposium, London, UK, 2001, pp. 88-94.

[54] M.A. Champ, Marine Testing Board for certification of ballast water technologies, Mar. Poll. Bull., 44 (2002) 1327-1335.

[55] J. Sassi, S. Viitasalo, J. Rytkönen, E. Leppäkoski, Experiments with ultraviolet light, ultrasound and ozone technologies for onboard ballast water treatment (VTT Research Notes 2313), in, VTT Technical Research Centre of Finland, 2005, pp. 1-80.

[56] X.P. Kong, Y.M. Zhu, M.X. Zhang, X.J. Sun, W. Zhang, Simulated experiment on minimizing the presence of chlorella and bacteria in ballast water by combination of micro-hole filtration and UV radiation, J. Adv. Oxid. Technol., 10 (2007) 186-188.

[57] B. Nilsen, H. Nilsen, T. Mackey, The Optimar ballast system, in: International Maritinme Organization 1st International Ballast Water Treatment R&D Symposium, London, UK, 2001, pp. 126-136.

[58] D.A. Wright, R. Dawson, C.E. Orano-Dawson, S.M. Moesel, A test of the efficacy of a ballast water treatment system aboard the vessel Coral Princess, Mar. Technol., 44 (2007) 57-67.

[59] T.F. Sutherland, C.D. Levings, C.C. Elliott, W.W. Hesse, Effect of a ballast water treatment system on survivorship of natural populations of marine plankton, Mar. Ecol. Prog. Ser., 210 (2001) 139-148.

[60] T.F. Sutherland, C.D. Levings, S. Petersen, W.W. Hesse, Mortality of zooplankton and invertebrate larvae exposed to cyclonic pre-treatment and ultraviolet radiation, Mar. Technol. Soc. J., 37 (2003) 3-12.

[61] Borosilicate. 2009. http://www.refmexgl.com/index.php/catalogo/detalle/producto/9

[62] VWR. VWR VistaVision™ Cover Glasses.

[63] Aldrich, AL-228 Suggestions for Cleaning Glassware.

[64] Ghazzal, M.N., et al., Effect of compressive stress inducing a band gap narrowing on the photoinduced activities of sol-gel TiO2 films. Thin Solid Films, 2011. **520**(3): p. 1147-1154.

[65] Ghazzal, M.N., et al., Photocatalytic degradation of Rhodamine 6G on mesoporous titania films: Combined effect of texture and dye aggregation forms. Applied Catalysis B-Environmental, 2012. **115**: p. 276-284.

[66] Wang, W.Y., A. Irawan, and Y. Ku, Photocatalytic degradation of Acid Red 4 using a titanium dioxide membrane supported on a porous ceramic tube. Water Research, 2008. **42**(19): p. 4725-4732.

[67] Guillard, C., et al., Influence of chemical structure of dyes, of pH and of inorganic salts on their photocatalytic degradation by TiO2 comparison of the efficiency of powder and supported TiO_2. Journal of Photochemistry and Photobiology a-Chemistry, 2003. **158**(1): p. 27-36.

[68] Yang, J., et al., Effects of hydroxyl radicals and oxygen species on the 4-chlorophenol degradation by photoelectrocatalytic reactions with TiO_2-film electrodes. Journal of Photochemistry and Photobiology a-Chemistry, 2009. **208**(1): p. 66-77.

[69] Alinsafi, A., et al., Treatment of textile industry wastewater by supported photocatalysis. Dyes and Pigments, 2007. **74**(2): p. 439-445.

[70] Balasubramanian, G., et al., Evaluating the activities of immobilized TiO_2 powder films for the photocatalytic degradation of organic contaminants in water. Applied Catalysis B-Environmental, 2004. **47**(2): p. 73-84.

[71] Ao, C.H., et al., Photocatalytic decolorization of anthraquinonic dye by TiO_2 thin film under UVA and visible-light irradiation. Chemical Engineering Journal, 2007. **129**(1-3): p. 153-159.

[72] Ghazzal, N.M., et al., A simple procedure to quantitatively assess the photoactivity of titanium dioxide films. Journal of Photochemistry and Photobiology a-Chemistry, 2010. **215**(1): p. 11-16.

CHAPTER 3. PHOTOCATALYTIC INACTIVATION OF HUMAN ADENOVIRUS 40 IN NATURAL SURFACE WATER: EFFECT OF WATER QUALITY

3.1 Introduction

Adenoviruses, members of the family Adenoviridae, are non-enveloped viruses ranging from 70 to 90 nm in diameter and are icosahedral in shape [1]. Represented by 7 species (A through G) and 51 serotypes [1], adenoviruses are double-stranded DNA viruses, ubiquitous in the aqueous environment . Adenoviruses have been shown to be the etiologic agents of various types of diseases, including respiratory infections, conjunctivitis, gastroenteritis and pneumonia [2]. The viruses can be transmitted through direct contact, fecal-oral transmission or occasionally waterborne transmission [2]. The most common symptoms of HAdV infection are fever and coughing; however, life-threatening multi-organ diseases can also be caused by HAdV infection in extreme cases [3]. Adenoviruses have been on the Drinking Water Contaminant Candidate List of the U.S. Environmental Protection Agency (EPA) since 1998 [4].

Numerous studies have shown that adenoviruses can be stable for days and even months in water and on dry surfaces [5, 6]. Moreover, adenoviruses have been recognized as the most UV-resistant virus known to date, requiring a much higher dose for disinfection than other EPA regulated viruses [7] (see Appendix, Fig. S.1). This property is associated with the double-stranded DNA: it has been demonstrated that the viruses can utilize the host cell's DNA repairing capability [8, 9]. Since both DNA strands can serve as a template for replication, when only one of them is damaged by external factors (e.g. UV light irradiation), the other strand can still be used to repair the damaged sites [9]. The U.S. EPA has specified a UV dose of 186 mJ/cm^2 for achieving a 4-log inactivation of all viruses (99.99% removal) [10]. However, human adenovirus serotype 40

(HAdV40) requires a UV dose of up to 226 mW/cm^2 to achieve a 4-log reduction [11]. HAdV40 has been identified as the most UV resistant serotype of the adenoviruses [12]. Species F of HAdV40 has been recognized as a very important pathogenic agent associated with gastroenteritis, primarily in children [13-16]. Every year, millions of deaths are caused by adenoviruses, costing billions of dollars worldwide [17]. The concerns over the health risks of adenoviruses prompt further research on the disinfection of these microorganisms.

Effective against a variety of waterborne pathogens [18-20], photocatalytic disinfection offers an alternative to traditional disinfection by chlorine. However, much of the reported studies on photocatalytic disinfection focus only on bacteria [21-23], particularly using E. coli as an indicator organism, which may not be representative of viruses [24-30]. The studies that have examined the inactivation of viruses with photochemical methods have often used bacteriophages, such as MS2 or P22, as their target agents [31-34]. Human viruses, such as adenoviruses, have received much less attention, due the more challenging culturing protocols. To our knowledge, there have been only three published reports on the photocatalytic disinfection of adenoviruses [35-37]. All three studies used UV as the light source. Gorvel et al. [35] and Li et al. [36] coupled UV irradiation with titanium dioxide for inactivation of replication-deficient recombinant adenoviruses and serotype 5 adenoviruses. Bounty et al. [37] used H_2O_2 in the UV treatment of serotype 2 adenoviruses. The photocatalytic inactivation of human adenovirus serotype 40 has not been explored. This knowledge is needed, given the essential role of HAdV40 as an etiologic agent of waterborne disease and it is resistance to UV disinfection.

An important challenge to photocatalytic disinfection is the influence of natural organic matter, which can quench the ROS produced as disinfectants. Recent work has pointed to the importance of NOM interactions with photocatalytic processes and noted a distinction between surface-based and bulk quenching of radicals [38]. None of the aforementioned studies on adenovirus disinfection investigated the role of NOM in the photocatalytic process [39]. The nature of these interactions is important when considering strategies to mitigate the quenching. Membrane filtration may provide a route to eliminate key fractions of NOM that quench ROS.

The goal of this study is twofold. First, we investigate the kinetics of photocatalytic disinfection of HAdV40 in DI water and filtered surface water of different quality. Second we evaluate a photocatalytic membrane reactor as a method for high throughput inactivation and removal of HAdV40.

3.2 Experimental

3.2.1 Reagents

Aeroxide TiO_2 P25 powder was provided by Evonik Industries. Minimum essential medium (MEM), sodium pyruvate solution (100 mM), trypsin 1×, modified eagle's medium eagle non-essential amino acid solution (NEAA), HEPES buffer (1 M), 1×PBS with W/EDTA (pH=7.4), antibiotic-antimycotic solution, and kanamycin sulfate solution (5,000 µg/mL) were purchased from VWR International. Cell culture Tris-buffered saline solution (10×) was purchased from Fisher Scientific International, Inc. Fetal bovine serum (FBS) was purchased from Atlanta Biologicals, Inc. Ultrapure water (~ 17 MΩ/cm) was produced by a Barnstead E-pure water purification system (Thermo Fisher Scientific). Polyelectrolytes used for the LbL deposition of catalyst included reagent grade polydiallyldimethylammonium chloride (PDADMAC, Aldrich, MW 100,000 -200,000 Da), and polyacrylic acid (Aldrich, MW 1,800 Da). Commercially available titanium dioxide (Evonik P25) was used as a catalyst in all coatings.

3.2.2 A549 cell line and HAdV40 propagation

HAdV40 was obtained from the American Type Culture Collection (ATCC) and propagated in A549 cell lines (human carcinoma cells). A549 cell lines were propagated in growth medium (containing 10% FBS, see Appendix, Table S.1, for the complete composition of the growth medium) until the confluence reached 80%; after that growth medium was replaced with maintenance medium (containing 2% FBS) to retain cell activity. Typically, maintenance medium was renewed every three days.

The HAdV40 propagation process was conducted as follows: when the monolayer cell line was determined to reach confluence of at least 80%, the old medium was emptied from the 150 cm^2 tissue culture flask and the monolayer cell line was rinsed with sterile, Tris-buffered saline. Afterwards, 4 mL of HAdV40 stock were added into each flask, which were then incubated at 37 °C and vigorously shaken every 15 min for 1 to 1.5 h. After the incubation, 46 mL of maintenance medium were added to each flask sequentially and then all flasks were incubated for 3 to 4 days until 90% of the cell monolayer was destroyed. The flasks were frozen and thawed three times, then the entire mixture was transferred to 50 mL centrifuge tubes and centrifuged at 12,000g at 4°C for 10 min [37]. After centrifugation, the supernatant was filtered using 0.22 µm syringe filter to remove cell debris. The filtrate was stored at −80 °C and used as HAdV40 stock in filtration experiments.

3.2.3 Batch UV photoreactor

Figure 3.1 shows the schematic of the photoreactor used in the batch UV disinfection experiments. The photoreactor has two chambers connected through a circular opening 9.3 cm in diameter. In the upper chamber, a preheated germicidal UV lamp (16 W, model GPH330T5L/4, Atlantic Ultraviolet Corp.) was fixed above the center of the opening. The temperature within reactor was maintained constant by circulating air by a fan. A beaker with a solution was placed in the lower chamber and the solution was mixed with a magnetic stirrer to ensure its homogeneous irradiation by the UV light. A shutter positioned between two chambers controlled the irradiance of UV light to the solution.

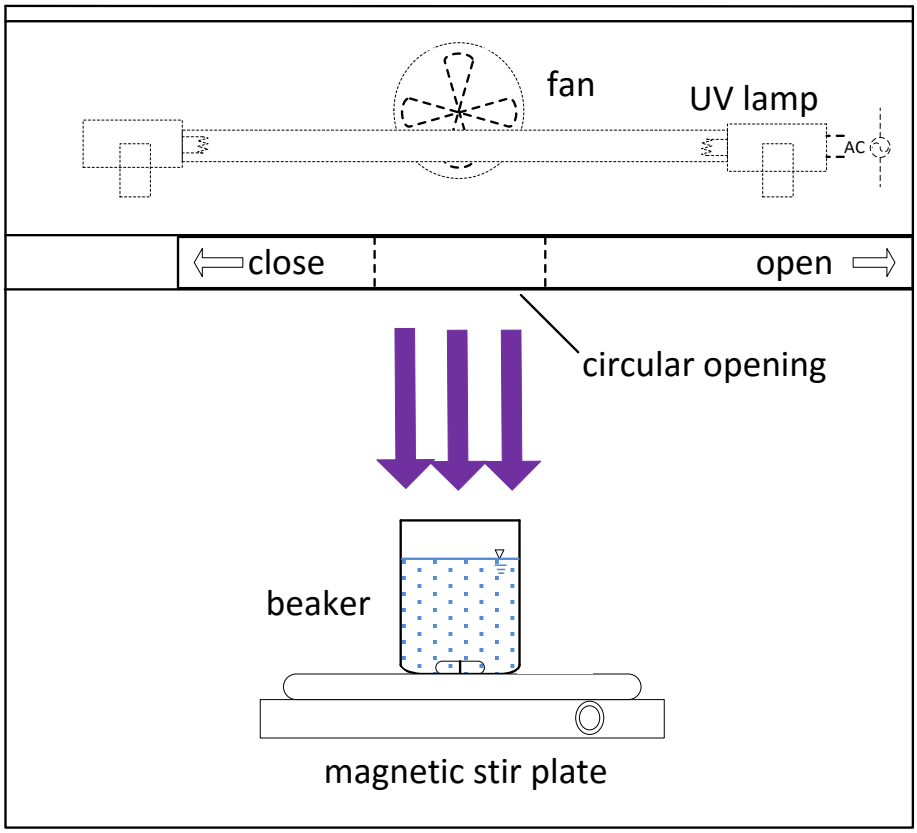

Figure 3.1 Schematic diagram of the batch UV reactor

3.2.4 Photocatalytic membrane and membrane reactor

A tubular ceramic (TiO_2) membrane (TAMI Industries) with the nominal pore size of 0.8 µm was coated with TiO_2 nanoparticles (100% anatase, Sigma) by the layer-by-layer method as described earlier [40]. The design of the photocatalytic membrane reactor was also described previously [41]. Crossflow rate and permeate mass flow rate were automatically logged into a computer at 1 s intervals. The crossflow rate was maintained constant in the 1.1 to 1.2 L/min range, which translates to the crossflow velocity of ~ 0.17 m/s. Transmembrane pressure was measured by two pressure gauges installed on the feed and retentate sides of the membrane unit.

3.2.5 Sample collection and storage

Surface water was collected from Lake Lansing at the boat ramp in Lake Lansing Park-South (Haslett, MI) in November, 2015 and stored at 4 ^{o}C. All feed water samples were characterized in for UV/Vis absorbance (MultiSpec 1501 spectrophotometer, Shimadzu) and total organic carbon (TOC) content. The TOC in each water sample was measured at least in triplicate (OI Analytical model 1010 analyzer, OI Analytical, College Station, TX). In batch tests, samples were collected at 0, 1, 5, 10, 15, 20, 30, 45, and 60 min into each experiment and stored in 5 mL cryogenic vials at −80 °C. In crossflow filtration experiments, samples of both feed and permeate solutions were collected. Feed solution was withdrawn from the feed tank prior to the start of the filtration test. Permeate samples were first collected into a foil-wrapped Erlenmeyer flask positioned on an electronic mass balance, and then after the filtration, three or four mL sample was withdrawn from the flask for qPCR analysis. The remaining permeate solution was transferred to the pressurized tank (see Appendix, Fig. S.2) for concentration using 50 kDa ultrafiltration membrane discs (PBQK06210, EMD Millipore) and then the concentrated samples were used for cell culture assays. All the samples were stored in a −80 °C freezer.

3.2.6 Lake water pre-treatment

In batch tests, both raw lake water and pre-filtered lake water were tested. Lake water was pre-filtered through membranes of one of three different nominal pore sizes: 0.8 µm (tubular TiO_2 membrane, TAMI Industries), 0.45 µm (mixed cellulose esters membrane, HAWP09000, Merck Millipore Ltd.) and 0.03 µm (PVP-treated, low non-specific binding polycarbonate track etch membranes, PCT0039030, Sterlitech Corp.) and stored in separate glass flasks at 4 ^{o}C. In all

crossflow filtration experiments, lake water pre-filtered through 0.45 µm membrane (HAWP09000, Merck Millipore Ltd.) was used to prepare the feed solution.

3.2.7 UV dose quantification

A UVX Radiometer (UVP, LLC) was used to measure the incident light intensity (254 nm) at the surface of the reaction solution. Based on the measured value of 425 $\mu W/cm^2$ for the initial time point, the average fluence throughout the reactor for each water source was estimated using a standard procedure described by Bolton and Linden [43]. The fluence was re-calculated iteratively after each sample aliquot withdrawn to account for the changes in reaction volume.

3.2.8 Photochemical characterization

The batch photochemical reactor was used to determine steady state OH• concentrations in experiments with different waters. The concentrations of OH• was determined indirectly by measuring the degradation of a probe compound, pCBA, with a known rate constant for reaction with OH• ($5 \cdot 10^9$ L $mol^{-1}s^{-1}$) [44]. The degradation of pCBA was measured as a function of irradiation time using a Perkin Elmers Series 200 HPLC equipped with a Waters 2487 Dual Lambda absorbance detector, at 235 nm, and a C-18 column.

3.2.9 Total virus quantification with qPCR

All samples from batch UV and crossflow filtration tests were subjected to qPCR analysis. The DNA extraction process was the same as described earlier [41]. The generic primers and TaqMan probe used for quantification were described previously [45]. The qPCR analysis started with 15 min denaturation at 95 °C then followed by 45 amplification cycles at 95 °C for 10 s, 60 °C for 30

s and 72 °C for 12 s and finally cooling at 40 °C for 30 s. To relate the crossing-point values to the numbers of HAdV40 DNA copies, a standard curve developed earlier was used [45].

3.2.10 Quantification of culturable virus: Cell culture assays and most probable number (MPN) calculation

The culturable virus from both batch and membrane reactor samples was quantified by cell culture assays [46]. Each sample was prepared in a ten-fold series dilutions (10^{-1} to 10^{-4}) and cell culture assays were conducted. First, the monolayer cell line in 25 cm^2 tissue culture was checked for a confluence of at least 90%. The old medium was then emptied and the monolayer of cells was rinsed with sterile Tris-buffered saline (1×). Second, 1 mL of diluted sample was inoculated into a flask. Each diluted sample was analyzed in triplicate. Third, flasks were incubated at 37 °C and vigorously shaken every 15 min for approximately 1 to 1.5 h. After the incubation, the 1 mL sample was decanted and 8 mL of maintenance medium was added. Cytopathic effects (CPE), which indicate viral infection in the cell cultures, were monitored for up to 14 days. Maintenance media in the flasks was changed every 7 days. Positive and negative results of the samples were determined according to the U.S. EPA protocol [46]. The mean concentration of HAdV40 in each sample was estimated using MPN calculator [47].

3.3 Results and discussion

3.3.1 OH• radical production and quenching: Effect of water quality

In order to design an effective PMR, it is critical to understand how permeate quality affects the photocatalytic process. Water quality is an important factor that affects UV fluence and OH• lifetimes. Specifically, DOM is a potent OH• scavenger and typically absorbs UV light effectively. Further, suspended and dissolved organics can scatter light, which, combined with the absorption, reduces the intensity of radiation available for disinfection in the bulk of the water sample. Thus, knowledge of UV absorbance by organic matter is needed for attenuation calculations. Spectrophotometry can also provide insights into the type and quantity of organics in solution.

To explore the effects of permeate water quality on photocatalysis, a photocatalytic batch reactor was used to evaluate the role of OH• in the inactivation of HAdV40. First, raw feed samples were filtered through membranes of different pore sizes and UV absorbance as well total organic content (TOC, Appendix Fig. S.3, Fig. 3.2) were measured. The absorptivity values for DI water containing TiO_2, MEM, or both were also determined to assess the impact of these two constituents (Fig. 3.2). As expected, using membranes with smaller nominal pore sizes led to improved water quality, where improvement is defined as reduced UV absorbance in the UVC range. A notable difference in water quality was observed between samples prefiltered through membranes with 0.45 and 0.03 μm nominal pore sizes. The contribution of MEM (essentially an amino acid mixture, see Appendix, Table S2), was commensurate with that due to organics in the lake water. TiO_2 also exerted significant, broad-band absorption of UV light. Figure 3.2 presents total organic carbon (TOC) and UV_{254} absorbance values in the lake water samples. The small difference in DOC between the 0.03 and 0.45 μm prefiltered samples suggests that membrane selection in this pore

size range does not significantly affect DOC rejection for clean membranes. The difference in DOC rejection for the different filters could become significant with the addition of fouling layers after continued membrane use. Therefore, the effects of DOC concentration on photocatalysis are not expected to be significantly different between the prefiltered lake water samples, since clean membranes were used.

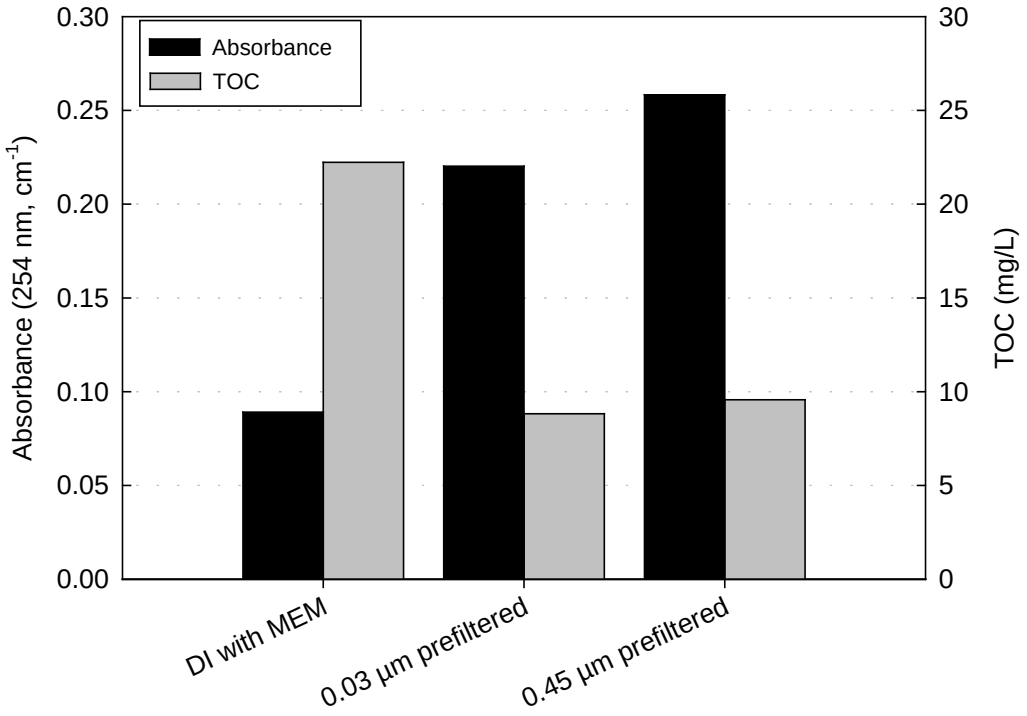

Figure 3.2 UV absorptivity (254 nm) and TOC of water samples used in photocatalytic tests

Note: To parallel the photocatalytic batch experiments (Figures 3.3 ~ 3.7 in sections 3.3.1 and 3.3.2 and Figures S4 and S5 in the Appendix), each water sample contained TiO_2 (0.83 mg/L). In addition, DI water sample contained MEM (1% v/v).

Specific UV absorbance (SUVA), a common metric for the aromaticity of organic matter, is given by UV_{254} absorbance normalized by dissolved organic carbon (DOC) contents of the sample. In this study we used TOC as an estimate of DOC. To maintain this assumption, the raw water and

0.8 μm filtered solutions were not included in the analysis, as they do not meet the requirement of 0.45 μm filtration, a criterion used to operationally define the dissolved fraction of organic carbon in water. SUVA values of 0.40, 2.5, and 2.7 $L \cdot mg^{-1} \cdot m^{-1}$ were obtained for the pure water with 1% MEM, 0.03 μm, and 0.45 μm prefiltered samples, respectively. SUVA is known to be a predictor of chemical reactivity of DOC; disinfection byproduct formation, for example, was shown to increase with increasing SUVA values [51]. Given that SUVA is a predictor of aromaticity of DOC and that aromatic compounds are electron rich, higher SUVA values may also be predictive of higher reactivity with OH•. Increased reactivity of water constituents with OH• would directly correlate to a decrease in efficacy of photocatalytic disinfection; thus waters with high SUVA are likely to inhibit OH• driven disinfection more than those with lower SUVA. If this mechanism proves significant in mediating the photocatalytic efficiency, then higher photoactivity should be observed in DI water with MEM (low SUVA sample) than in the lake water samples.

The observation of pCBA degradation provides a convenient method for the estimation of a pseudo steady state OH• concentration in a photocatalytic reaction. The steady state estimation is possible given the known reaction rate of OH• with pCBA. While it was expected that the presence of DOM would impact the photocatalytic production of OH•, the magnitude of this effect (see Appendix, Fig. S.4) was surprisingly high. The difference in pCBA degradation was not significant in 0.03 μm prefiltered lake water for the cases of direct (i.e. non-photocatalytic) UV and photocatalytic UV. In the lake water, the NOM quenched OH• significantly and more rapidly than the quenching reaction with pCBA. The steady state OH• concentration estimation for pure water resulted in a value of $1.2 \times 10^{-13} \pm 7.2 \times 10^{-15}$ M after subtracting the degradation caused by UV alone.

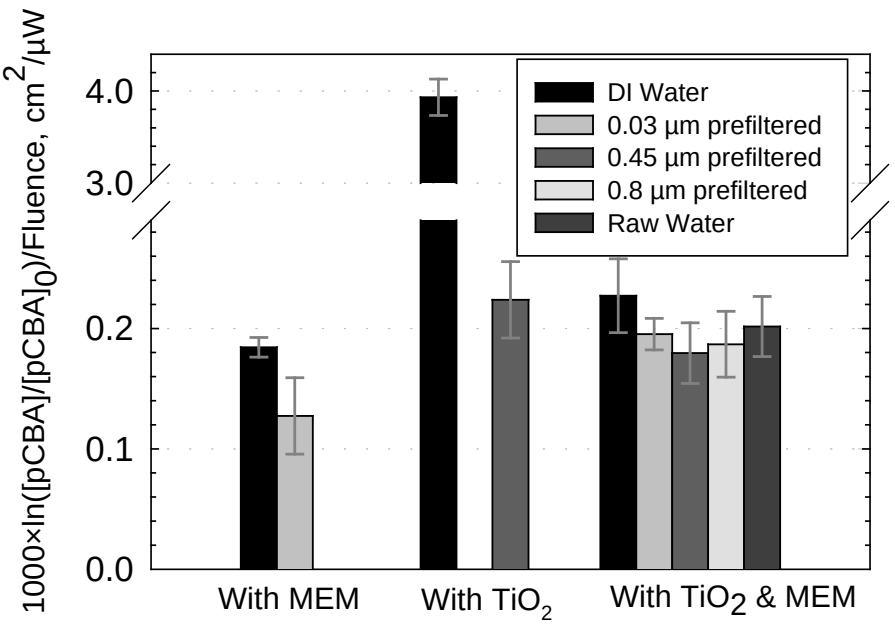

Figure 3.3 Degradation of pCBA normalized by UV_{254} fluence for different water types with and without TiO_2 (0.83 mg/L) and MEM (1%) in the solution

Note: Error bars correspond to 95% confidence intervals for the linear fit of the dependence of pCBA degradation on UV_{254} fluence.

Given the difficulty with distinguishing the degradation of pCBA by direct UV from that caused by reaction with OH•, pCBA degradation rates normalized by fluence (Fig. 3.3) were calculated in lieu of steady state OH• concentrations. The data shows that there is no significant difference between any of the prefiltered lake water samples used for HAdV40 experiments. Likewise, MEM is observed to quench OH• to the same extent as the NOM present in the lake water. Comparing the pure water case to any other sample, it is clear that the DOM exerts a strong quenching action on OH•. If viruses react with OH• more readily than pCBA, then enhanced viral inactivation by photocatalytically produced OH• can be expected even in the presence of DOM.

3.3.2 HAdV40 removal and inactivation in a batch UV reactor

Batch experiments were conducted to investigate the removal and inactivation of HAdV40 in four different waters: (1) raw lake water, (2) lake water prefiltered through 0.8 µm membrane, (3) lake water prefiltered through 0.45 µm membrane and (4) lake water prefiltered through 0.03 µm membrane. UV fluence was measured following the procedure described in section 2.6. Total numbers of HAdV40 were quantified using the qPCR method (see section 2.7).

Figure 3.4 shows log removal values (LRVs) of total HAdV40 as a function of UV fluence. The combined dataset can be fit well (R^2 = 0.9026) by a linear dependence on the UV fluence. Since the qPCR method quantifies the number of organisms by counting the number of target DNA sequences in the sample, the only direct way to reduce the qPCR count is to damage the DNA. Thus, the increased LRVs can be attributed to the UV-induced DNA damage, including dimerization and the oxidation of DNA by ROS formed in the photocatalytic UV process [19].

All experiments were conducted with identical sample time points. The fluence was highest for the experiments conducted with 0.03 µm, due to the relatively lower absorbance in that water type. In samples with higher water quality (i.e. lower TOC values), more UV-induced DNA damage was observed leading to higher LRVs of total HAdV40. The LRVs for each water type at a given fluence value were not significantly different; UV fluence was the main determinant of DNA damage. These observations suggest that water quality impacted the DNA damage pathway via fluence attenuation only.

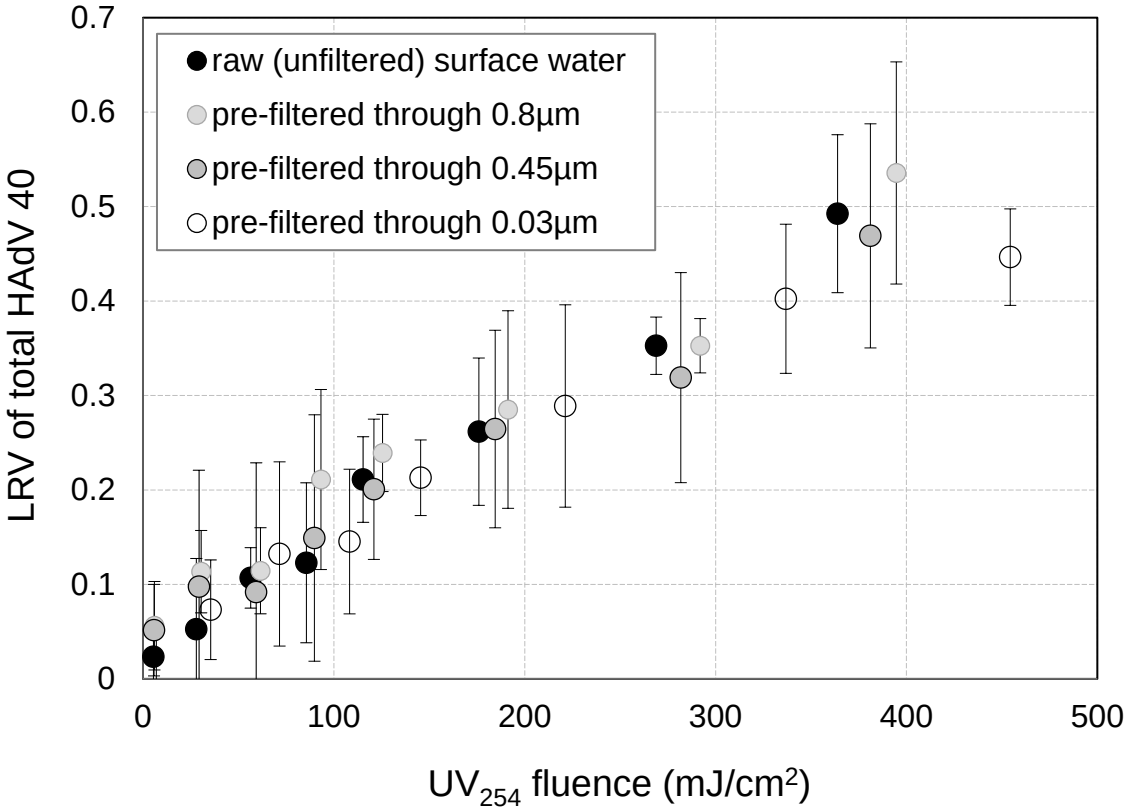

Figure 3.4 Log removal of total HAdV40 (as measured by qPCR) in photocatalytic UV tests with different waters

Note: Error bars represent standard deviations (n = 3).

Comparison of total HAdV40 removal with and without catalysts was performed in lake water pre-filtered through 0.03 µm and 0.45 µm membranes (Fig. 3.5). In each situation, no significant differences in the removal of total virus with and without catalysts were observed. In other words, the presence of TiO_2 catalyst did not cause apparent increase of total HAdV40 removal. Thus, we conclude that UV-induced damage, such as dimerization, rather than the ROS generated during photochemical process was the main mechanism for the total virus removal in high quality water.

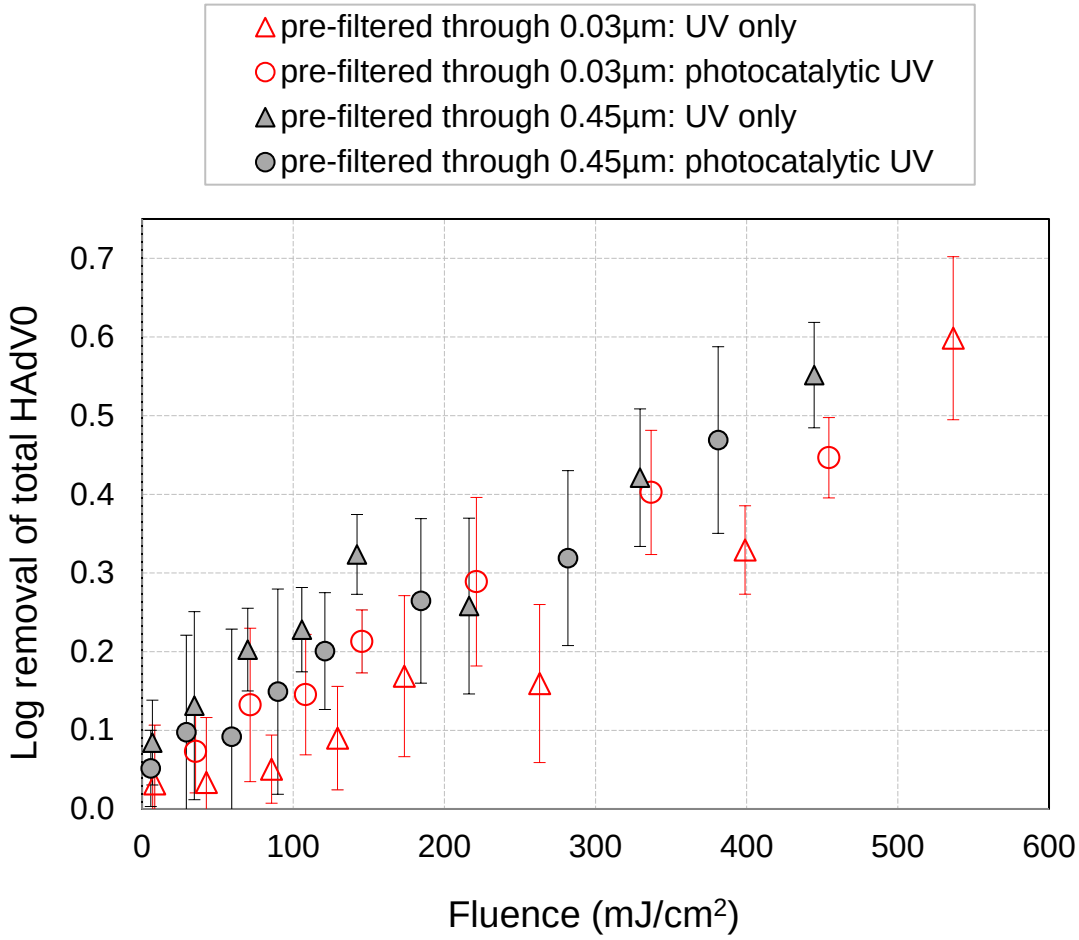

Figure 3.5 Comparison of total HAdV40 removal (as determined by qPCR) by direct UV (-Δ-, -▲-) and by photocatalytic UV (-○-, -●-) in batch inactivation tests

Note: Error bars represent standard deviations (n = 3). The data points representing photocatalytic tests (-○-, -●-) are the same as shown in Figure 3.4.

Figure 3.6 shows LRVs of culturable HAdV40 in different waters. Because of the limitation of the measurement method, no culturable virus could be detected after 10 min in all experiments. Thus, only four samples (initial, 1 min, 5 min and 10 min into the experiment) were analyzed for viable virus concentration in each test. An increase in LRVs with irradiation time was observed for each water type. The LRVs of culturable HAdV40 were much higher (Fig. 3.6) than the LRVs of total

HAdV40 under the same fluence (Fig. 3.5). This enhanced removal efficacy may be attributed to the fact that in addition to the UV-induced DNA damage, the oxidation by reactive oxygen species may also lead to the loss of viability [19]. The cell culture method is more sensitive than the qPCR technique, since it is capable of observing these losses to viability that are not detected with qPCR.

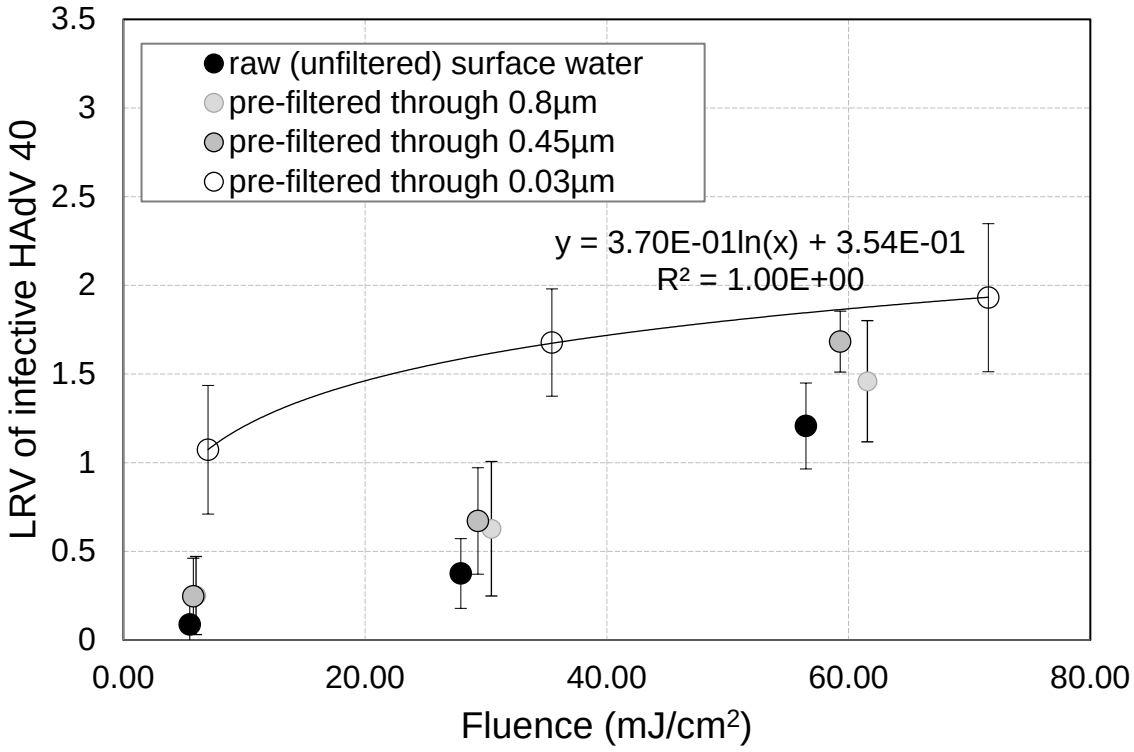

Figure 3.6 Photocatalytic inactivation of culturable HAdV in different waters

Note: Error bars represent standard deviations (n = 3).

LRVs of culturable HAdV40 in lake water pre-filtered through 0.03 µm membrane at all sampling time were much higher than that in the other water samples (i.e. raw, prefiltered through 0.8 µm, prefiltered through 0.45 µm). The kinetics of HAdV40 inactivation in lake water pre-filtered with 0.03 µm membrane fit the Collins-Selleck model [52, 53] reasonably well with Collins-Selleck

coefficient Λ_{CS} = 0.8513 and with the lag coefficient b = 0.6596 mJ/cm^2 (see Appendix, Fig. S.5). The decelerating kinetics showed that at higher UV fluence, the inactivation of HAdV40 exhibited a "tailing" effect, where large increases in fluence resulted in only gradual increases in LRVs. Similar "tailing" effects were also reported in other studies on photocatalytic inactivation of viruses [54, 55]. Possible reasons for tailing include the presence of resistant subpopulation due to genetic or morphological differences [56], aggregated state of viruses [57] and the competition for adsorption sites between the remnants of inactivated viruses and infective viruses [54].

The virus inactivation due to direct UV and photocatalytic oxidation is presented in Figure 3.7. In both waters, the LRVs with UV only were similar, which indicates that water quality has little effect on the viral DNA damage due to dimerization. In water pre-filtered through a 0.03 µm membrane, photocatalytic oxidation appeared to contribute significantly to HAdV40 inactivation, where the LRV due to direct UV was approximately one log lower than that of the photocatalytic process. However, the inactivation of HAdV40 in water pre-filtered through a 0.45 µm membrane relied more on direct UV, especially at low UV fluence. This observation may be attributed to the presence of NOM in water, which consume the OH• produced by the photocatalytic process, thereby reducing the effects of photocatalysis

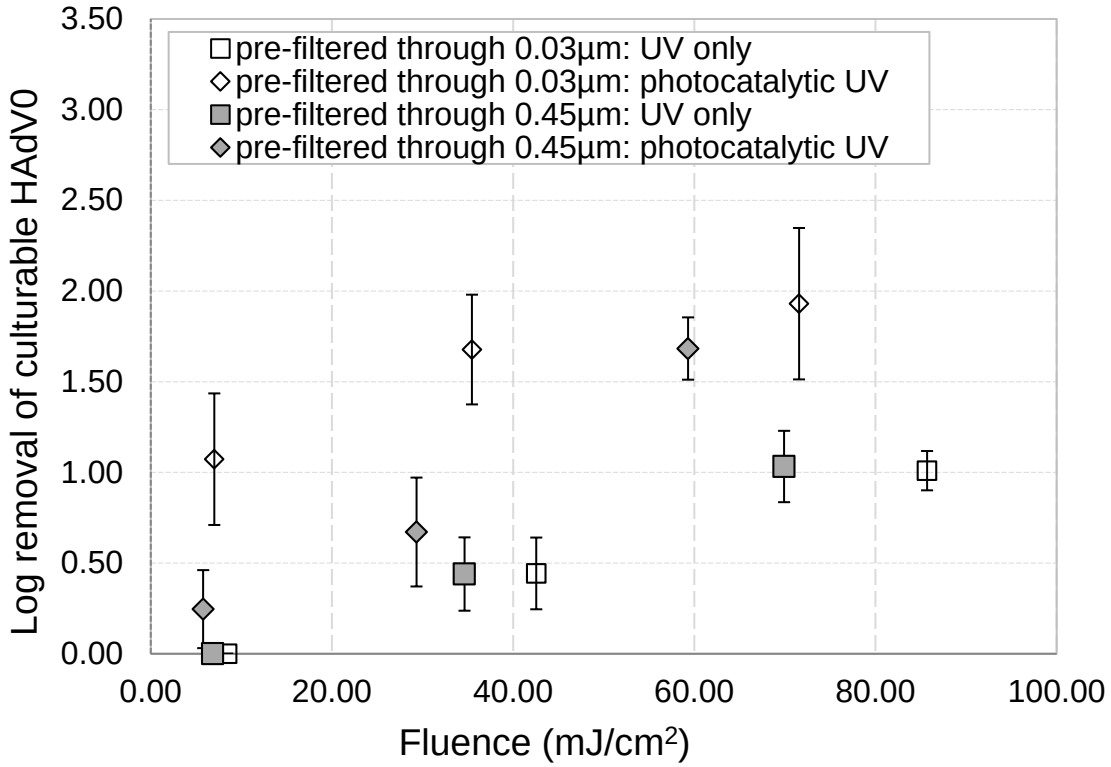

Figure 3.7 Comparison of culturable HAdV40 inactivation with and without catalysts

Note: Error bars represent standard deviations (n = 3).

3.3.3 Virus removal and inactivation in photocatalytic membrane reactor

Three different processes: (1) MF only, (2) non-photocatalytic hybrid MF–UV process, and (3) photocatalytic hybrid MF–UV process, were conducted using the crossflow filtration system. To minimize membrane fouling, lake water used this study was pre-filtered through 0.45 µm membrane. However, a decline in the permeate flux was still observed in all types of filtration processes (see Appendix, Fig. S.2). For one hour filtration, the permeate flux shows a 67±9.7% decline in microfiltration only process, 55±4.9% in the non-photocatalytic hybrid MF-UV process and 31±19.7% in the photocatalytic hybrid MF-UV process. Therefore, with the layer-by-layer TiO_2 coating, the coated membrane shows less permeate flux decline, which indicates that the

coating layer may relieve membrane fouling to some extent. The fully explanation for this improvement caused by coating is unclear and further investigation is needed.

The removal of total HAdV40 was quantified by qPCR for all three processes and expressed in terms of LRV (Fig. 3.8). Permeate samples were collected at 30 min and 60 min into the filtration experiment. Due to the large nominal pore size of the membrane (d_{pore} = 0.8 μm) relative to the diameter of HAdV40 (d_v = 90 to 100 nm) [58], the MF process was the least effective in removing HAdV40 (LRV = 0.96 ± 0.08). The non-photocatalytic hybrid MF–UV process gave LRV of 1.37 ± 0.24 and the photocatalytic hybrid MF–UV process gave the highest LRV of 1.58 ± 0.24.

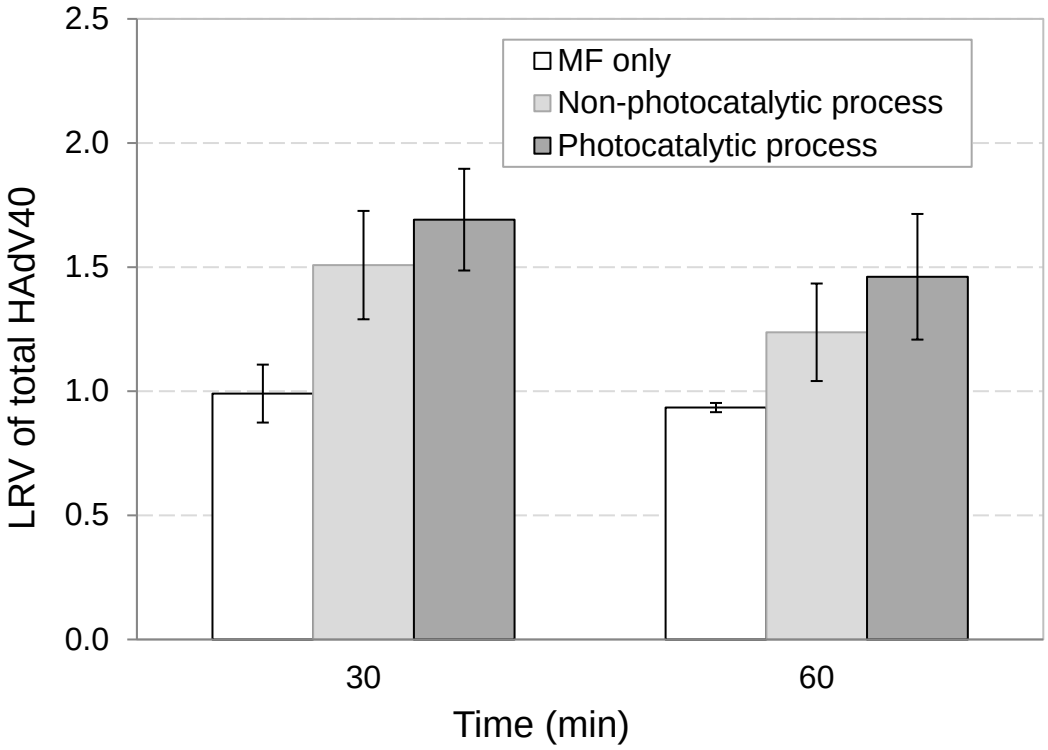

Figure 3.8 Removal of total HAdV40 by (1) microfiltration only (2) non-photocatalytic hybrid MF–UV process and (3) photocatalytic hybrid MF–UV process

Note: Error bars represent standard deviations (n = 3).

Figure 3.9 shows the inactivation of culturable HAdV40 by each of the three processes. The MF process and the non-photocatalytic hybrid MF–UV process have almost same LRVs (2.21 ± 0.02 and 2.09 ± 0.22). By contrast, the removal efficacy of the photocatalytic hybrid MF–UV process is significantly larger: 3.03 ± 0.35. The difference could be a consequence of the combined effect of membrane adsorption, size exclusion (for the possible existence of very small pore size), and the UV-induced inactivation of viruses in the permeate.

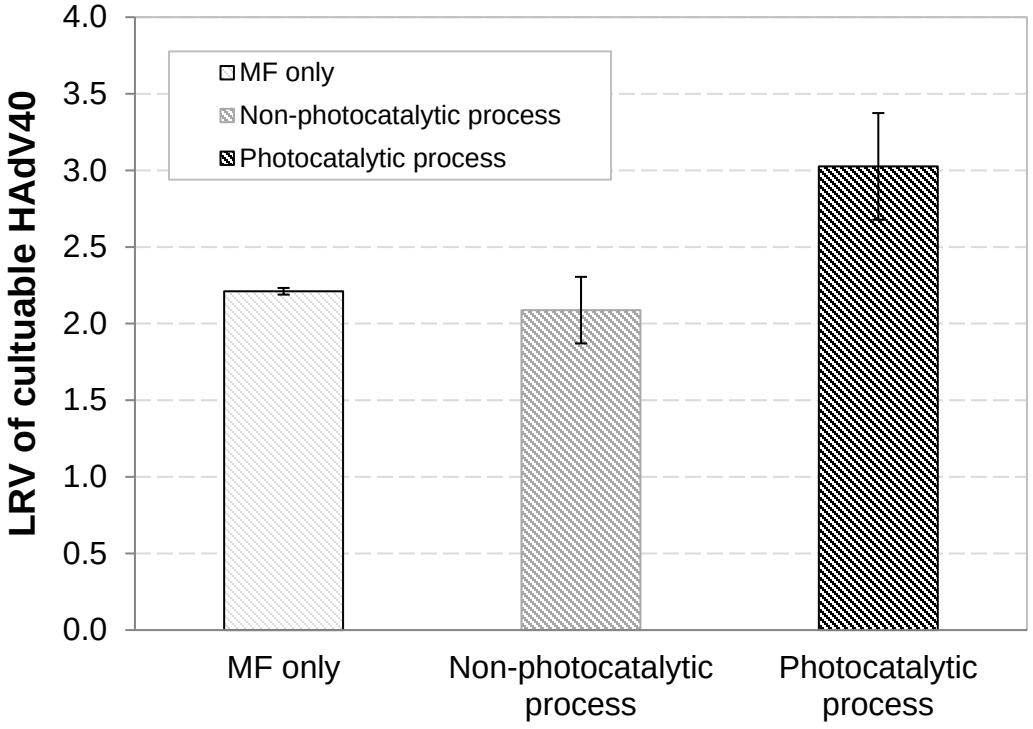

Figure 3.9 Inactivation and/or removal of culturable HAdV40 by microfiltration only, in a sequential MF–UV process, and in a photocatalytic MF membrane reactor

Note: Error bars represent standard deviations (n = 3).

Figure 3.10 provides the ratio of culturable to total HAdV40 in the feed and in the effluent of each of the three treatment processes. Approximately 13.5% of the total virus load in the feed was culturable, and after membrane filtration the ratio decreased to 1.5%. This significant decrease

may due to adsorption, size exclusion and possibly damage to the virus capsid during permeation, leading to infectivity loss. The addition of UV source did not lead to a major change in the viable-to-total ratio. However, after the photocatalytic process, the ratio of culturable to total virus dropped dramatically to 0.1%. This large drop is believed to be a result of the synergistic effects of combining membrane filtration with photocatalytic UV disinfection. The ROS generated at the surface of TiO_2 coating layer can oxidize the protein capsid of viruses, which complements the direct DNA damage due to the germicidal property of the UV lamp.

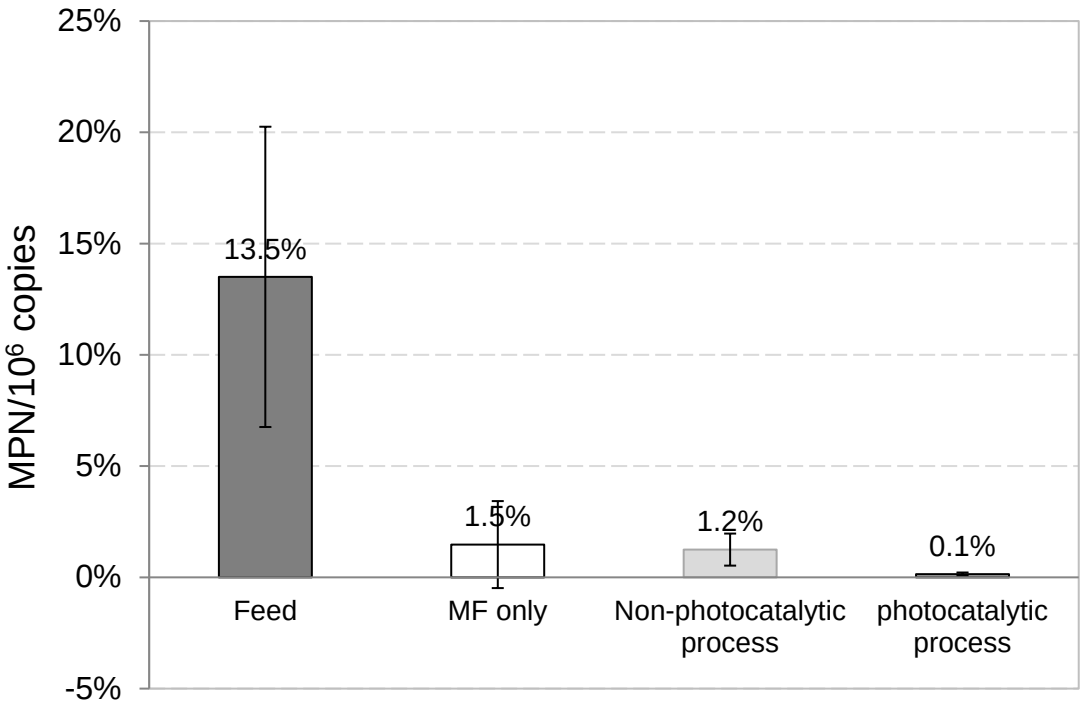

Figure 3.10 Concentration ratio of culturable and total HAdV40 in feed and permeates

Note: Error bars represent standard deviations (n = 3).

In summary, the photocatalytic hybrid MF–UV process developed in our group was successfully applied for turbid water treatment and has proven to be highly efficient in virus removal and inactivation. The combined process overcomes the limitations of UV disinfection due to turbidity and the existence of UV-resistant viruses. Moreover, it also relives the permeate flux decline.

3.4 Conclusions

In this study, we extended the application of the photocatalytic hybrid MF–UV process for the removal and inactivation of widespread naturally occurring virus from natural water resource. The batch experiments conducted with HAdV40 and natural surface water suggested that the inactivation kinetics may varied in different water quality, especially under lower light source. The total virus removal linearly depend on the UV fluence, and the removal mechanism mainly due to the UV-induced DNA dimerization. The removal of culturable virus in higher water quality (e.g. lake water pre-filtered through 0.03 μm membrane) had a "tailing" effect and fit Collins-Selleck model. However, the removals in lower water quality, such as raw lake water, lake water pre-filtered through 0.45 μm and through 0.8 μm membrane, were fit a two-stage linear relationship. To investigate the performance of the photocatalytic hybrid MF-UV process, a number of experiments with filtration alone, non-photocatalytic membrane and photocatalytic membrane were performed respectively. Although challenged with the most UV resistant virus – HAdV40 and complex surface water, the photocatalytic hybrid process showed its superiority as a promising treatment process for water disinfection. It achieved a 96.8% removal of total virus (LRV of 1.58 ± 0.24), while more significantly, a 99.9% inactivation of infectious virus (LRV of 3.03 ± 0.35). Nevertheless, reasons for the improved permeate flux observed by adding UV and TiO_2 coating are still unclear, and further studies are very necessary.

APPENDIX

APPENDIX: Supporting Information

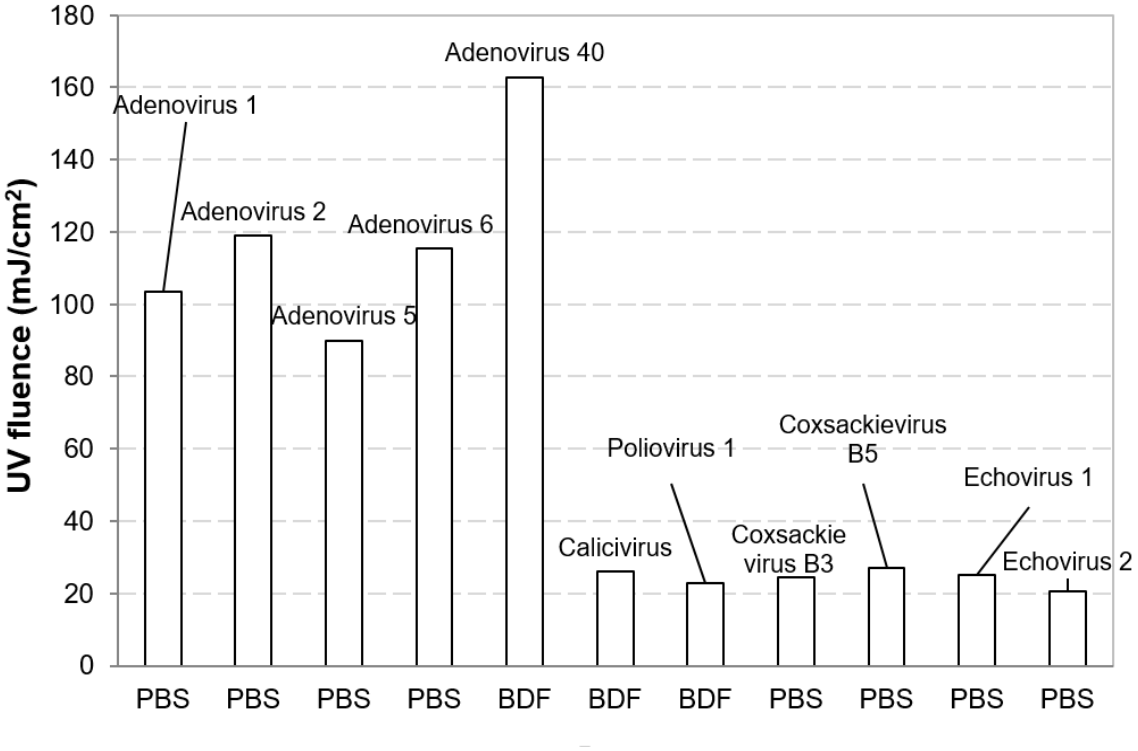

Figure S.1 UV fluence required for 99.9% reduction of representative human enteric viruses

Notes: BDF-buffered demand-free; SDW-sterile distilled water; SEW-steriie estuarine water; PBS-phosphate buffered saline; PBW- phosphate buffered water.

Table S.1 Composition of tissue culture medium

Composition	Volume (mL)	
	Growth medium	**Maintenance medium**
FBS	50	10
antibiotic-antimycotic solution	6	6
kanamycin sulfate solution	6	6
sodium pyruvate solution	6	6
NEAA	6	6
HEPES buffer	10	10
MEM	500	500

Table S.2 Media formulations of Basal Medium Eagle

Amino Acids	Molecular weight, Da	Concentration, mg/L
L-Arginine hydrochloride	211.0	21.0
L-Cystine 2HCl	313.0	16.0
L-Histidine	155.0	8.0
L-lsoleucine	131.0	26.0
L-Leucine	131.0	26.0
L-Lysine hydrochloride	183.0	36.47
L-Methionine	149.0	7.5
L-Phenylalanine	165.0	16.5
L-Threonine	119.0	24.0
L-Tryptophan	204.0	4.0
L-Tyrosine disodium salt dihydrate	261.0	26.0
L-Valine	117.0	23.5

Note: Media purchased from Thermo Fisher Scientific Inc. (Catalog number: 21010-046)

Figure S.2 shows the concentration unit for permeate concentration after crossflow filtration. The stirred dead-end filtration cell (Model 8050, EMD Millipore) was connected to a feed tank (serial NO. 22111-041, Alloy Products Corp.) which was pressurized by compressed nitrogen at 30 psi. Biomax® 50 KDa ultrafiltration membrane discs (PBQK06210, EMD Millipore) was used to concentrate the permeate sample collected in the previous crossflow filtration. This entire process was stopped when the volume of residual solution in filtration cell was about 10 mL. Mass weights of initial permeate from crossflow filtration and final residual solution collected after concentration were measured by mass balance, which were used to calculate concentrate ratio for culturable virus quantification.

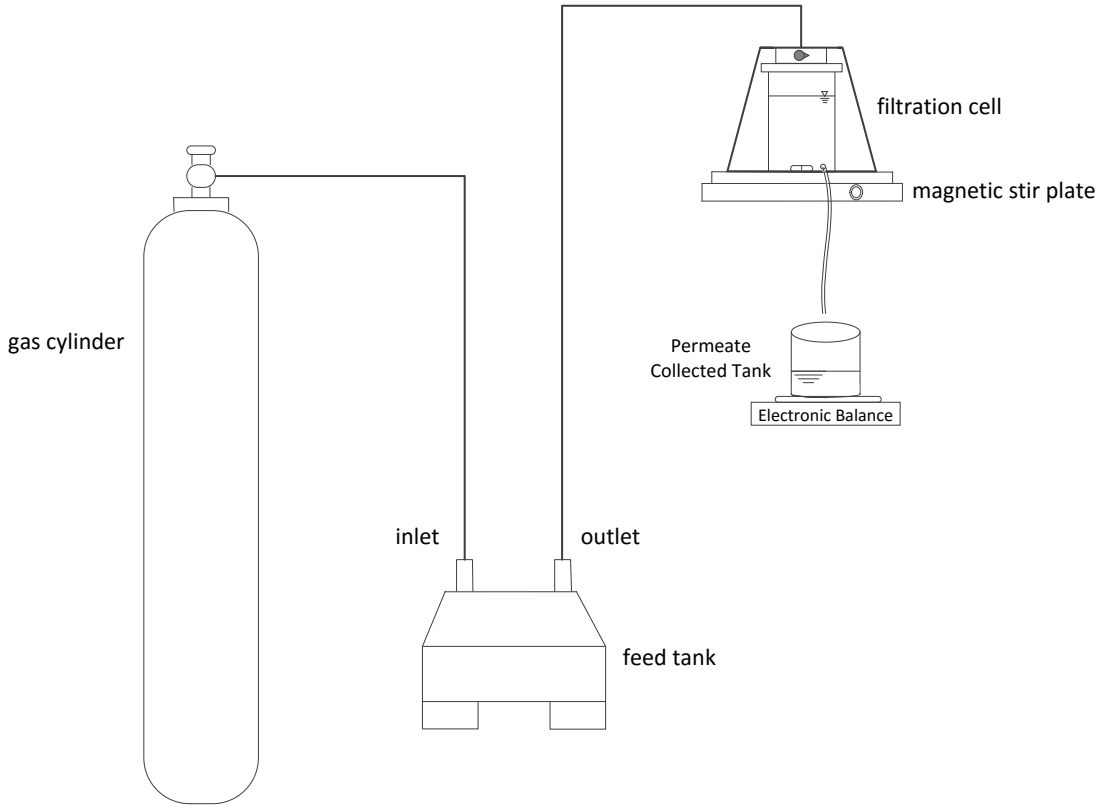

Figure S.2 Schematic diagram of concentrate system

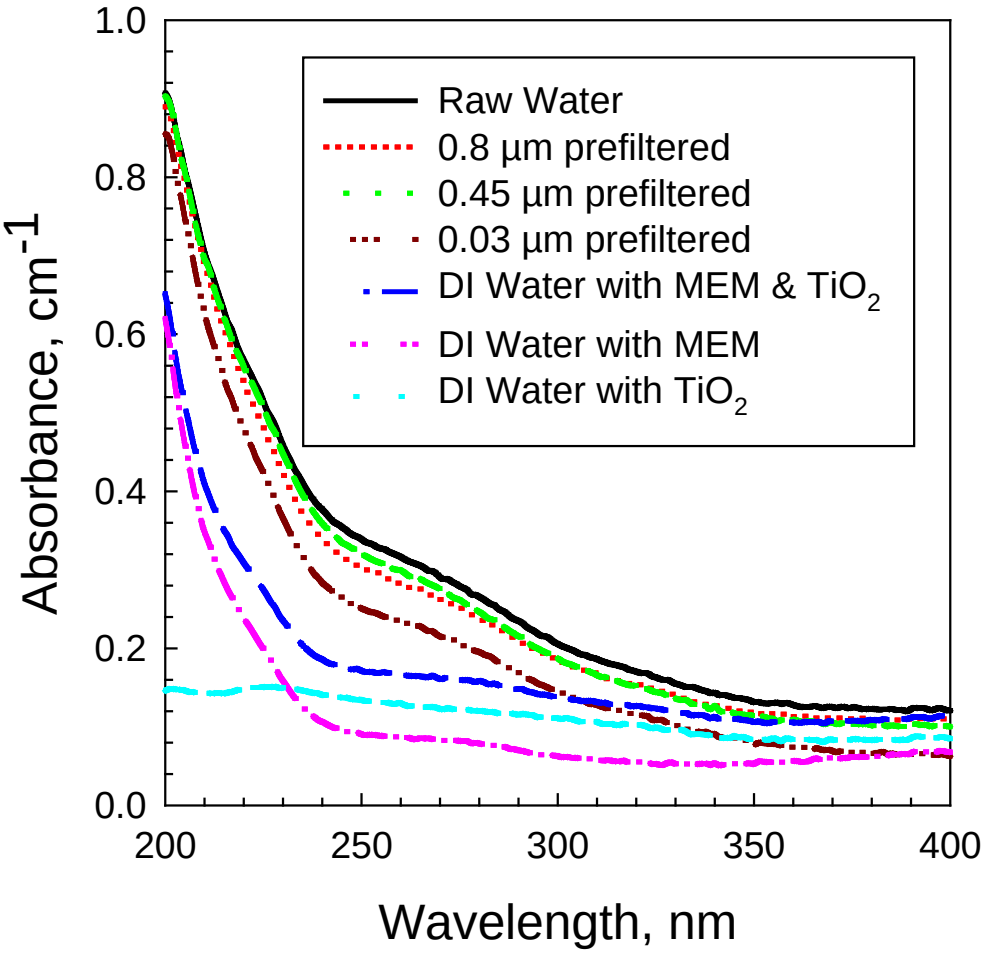

Figure S.3 UV absorbances for several experimental conditions

Note: Lake water solutions and the DI cases with MEM contained 1% MEM to parallel HAdV40 experiments.

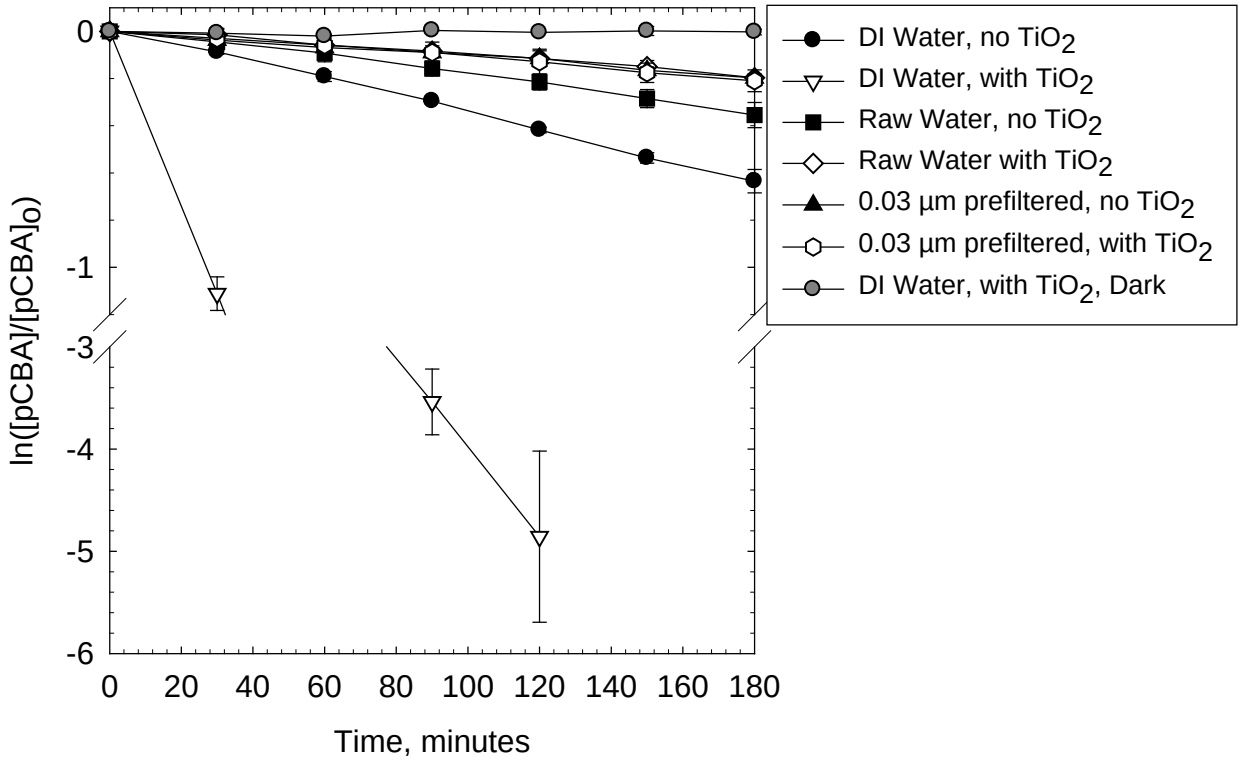

Figure S.4 pCBA degradation over time for various water sources

Note: The raw water and 0.03 µm prefiltered cases include 1% MEM to parallel the HAdV40 experiments.

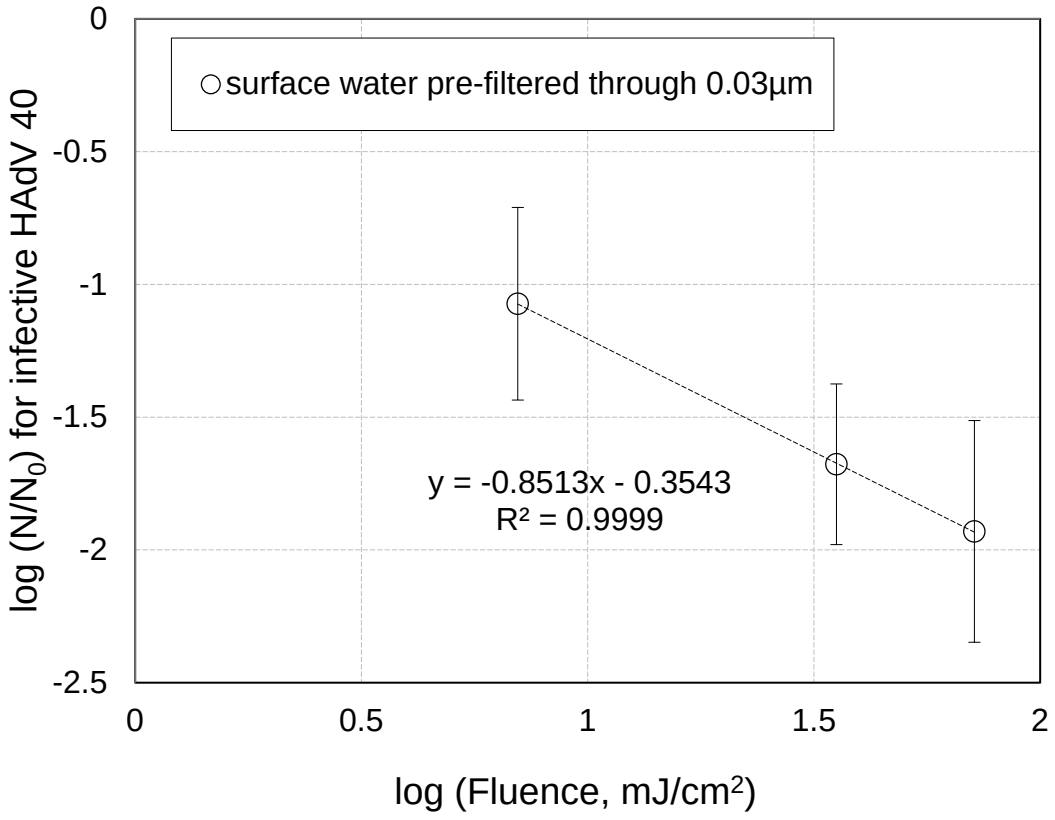

Figure S.5 Inactivation of culturable HAdV40 in lake water pre-filtered through 0.03 µm membrane

Note: Error bars represent standard deviations (n = 3).

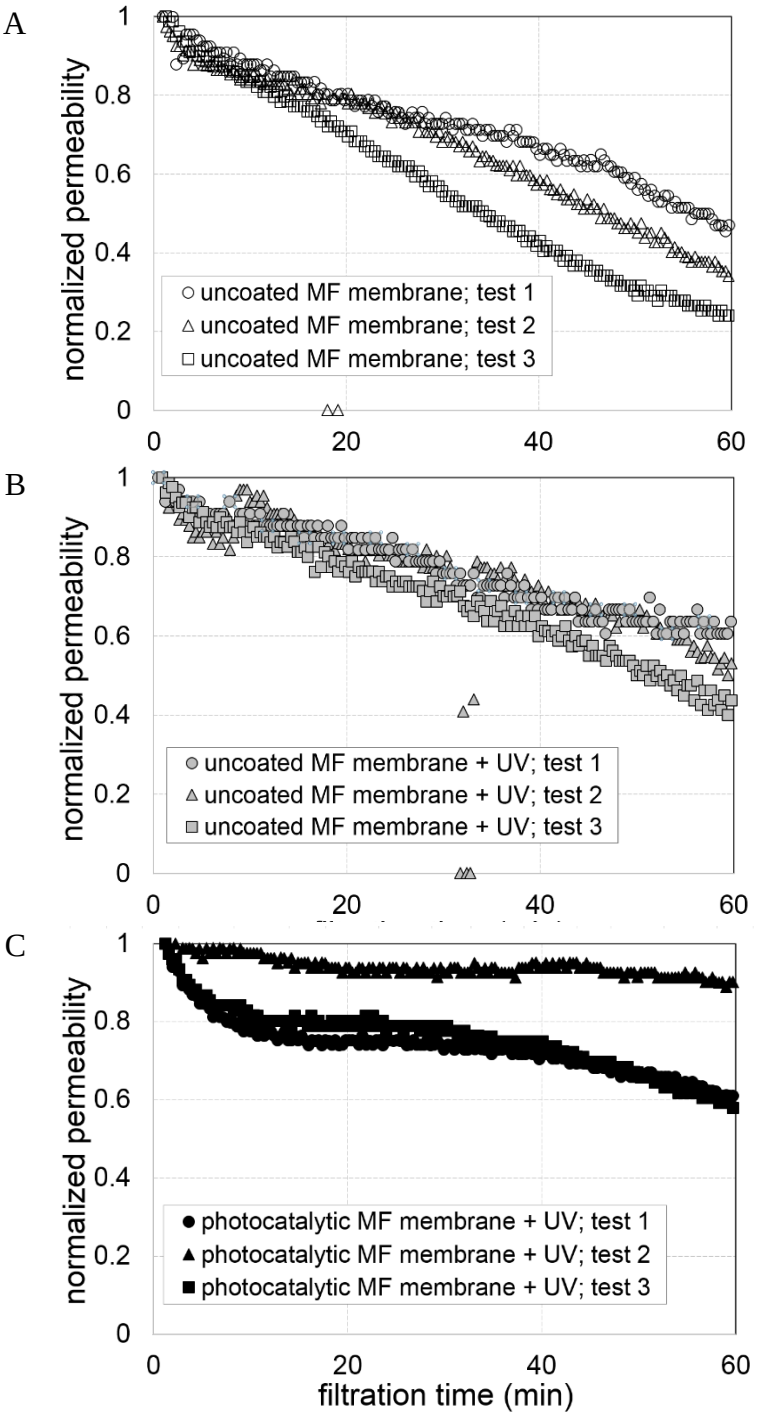

Figure S.6 Normalized permeability of microfiltration membranes to deionized water

Note: A) uncoated membrane; B) the same membrane with a photocatalytic coating in the absence of UV light; C) the same membrane with a photocatalytic coating exposed to UV light.

REFERENCES

REFERENCES

[1] J.H. Jorgensen, M.A. Pfaller, K.C. Carroll, G. Funke, M.L. Landry, S.S. Richter, D.W. Warnock, Manual of Clinical Microbiology, 11 ed., American Society of Microbiology, 2015.

[2] M.V. Yates, Adenovirus, in: S. Percival, M.V. Yates, D. Williams, R. Chalmers, N. Gray (Eds.) Microbiology of Waterborne Diseases. Microbiological Aspects and Risks, Elsevier, 2014, pp. 471-477.

[3] Y. Jin, R.-f. Zhang, Z.-p. Xie, K.-l. Yan, H.-c. Gao, J.-r. Song, X.-h. Yuan, Y.-d. Hou, Z.-j. Duan, Prevalence of adenovirus in children with acute respiratory tract infection in Lanzhou, China, Virol. J., 10 (2013) 271-271.

[4] EPA, https://www.epa.gov/ccl/contaminant-candidate-list-1-ccl-1. Retrieved May 14, 2016, in, 2006.

[5] C.E. Enriquez, C.J. Hurst, C.P. Gerba, Survival of the enteric adenoviruses 40 and 41 in tap, sea, and waste water, Water Res., 29 (1995) 2548-2553.

[6] A. Kramer, I. Schwebke, G. Kampf, How long do nosocomial pathogens persist on inanimate surfaces? A systematic review, BMC Infec. Dis., 6 (2006) 130-130.

[7] C.P. Gerba, N. Nwachuku, K.R. Riley, Disinfection resistance of waterborne pathogens on the United States Environmental Protection Agency's Contaminant Candidate List (CCL), J. Water Supply: Res. Technol. - Aqua, 52 (2003) 81-94.

[8] C. Bernstein, H. Bernstein, Aging, Sex, and DNA Repair, Academic Press, New York, 1991.

[9] T.J. Kelly, Adenovirus DNA replication, in: H.S. Ginsberg (Ed.) The adenoviruses, Plenum Press, New York, 1984, pp. 271-308.

[10] EPA, U.S. Environmental Protection Agency. EPA 815-R-06-007, Office of Water. Ultraviolet Disinfection Guidance Manual for the Final Long Term 2 Enhanced Surface Water Treatment Rule, in, Washington, DC, 2006.

[11] J.A. Thurston-Enriquez, C.N. Haas, J. Jacangelo, K. Riley, C.P. Gerba, Inactivation of feline calicivirus and adenovirus type 40 by UV radiation, Appl. Environ. Microbiol., 69 (2003) 577-582.

[12] N. Nwachuku, C.P. Gerba, A. Oswald, F.D. Mashadi, Comparative inactivation of adenovirus serotypes by UV light disinfection, Appl. Environ. Microbiol. , 71 (2005) 5633-5636.

[13] I. Uhnoo, G. Wadell, L. Svensson, E. Olding-Stenkvist, E. Ekwall, R. Mölby, Aetiology and epidemiology of acute gastro-enteritis in Swedish children, J. Infec., 13 (1986) 73-89.

[14] J.R. Cruz, P. Cáceres, F. Cano, J. Flores, A. Bartlett, B. Torún, Adenovirus types 40 and 41 and rotaviruses associated with diarrhea in children from Guatemala, J. Clin. Microbiol., 28 (1990) 1780-1784.

[15] S. Chiba, I. Nakamura, S. Urasawa, S. Nakata, K. Taniguchi, K. Fujinaga, T. Nakao, Outbreak of infantile gastroenteritis due to type 40 adenovirus, Lancet, 322 (1983) 954-957.

[16] S. Levidiotou, C. Gartzonika, D. Papaventsis, C. Christaki, E. Priavali, N. Zotos, E. Kapsali, G. Vrioni, Viral agents of acute gastroenteritis in hospitalized children in Greece, Clin. Microbiol. Infec., 15 (2009) 596-598.

[17] C.W. LeBaron, N.P. Furutan, J.F. Lew, J.R. Allen, V. Gouvea, C. Moe, S.S. Monroe, Viral agents of gastroenteritis: public health importance and outbreak managemen, in: C.f.D.C.a.P.M.a.M.W. Report (Ed.), 1990, pp. 1-24.

[18] L. Belháčová, J. Krýsa, J. Geryk, J. Jirkovský, Inactivation of microorganisms in a flow-through photoreactor with an immobilized TiO2 layer, J. Chem. Technol. Biotechnol., 74 (1999) 149-154.

[19] O.K. Dalrymple, E. Stefanakos, M.A. Trotz, D.Y. Goswami, A review of the mechanisms and modeling of photocatalytic disinfection, Appl. Catal. B: Environ., 98 (2010) 27-38.

[20] S. Pigeot-Rémy, F. Simonet, E. Errazuriz-Cerda, J.C. Lazzaroni, D. Atlan, C. Guillard, Photocatalysis and disinfection of water: Identification of potential bacterial targets, Appl. Catal. B: Environ., 104 (2011) 390-398.

[21] Y.W. Cheng, R.C.Y. Chan, P.K. Wong, Disinfection of Legionella pneumophila by photocatalytic oxidation, Water Res., 41 (2007) 842-852.

[22] J. Lonnen, S. Kilvington, S.C. Kehoe, F. Al-Touati, K.G. McGuigan, Solar and photocatalytic disinfection of protozoan, fungal and bacterial microbes in drinking water, Water Res., 39 (2005) 877-883.

[23] S. Navalon, M. Alvaro, H. Garcia, D. Escrig, V. Costa, Photocatalytic water disinfection of Cryptosporidium parvum and Giardia lamblia using a fibrous ceramic TiO2 photocatalyst, Water Sci. Technol., 59 (2009) 639-645.

[24] P.-C. Maness, S. Smolinski, D.M. Blake, Z. Huang, E.J. Wolfrum, W.A. Jacoby, Bactericidal activity of photocatalytic TiO(2) reaction: toward an understanding of its killing mechanism, Appl. Environ. Microbiol., 65 (1999) 4094-4098.

[25] T. Matsunaga, R. Tomoda, T. Nakajima, H. Wake, Photoelectrochemical sterilization of microbial cells by semiconductor powders, FEMS Microbiol. Lett., 29 (1985) 211-214.

[26] J. Marugán, R. van Grieken, C. Sordo, C. Cruz, Kinetics of the photocatalytic disinfection of Escherichia coli suspensions, Appl. Catal. B: Environ., 82 (2008) 27-36.

[27] O.A. McLoughlin, P.F. Ibáñez, W. Gernjak, S.M. Rodríguez, L.W. Gill, Photocatalytic disinfection of water using low cost compound parabolic collectors, Solar Energy, 77 (2004) 625-633.

[28] A.G. Rincón, C. Pulgarin, Photocatalytical inactivation of E. coli: effect of (continuous–intermittent) light intensity and of (suspended–fixed) TiO2 concentration, Appl. Catal. B: Environ., 44 (2003) 263-284.

[29] A.-G. Rincón, C. Pulgarin, Bactericidal action of illuminated TiO2 on pure Escherichia coli and natural bacterial consortia: post-irradiation events in the dark and assessment of the effective disinfection time, Appl. Catal. B: Environ., 49 (2004) 99-112.

[30] C.P. Rodrigues, R.L. Ziolli, J.R. Guimarães, Inactivation of Escherichia coli in water by TiO2-assisted disinfection using solar light, J. Bras. Chem. Soc., 18 (2007) 126-134.

[31] A.R. Badireddy, J.F. Budarz, S. Chellam, M.R. Wiesner, Bacteriophage Inactivation by UV-A Illuminated Fullerenes: Role of Nanoparticle-Virus Association and Biological Targets, Environmental Science & Technology, 46 (2012) 5963-5970.

[32] M. Cho, J. Lee, Y. Mackeyev, L.J. Wilson, P.J.J. Alvarez, J.B. Hughes, J.H. Kim, Visible Light Sensitized Inactivation of MS-2 Bacteriophage by a Cationic Amine-Functionalized C(60) Derivative, Environmental Science & Technology, 44 (2010) 6685-6691.

[33] H. Mamane, H. Shemer, K.G. Linden, Inactivation of E. coli, B. subtilis spores, and MS2, T4, and T7 phage using UV/H2O2 advanced oxidation, Journal of hazardous materials, 146 (2007) 479-486.

[34] S.D. Snow, K. Park, J.-H. Kim, Cationic Fullerene Aggregates with Unprecedented Virus Photoinactivation Efficiencies in Water, Environmental Science & Technology Letters, 1 (2014) 290-294.

[35] L. Gorvel, M. Yver, E. Robert, M. Harmant, M. Rosa-Calatrava, B. Lina, J.P. Gorvel, V. Moulès, R. Albalate, C. Gaüzère, Innovative germicidal UV and photocatalytic system dedicated to aircraft cabin eliminates volatile organic compounds and pathogenic micro-organisms, CLEAN – Soil Air Water, 42 (2014) 703-712.

[36] G. Li, X. Liu, H. Zhang, P.-K. Wong, T. An, W. Zhou, B. Li, H. Zhao, Adenovirus inactivation by in situ photocatalytically and photoelectrocatalytically generated halogen viricides, Chem. Eng. J., 253 (2014) 538-543.

[37] S. Bounty, R.A. Rodriguez, K.G. Linden, Inactivation of adenovirus using low-dose UV/H2O2 advanced oxidation, Water Res., 46 (2012) 6273-6278.

[38] J. Brame, M.C. Long, Q.L. Li, P. Alvarez, Inhibitory effect of natural organic matter or other background constituents on photocatalytic advanced oxidation processes: Mechanistic model development and validation, Water Research, 84 (2015) 362-371.

[39] P.L. Brezonik, J. Fulkerson-Brekken, Nitrate-induced photolysis in natural waters: Controls on concentrations of hydroxyl radical photo-intermediates by natural scavenging agents, Environ. Sci. Technol., 32 (1998) 3004-3010.

[40] B.J. Starr, V.V. Tarabara, M. Herrera-Robledo, M. Zhou, S. Roualdès, A. Ayral, Coating porous membranes with a photocatalyst: Comparison of LbL self-assembly and plasma-enhanced CVD techniques, J. Membr. Sci., 514 (2016) 340-349.

[41] B. Guo, E.V. Pasco, I. Xagoraraki, V.V. Tarabara, Virus removal and inactivation in a hybrid microfiltration-UV process with a photocatalytic membrane, Separ. Purif. Technol., 149 (2015) 245.

[42] R.O. Rahn, Potassium iodide as a chemical actinometer for 254 nm radiation: Use of iodate as an electron scavenger, Photochem. Photobiol., 66 (1997) 450-455.

[43] J.R. Bolton, K.G. Linden, Standardization of methods for fluence (UV dose) determination in bench-scale UV experiments, ASCE J. Environ. Eng., 129 (2003) 209-215.

[44] G.V. Buxton, C.L. Greenstock, W.P. Helman, A.B. Ross, Critical review of rate constants for reactions of hydrated electrons, hydrogen atoms and hydroxyl radicals (.OH/.O-) in aqueous solution, J. Phys. Chem. Ref. Data, 17 (1988) 513-886.

[45] I. Xagoraraki, D.H.W. Kuo, K. Wong, M. Wong, J.B. Rose, Occurrence of human adenoviruses at two recreational beaches of the Great Lakes, Appl. Environ. Microbiol., 73 (2007) 7874.

[46] USEPA, Manual of Methods for Virology. Chapter 15, in, Washington, DC: Office of Research and Development, United States Environmental Protection Agency, 2001.

[47] MPN Calculator, http://www.i2workout.com/mcuriale/mpn/

[48] R.O. Rahn, J. Bolton, M.I. Stefan, The iodide/iodate actinometer in UV disinfection: Determination of the fluence rate distribution in UV reactors, Photochem. Photobiol., 82 (2006) 611-615.

[49] R.O. Rahn, S. Echols, Iodide/iodate chemical actinometry using spherical vessels for radiation exposure as well as for monitoring absorbance changes, Photochem. Photobiol., 86 (2010) 990-993.

[50] A. Fujishima, X. Zhang, Titanium dioxide photocatalysis: present situation and future approaches, C. R. Chimie, 9 (2006) 750-760.

[51] J.L. Weishaar, G.R. Aiken, B.A. Bergamaschi, M.S. Fram, R. Fujii, K. Mopper, Evaluation of specific ultraviolet absorbance as an indicator of the chemical composition and reactivity of dissolved organic carbon, Environ. Sci. Technol., 37 (2003) 4702-4708.

[52] H. Collins, R. Selleck, G.C. White, Problems in obtaining adequate sewage dinsinfection, J. San. Eng. Div. ASCE, 97 (1971) 549-562.

[53] R. Selleck, B. Saunier, Kinetics of bacterial deactivation with chlorine, J. Environ. Eng. ASCE, 104 (1978) 1197-1212.

[54] M.V. Liga, E.L. Bryant, V.L. Colvin, Q. Li, Virus inactivation by silver doped titanium dioxide nanoparticles for drinking water treatment, Water Res., 45 (2011) 535-544.

[55] D.B. Misstear, L.W. Gill, The inactivation of phages MS2, ΦX174 and PR772 using UV and solar photocatalysis, J Photochem Photobiol B., 107 (2012) 1-8.

[56] H. Ryu, D. Gerrity, J.C. Crittenden, M. Abbaszadegan, Photocatalytic inactivation of Cryptosporidium parvum with TiO2 and low-pressure ultraviolet irradiation, Water Res., 42 (2008) 1523-1530.

[57] M.J. Mattle, T. Kohn, Inactivation and tailing during UV254 disinfection of viruses: Contributions of viral aggregation, light shielding within viral aggregates, and recombination, Environ. Sci. Technol., 46 (2012) 10022-10030.

[58] Z. Yin, V.V. Tarabara, I. Xagoraraki, Human adenovirus removal by hollow fiber membranes: Effect of membrane fouling by suspended and dissolved matter, J. Membr. Sci., 482 (2015) 120-127.

CHAPTER 4. CONCLUSIONS AND FUTURE WORK

4.1 Conclusions

The hybrid photocatalytic UV-membrane filtration system developed in this study is the first application of PMR with immobilized catalysts for the removal and inactivation of viruses. The major contribution of this study is to propose an innovative treatment process that improves the efficacy of water disinfection, especially the removal and inactivation of viruses.

In theory, there are no harmful disinfection by-products generated by using this hybrid system. The hybrid system retains the advantages of photocatalytic UV disinfection and membrane filtration while mitigating drawbacks of each of these two processes. The membrane, operated in the inside-out geometry, removes the turbidity of the water thereby enhancing the efficacy of UV disinfection. The membrane also serves as a support for immobilized catalysts to avoid the recovery and secondary separation of catalysts. The presence of catalysts complements direct UV to enhance pathogen removal. The additional photocatalytic UV disinfection applied on the permeate side of the membrane enables trade-offs in pore sizes and product water fluxes.

A number of experiments were conducted to determine the optimized operational parameters, understand mechanisms of virus inactivation in complex water matrices and evaluate the performance of the hybrid photocatalytic UV-membrane filtration system. To make this investigation feasible, we started from a simple model system of bacteriophage P22 suspended in DI water (chapter 2). The hybrid process was shown to be considerably more effective in inactivating bacteriophage P22 than the constituent processes applied in series. P22 inactivation

by direct UV in a batch rector followed Collins-Selleck model. Similar results were observed in the second part of the study (chapter 3) that involved human adenovirus suspended in lake water pre-filtered through membranes of different porosities. The virus inactivation by the hybrid photocatalytic UV-membrane filtration process was ~1.5 times higher than that with the non-photocatalytic UV-membrane filtration process. UV disinfection experiments in a batch reactor with adenovirus suspended in pre-filtered lake water showed that the water quality has a major impact on the efficacy of virus inactivation but does not affect qPCR count.

4.2 Future research work

The efficiency of photocatalysis depends upon many factors: photocatalyst loading, initial concentration of the substance, characteristics of UV lamp, and composition of the solution. Besides, the operational parameters, such as crossflow rate, distance between the photocatalytic surface of the membrane and light source as well as membrane's pore size, also affect the performance of the hybrid system. Table 4.1 summarizes what is known and unknown knowledge of this novel hybrid photocatalytic UV-membrane filtration system. From this table, we can see that there are still many areas that lack of the comprehensive understanding. Therefore, plenty of experiments with more in-depth researches are necessary to be conducted to find out the optimal combination for this hybrid system.

Table 4.1 Knowledge gaps of the novel hybrid photocatalytic UV-membrane filtration system

Parameters	Knowns	Unknowns
photocatalysts loading	a) The photocatalytic efficiency is proportional to the mass of catalysts on the membrane within a reasonable range. Adding catalyst in excess of the optimum does not lead to increased reactivity. b) Excessive coverage by the photocatalyst results in a dense coating layer causing significant decrease in membrane permeability.	The optimal amount of catalysts.
initial concentration of the substance	-	Whether and how the change of the initial concentration affects the treatment efficiency.
characteristics of UV lamp	-	a) How do the wavelength and the intensity of the UV irradiation influence the treatment efficiency? b) What is the optimal intensity?
components of the solution	Water quality affects the treatment efficiency, especially the results of virus inactivation.	a) How does the pH of the solution affect the treatment efficiency? b) What is the treatment efficiency when more than one type of microbial species exists in the solution?
crossflow rate	-	How does the crossflow rate affect the treatment efficiency?
distance between membrane and light source	-	The optimal distance.
membrane pore size	-	How does the membrane pore size influence the treatment efficiency?